Dissertation zur Erlangung des Doktorgrades der Fakultät für Chemie und Pharmazie der Ludwig-Maximilians-Universität München

Lyophilization process design for protein drugs using α-relaxations and thermal history

Sebastian Groel

aus

Darmstadt, Deutschland

2023

Erklärung

Diese Dissertation wurde im Sinne von § 7 der Promotionsordnung vom 28. November 2011 von Herrn Prof. Dr. Gerhard Winter betreut.

Eidesstattliche Versicherung

Diese Dissertation wurde eigenständig und ohne unerlaubte Hilfe erarbeitet.

München, 29.06.2023

_____

Sebastian Groel

Dissertation eingereicht am 29.06.2023

1. Gutachter: Prof. Dr. Gerhard Winter

2. Gutachter: Prof. Dr. Wolfgang Frieß

Mündliche Prüfung am 18.07.2023

To my family

Acknowledgements

I want to express my sincere gratitude to Prof. Gerhard Winter for the opportunity and trust to work on several exciting research topics. The created working atmosphere gave me the possibility to not only grow on my scientific expertise but furthermore helped me a lot for my personal development. Also, I want to thank for the great chance to visit several conferences in Europe as well as beyond in the USA and to spend a research stay at the Georgia Institute of Technology (Georgia Tech), Atlanta, USA.

I want to thank Tim Menzen for the co-supervision of my work. His creativity and analytical discussions helped me to overcome difficulties and to find the right path to proceed.

For the hosting at the Georgia Institute of Technology I want to thank Prof. Marcus T Cicerone and Kelly Badilla-Nunez. I incredibly appreciate the really great time I had and the chance to learn a lot about optics, Raman Scattering and β-relaxation.

Further thanks also to Jürgen Seidel from the Institut für Physikalische Chemie of the TU Bergakademie Freiberg for the teaching of the basics of calorimetry and the help to set up the isothermal microcalorimeter.

I want to thank my former labmates Andreas Stelzl, Ute Rockinger and Bernard Manuel Haryadi for the nice time in the office at the end of the hallway, as well as all members of AK Winter, AK Frieß and AK Merkel, for the scientific and social activities inside and outside the LMU, like the ski trips in winter, hiking tours in summer, conferences in Rotterdam and Breckenridge.

Especially I want to thank Ruth Rieser, Nicole Härdter, Katharina Prüßmann and Alice Hirschmann for the lunch breaks and the good coffee as well as Ken Lo Presti for the great time in Breckenridge and for the relaxing evenings to compensate the lab work (← → ↓ ← → ↓ Δ).

Last but not least many thanks to my friends at home, Christian Peter and Maximilian Molitor, the phone calls felt like you were here in person.

Infinite thanks to my parents Brigitte and Michael who remove nearly every obstacle out of my path to find my way since almost 30 years. From the bottom of my heart, I want to thank Sina. The person that motivates me to start when I was paralyzed, forced me to take a break when I could not stop, cheering me up when I was down and was always on my side.

Table of Content

Chapter I Calorimetric Investigation of the Relaxation Phenomena in Amorphous Lyophilized Solids

This chapter is published as: Groël, S.; Menzen, T.; Winter, G. (2021). Calorimetric Investigation of the Relaxation Phenomena in Amorphous Lyophilized Solids. *Pharmaceutics* 2021, 13, 1735.

This article belongs to the Special Issue New Trends in Freeze-Drying of Pharmaceutical Products

Note from the authors: To establish a coherent numbering and pagination within this document the numbers of references, figures and tables were adapted. Apart the minor changes, the version included in this thesis is identical with the published article.

The published article can be accessed online via:

https://doi.org/10.3390/pharmaceutics13101735

I.1 Abstract

Studying the thermal history and relaxation of solid amorphous drug product matrices by calorimetry is a well-known approach, particularly in the context of correlating the matrix parameters with the long-term stability of freeze-dried protein drug products. Such calorimetric investigations are even more relevant today, as the application of new process techniques in freeze-drying (which strongly influence the thermal history of the products) has recently gained more interest. To revive the application of calorimetric methods, the widely scattered knowledge on this matter is condensed into a review and completed with new experimental data. The calorimetric methods are applied to recent techniques in lyophilization, such as controlled nucleation and aggressive/collapse drying. Phenomena such as pre-T_g events in differential scanning calorimetry and aging shoulders in isothermal microcalorimetry are critically reviewed and supplemented with data of freeze-dried products that have not been characterized with these methods before.

Keywords: collapse; controlled nucleation; differential scanning calorimetry (DSC); freeze-drying; isothermal microcalorimetry (IMC); lyophilization; molecular mobility; relaxation

I.2 Introduction

In the pharmaceutical field, there is still a tremendous need for lyophilized products with increasing tendency. More and more biological compounds are being developed and used to improve the treatment of severe diseases [1]. The advantages of biotec products are obvious. Monoclonal antibodies, for instance, provide improved targeting upon conjugation with small-molecule drugs with low side effects for specific cancer treatments [2]. Protein- or RNA-based vaccines allow us to react quickly to pandemic infections, as we have experienced recently. These are only a few of the manifold reasons to use these products [3–5]. However, many biological drug products suffer from physico-chemical instabilities, which compromise their long-term stability [6]. Several instabilities, such as oxidation, hydrolysis, or aggregation, make it difficult to develop a stable pharmaceutical formulation that can be shipped, stored, and administered conveniently [7–11]. Therefore, liquid biological drug products typically require long-term storage under frozen or refrigerated temperatures. In contrast, freeze-drying as a gentle method to remove the water provides an opportunity for the storage of freeze-dried drug products under ambient conditions by overcoming most of physico-chemical instabilities [12,13]. The resulting dry solid matrix is able to protect the biological ingredients, although most of the water, which is the natural habitat of these compounds, is missing [13]. This is not trivial and only a few drying methods are able to provide a stabilizing matrix [14,15]. The secret of these methods is hidden in the special properties of the resulting matrix, which will be explained in the following.

A typical freeze-drying process leads to a fully amorphous, glassy system or at least a partly amorphous one [16]. Several studies proved that biologicals such as proteins are much better preserved in the amorphous state compared to a crystalline one [17,18]. There are two main theories that try to explain why this is the case. One is the water replacement theory that states that biologicals are best preserved in their native state, which is surrounded by water [19]. When the water is removed during the freeze-drying process, excipients such as sugars stabilize this native structure by replacing the water with their own hydroxyl groups [19,20]. This can only work when the excipient is in an amorphous state. The other approach is the glassy dynamics theory, also called the vitrification hypothesis [19,21]. Summarized, it states that the matrix becomes more and more rigid during its formation in such a manner that any movement of molecules and functional groups is finally impossible. In this context, movement is seen as an essential factor for reaction processes that are impeded in this way [22,23]. This theory is the major basis of the topics discussed in this review and thus is further explained in the Theoretical Background section.

Importantly, these amorphous products are thermodynamically instable or metastable, which is, on the one hand, helpful due to the improved solubility of the formulations but is a problem for long-term stability [17]. Thus, the formulations will rearrange their structure, which is called structural relaxation, or even crystallize during storage, thereby at least partly losing their ability to stabilize the biological entity [24]. This is also relevant for small drug molecules. The reason to prepare an amorphous form is often not only to increase water solubility but to achieve an enabling rise in bioavailability [25–27]. Changes in this amorphous state over time or even crystallization can lead to critical dose fluctuations [28]. For this reason, it is in fact mandatory to analyze the solid state with respect to the stability predicting factors. Most common solid state properties in this context are residual moisture, specific surface area, glass transition temperature, and crystallinity. Furthermore, one of the more recent techniques is the investigation of the ability of a lyophilized molecule to exchange hydrogen atoms with deuterium (solid state hydrogen deuterium exchange, ssHDX), thereby indicating the accessibility and reaction rate of degradation or—in other words—the ability of a matrix to provide immobilization to the molecule that shall be stabilized [29]. All these methods and properties are indeed very important for the characterization of a freeze-dried product but do not directly mirror (except the glass transition temperature) the thermal history of the lyophilized matrix, which is strongly connected to the thermodynamic properties and thus the long-term stability of freeze-dried products.

Different researchers agree that relaxation processes in freshly prepared glasses (amorphous excipient/drug matrices) can be used as a good surrogate to characterize their thermal history and thermodynamic properties and can also be taken as a predictive tool for the long-term stability of the created products [30,31]. Several methods were used and developed in the last few decades to investigate matrix relaxations. These include, inter alia, measurements of viscosity [16,32], solid state nuclear magnetic resonance spectroscopy (ss-NMR) [22,33], dielectric spectroscopy [16,22,34], terahertz spectroscopy [22,35], thermally stimulated depolarization current [36,37], electron spin resonance spectroscopy [38], incoherent neutron scattering [39,40] and, last but not least, calorimetric methods [17,22,41,42]. With the exception of the latter, all these methods require very well-trained scientific operators and a great deal of experience to obtain and evaluate the relaxation data. Furthermore, most laboratories that deal with pharmaceutical freeze-drying have only limited access to these methods. In contrast, almost every formulation laboratory has access to at least one calorimetric method—typically differential scanning calorimetry (DSC)—but only a few scientists make use of the full potential of this device.

With this review, we wish to offer a summary of the thermal history and relaxation determination of lyophilized pharmaceutical products with calorimetric methods. We hope to encourage the reader to "revive" the partly neglected and surprisingly simple techniques and re-evaluate their use, particularly regarding the recent updates in freeze-drying techniques. We provide a guideline on calorimetric methods and encourage researchers to acquire more information from calorimetric measurements. We complete this review with our own data and look at the calorimetric methods from a different angle in the context of collapse freeze-drying, controlled nucleation, and highly concentrated protein formulations.

I.3 Theoretical Background

A thermodynamic equilibrated state can be described as a system where every molecule or functional group possesses its full degree of freedom [43]. This means, for example, that the system adapts to changes in temperature with modifications in its structure or other thermodynamic properties such as configurational entropy immediately [23,43]. This system is called "ergodic" [44]. Examples of thermodynamic equilibrated material are crystalized solids and liquids, even when the latter are supercooled (exceptions may exist).

Usually, when a liquid is cooled, at a certain point, the melting temperature (T_m), the liquid crystallizes and forms a solid [23]. During the freezing step of a lyophilization process, the solution normally fails to fully crystallize. In detail, parts of the water will crystallize, leading to an up-concentration of the remaining solution. This solution, containing the active pharmaceutical ingredient (API) and the excipients, will thereby form a supercooled liquid [23]. With further cooling of this supercooled liquid, at a certain point, the glass transition temperature (T_g), the system becomes too slow to follow the cooling rate with thermodynamic changes. Thus, it leaves the equilibrated state and the material forms a glass. Concerning lyophilizates, it is important to bear in mind that we can essentially identify two glassy systems. One glass system is the solution before drying, with T_g values of around −30 °C, also called T_g', and the other system after drying, with only little remaining water content. Depending on the excipients, the T_g can be at temperatures far above 100 °C. Important is that also the latter system is called a supercooled liquid, from the thermodynamic perspective, when it is heated above its T_g. Although the system can be considered a solid after freeze-drying, it is not in a thermodynamic equilibrium below T_g. Thus, the fresh glass will have an excess in entropy, enthalpy, and volume [23,31,44]. In Figure I.1a, an energetic model is provided that illustrates these explanations. The dashed line is a fictive, non-existent state that describes the thermodynamic equilibrated state of the system. Relaxation means the process of the new

material approaching the "equilibrated glassy state", which can be considered the prolonged energy state of the supercooled liquid (dashed line) [23]. This process, also called the physical aging of a glass, is connected to changes in other material properties, which strongly influences the protein stability [31,45]. The energy excess released below T_g during the aging provides the required energy for molecular movement and degradation [41,46]. Slowing down this processes hence has the potential to increase the stability of lyophilized products [47]. Therefore, an understanding and optimization of the thermodynamic properties of the host glass is essential to improve the long-term stability of a pharmaceutical formulation [47].

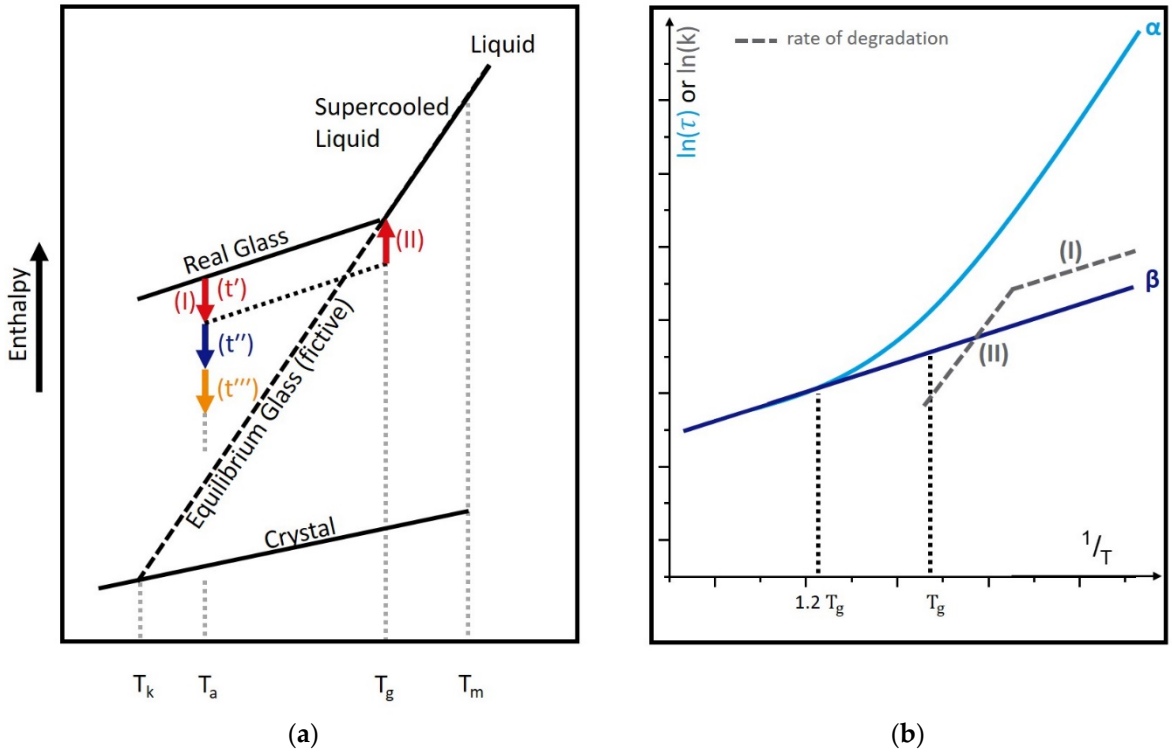

Figure I.1 Theoretical considerations concerning relaxation. (a) Enthalpy relaxation diagram of solids with the melting temperature T_m, the glass transision temperature T_g, the annealing or tempering temperature T_a, and the Kauzman temperature T_K. (t')–(t''') symbols indicate the tempering process of a glass at a certain temperature T_a. In the context of this review, the "real glass" represents our freshly prepared lyophilized formulation. The diagram is modified and adapted to the focus of this review [16,17,23,43,44,46,48]. (b) Model of the dominant relaxation modi. The influence of α- and β-relaxations on a degradation process with the constant k in dependence on temperature and T_g. (I) degradation is governed by β-mobility; (II) degradation is governed by α-mobility [43].

I.3.1 Nomenclature of Relaxation Modi

The relaxation processes themselves are classified into different modi concerning their behavior in a broadband relaxation spectroscopy measurement. They are sorted into α-, β-, and γ-relaxations [22,46,49], with α-relaxations being the slowest relaxations (time scale from seconds to months), followed by β-relaxations (time scales of milli- to picoseconds) and γ-

relaxations (beyond β-relaxations in the time scale of picoseconds) [22,43,46,50]. Apart from a limited number of exceptions, calorimetric methods capture only α-relaxations [51,52]. Thus, this review focuses on the properties of α-relaxations and refers to other excellent publications for more information on other types of relaxation modi [46,50,53]. For the investigation of further relaxation modi, other methods are appropriate, such as inelastic neutron scattering (β-relaxations), ss-NMR (β-relaxations), and dielectric spectroscopy (β- and γ-relaxations) [22,46].

α-Relaxations, also known as "structural relaxations", are strongly temperature-dependent and mostly linked to viscosity [23,46,47,50]. Thus, they describe the translational and rotational movement of whole molecules [22,23,31,54]. One well-known parameter that is connected to α-relaxations is the glass transition temperature and so it was a long-used idea to simply increase the temperature of the T_g of a formulation to slow down processes related to α-relaxations [47,55]. On the one hand, it is proven in several studies that α-relaxations as well as the T_g contribute to physical stability, but, on the other hand, for single amorphous drugs, sometimes, β-relaxations seem to be a better predictive tool [22,46,47,56]. Luthra and Cicerone developed a model that is able to explain this fact [43]. Whereas β-relaxations are temperature-independent on a wide temperature scale and thus always contribute the same amount of energy to mobility, the influence of α-relaxations strongly increases near T_g and dominates the glassy dynamics in this temperature range (Figure I.1b) [43]. The exact intersection temperature varies between formulations and this leads to different scenarios about whether α- or β-relaxations are the best stability predictors in a certain range of $T_g - T_a$ [43].

As mentioned above, not many recent studies exist that use the calorimetric methods in the context of new process developments in freeze-drying, although it is emphasized in the community that the properties of a glass depend on the "history" (process) of how it was made [46,57]. Below, the theoretical considerations as well as the evaluation of α-relaxation processes of freeze-dried products with DSC and isothermal microcalorimetry (IMC) are described in detail, including the relevant thermodynamic terms and formulas.

I.3.2 DSC

Firstly, it is of the utmost importance to point out that not all investigated parameters in glasses are thermodynamic parameters but rather of a kinetic nature [46]. This is easier to understand if the explanation above is combined with the practical example of the DSC measurement. For a measurement, normally, 5–10 mg of sample is hermetically sealed in an aluminum pan. The pan is then placed in the oven of the DSC instrument next to an empty reference pan. During a

fixed heating ramp, the heatflow of the sample is compared to the reference, which makes it possible to detect thermal events that trigger changes in the heatflow. In the pharmaceutical environment, usually, heat ramps from 1 K/min up to 20 K/min [58–60] are used. Bearing in mind that "at a certain point the system becomes too slow to follow the cooling rate with thermodynamic changes" helps to explain the kinetic character. This "certain" point depends inter alia on the heating rate of the DSC. General advice and developments in DSC measurement methods are perfectly described elsewhere [58,61]. In the following, we wish to emphasize details that play a role in relaxation and molecular mobility and are often found in the non-pharmaceutical literature.

In nearly every DSC curve of a lyophilized sample, proof of sample aging or, rather, energy loss due to relaxation is observable but barely recognized. Figure I.2 shows different thermograms of a freeze-dried trehalose-based pharmaceutical placebo formulation. In Figure I.2a, a linear measurement mode is displayed. The following thermodynamic parameters can be evaluated:

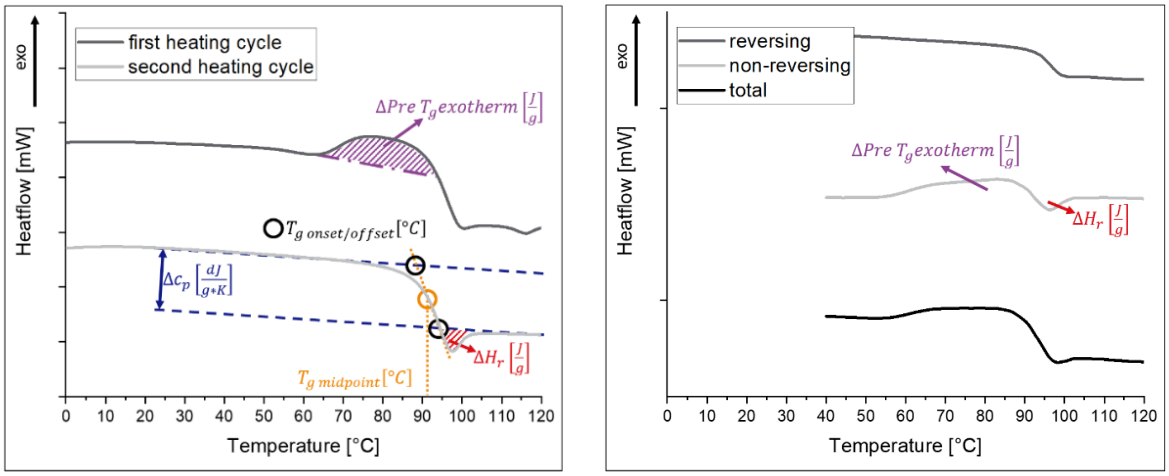

(**a**) (**b**)

Figure I.2 DSC thermograms of a freeze-dried trehalose-based pharmaceutical placebo formulation. The curves are displayed with offset for a better graphical presentation: (a) measured with a linear temperature program with two heating cycles; (b) measured in modulated mode (mDSC).

Δc_p *and* T_g*, Figure I.2a blue arrow and yellow circle, reversible.* These are the "standard" parameters to investigate freeze-dried formulations and thus are perfectly described elsewhere [62–65]. However, the authors wish to point out a few aspects.

At first, the T_g is strongly dependent on the heating rate and on the residual moisture of the formulation. Due to the fact that water works as a plasticizer, the rule of thumb is that per 1% more residual moisture, the T_g decreases by around 10 K [66].

Secondly, to pierce or not to pierce the crucible? In some publications, it is recommended to pierce the lid of the sealed aluminum pan. There is no right or wrong, but the following points have to be considered:

- At temperatures higher than 60 °C, residual moisture will evaporate out of the measured matrix, which lowers the T_g significantly and finally delivers data for the thermal behavior of a dry sample. However, this is not the property of the samples that is stored in the product vials after freeze-drying.
- In the context of the thermal history of an amorphous solid, the value of Δc_p at T_g is relevant. It is the comparison of the c_p ("baseline") between pre- and post-T_g and can be determined as shown in Figure I.2a. It must not be confused with the c_p value itself, which is a substance constant and declares the needed heat to raise 1 g of sample by 1 K. With a pierced lid, the values are determined isobaric in contrast to a hermetically sealed pan. Moreover, it has to be kept in mind that Δc_p at T_g depends on the absolute sample weight. Thus, in multiple measurements (e.g., triplicate), the values of Δc_p will differ more strongly than the T_g temperature due to additional weighing errors. The results of T_g are quite mass-independent.

Enthalpy recovery ΔH_r, Figure I.2a red area, non-reversible. This is also called T_g-overshoot and is the area that prolongs the post-T_g baseline [22]. It represents the weight-normalized restored enthalpy that a sample releases during storage at temperatures below T_g. This storage below T_g is also called annealing, aging, or tempering depending on the literature [22,67]. Throughout this review, tempering is used because it does not interfere with the name of certain process steps in a lyophilization process. The released enthalpy arises from the energy excess that an amorphous sample possesses in comparison to the thermodynamic equilibrated state (e.g., crystalline form). During storage below T_g, this energy excess is slowly released from the sample. This value is needed later for determining relaxation times with DSC.

ΔPre-T_g exo- or endothermal events, Figure I.2a magenta area, non-reversible. This event is rarely reported and is the most unclear observation in the DSC analysis of lyophilizates [43,68]. Dependent on the formulation, it can be sharp (e.g., sucrose) or broad (e.g., trehalose) as well as endothermic (e.g., sucrose) or exothermic (e.g., trehalose) [43]. Moreover, it is reported for pure protein formulations (lyophilized bovine serum albumin, BSA), where it is explained as "α-relaxation-like protein transition" and termed the "protein dynamical temperature" [68].

Because this event occurs in lyophilizates but not in amorphous melt-quenches, it is suggested that this peak arises from the special production procedure of a freeze-dried sample being frozen in an open structure with subsequent water removal [43,67,69,70]. One could describe the process in a way that the freezing step produces a glass, which is then converted into another glass by water sublimation. Because this pre-T_g event can be sharpened by sample tempering, it could be seen as a proof for widely distributed relaxation states that can be condensed during longer storage times [43,58,69]. The relaxation state theory is reasonable for a pre-T_g exotherm, but not for a pre-T_g endotherm. In this case, Luthra suggested that such samples are accidently tempered during the secondary drying step of the freeze-drying process, thereby losing their energy excess [43]. As a result, an endotherm occurs because the system receives enough energy to recover the lost energy excess at this point [43,71]. This is in agreement with Vyazovkin and Dranca, who investigated β-relaxations with a DSC method [52]. They stated that the endothermal peak occurs immediately above the annealing temperature and is a sign that α- and β-relaxations are coupled around the glass transition region [52]. Further, this would support the model of dominant relaxation modi of Luthra and Cicerone (Figure I.1b) [43]. In contrast, Reddy et al. oppose this idea in their studies comparing DSC and thermally stimulated current (TSC) by naming events "β-relaxations" when observed in the TSC but not visible in DSC [72]. Moreover, Wang et al. were not able to correlate these pre-T_g events with NMR- and neutron backscattering-measured β-relaxations [70]. On the contrary, these TSC events can be found in IMC measurements and it is suggested that IMC is able to measure some kinds of β-motions as well as more detailed α-motions [37]. For polymers, four properties of this pre-T_g phenomenon are reported; the effect is asymmetrical, the endotherm increases when the tempering time or temperature is raised, it can be superimposed from the glass transition, and the temperature peak is a function of tempering time ($\ln (t)_{tempering}$) and temperature ($(T)_{tempering}$) [73,74]. In the event that the pre-T_g event is missing, it is suggested that it is superimposed by the glass transition, as described previously [74]. It should be pointed out that this pre-T_g event is not based on a particular interaction between the protein and the placebo matrix because it occurs in placebo formulations as well as in pure freeze-dried protein and thus is a thermodynamic phenomenon (see also Thiewes and Steeneken [74]). Once the thermal history of a sample is erased by heating above T_g, this pre-T_g event disappears. The remarkable fact that the samples with missing pre-T_g events are often from quench-cooled melts and not from freeze-drying processes emphasizes the value of using calorimetric matrix investigations of lyophilizates. It is possible to distinguish between different production methods of the sample

by a single measurement and such observations make clear how strongly the process influences the sample properties.

If there is no interest in investigating the thermal history of a sample and only the T_g temperature is needed, it would be recommended to perform two heating cycles of the product with a T_g evaluation of the second heating cycle (Figure I.2a, second heating cycle). The potentially interfering influences of the matrix effects such as the pre-T_g exotherm throughout the thermal history of the sample would then be eliminated. This can clearly be seen in Figure I.2a. Even the enthalpy recovery (ΔH_r) could be removed if the sample is held at a temperature above T_g for a longer time, with subsequent rapid quench cooling. For this, a cooling rate of 20 K/min or higher is suggested [61]. With this, a quasi-fresh glass is produced in situ that is "free of any thermal history". However, it has to be ensured that no irreversible changes such as crystallization or decomposition happen when the sample is heated above T_g.

An even better way to capture all the thermal events of a sample would be DSC in the modulated mode (mDSC) [75,76]. With this method, the heat signals can be separated in reversing (e.g., T_g) and non-reversing signals (e.g., melting temperature, crystallization, ΔH_r, pre-T_g event). Further explanation of the methology can be found, e.g., in [77,78]. As seen in Figure I.2b, with one measurement, all described thermal events can be easily found and, in contrast to the linear mode, even superimposed events can be distinguished.

Determination of relaxation times with DSC, an indirect method. Figure I.1a shows, aside from crystallization and melting, practically all DSC events of an amorphous pharmaceutical sample. During an α-relaxation process, the relaxation energy is released, which is considered a certain part of the amorphous sample compared to the thermodynamic equilibrated state. To determine α-relaxation times with this DSC signal, an assumption has to be made. The relaxation energy itself, the value of interest (Figure I.1a, pathway (I)), is equal to the enthalpy recovery at T_g (Figure I.1a, pathway (II)). This enthalpy recovery corresponds to the red area in Figure I.1a and the red marked peak in Figure I.1b, dH_r. To point out the consequences for the practical (quite laborious) measurement: to obtain the complete relaxation curve at the temperature of interest (T), several DSC pans of the formulation that should be investigated have to be prepared. Afterwards, each pan must be stored at the same temperature (T) for a different amount of time (t) and then heated above the glass transition temperature. The value of $\Delta H_r(t)$ can be estimated in this way and the value should increase with increasing storage time (t) of the sample. At least one pan is needed for each point of $\Delta H_r(t)$. This enthalpy recovery energy

at time (t) can then be used to calculate the corresponding point in the relaxation curve. The theoretical considerations are described in the following.

Regularly, α-relaxations in pharmaceutical glasses follow a non-exponential decay. This arrives from independently relaxing substates of different size and distribution [43]. These substates can be imagined as different locations in the sample with individual energy excess. They might be compared (not connected) with the distribution of single compounds in a mixture. Mathematically, the overall relaxation process of a sample as a whole can be described best with the non-exponential decay function suggested by Kohlrausch–Williams–Watt (KWW), also called the stretched exponential function [48,79–81].

$$\phi_{\mathrm{KWW}}(\mathrm{t},\mathrm{T}) = \exp\left[\left(-\frac{\mathrm{t}}{\tau(\mathrm{T})}\right)^{\beta}\right] \tag{I.1}$$

In approximation, τ can be imagined as the relaxation time of each single relaxation step (in hours) and β as a distribution of the relaxation states [22,23,82]. β can only have values between 0 and 1, which should be used as limiting borders for the non-linear curve fitting [17,22,23]. The closer the values of β to 1, the more homogeneous is the distribution of relaxation states [53]. This means that the described substates of the whole sample possess a quite similar energy excess. Due to the fact that the KWW equation is an empirical equation, other interpretations are possible [23]. To obtain the single data points of the KWW equation, the obtained $\Delta H_r(t)$ as described above has to be converted by the following formula.

$$\phi_{\mathrm{KWW}}(\mathrm{t},\mathrm{T}) = 1 - \frac{\Delta \mathrm{H_r(t)}}{\Delta \mathrm{H_r}(\infty)} \tag{I.2}$$

In this equation, $\Delta H_r(t)$ was already explained in Figure I.2a (red area) and $\Delta H_r(\infty)$ is the infinite relaxation. The latter is the theoretically possible maximum enthalpy recovery at infinite time [17]. This maximum enthalpy recovery could be represented by one of the DSC pans described above that age over several years. They have been aged for so long (infinite) that the energy recovery will not increase anymore, even with a longer aging time (t). Because this would not work in practical experiments, Formula (3) is used to determine the value of $\Delta H_r(\infty)$.

$$\Delta \mathrm{H_r}(\infty) = \left(\mathrm{T_g} - \mathrm{T}\right) \times \Delta \mathrm{c_p} \tag{I.3}$$

T is the temperature of interest for which we wish to determine the relaxation times. T_g and Δc_p are the glass transition temperature and the heat capacity change at the glass transition temperature, respectively. More simply, the idea behind Formula (3) is that, at temperatures above T_g, the thermodynamics of our sample correspond to a supercooled liquid. As already described, the T_g is the point during cooling where a supercooled liquid falls out of equilibrium

and forms a glass. Thus, reversing this step, heating above T_g brings the formulation back to thermodynamic equilibrium. As a result, all energy excess is released at T_g and is measurable as Δc_p at this point. Thus, Δc_p at T_g (Figure I.2a blue description) makes it possible to determine the maximum energy release that is possible during the storage time even below T_g at a certain temperature. As seen in Figure I.1a, the discrepancy between the equilibrated state (dotted line) and the glass increases with growing distance to T_g. Therefore, Formula (3) simplifies the temperature dependence in Δc_p and is considered state of the art for the determination of $\Delta H_r(\infty)$ [23,83].

To summarize the analytical process, ΔH_r values are measured for different times (t) at the temperature of interest (T) and then converted into data points for the relaxation curve using Formula (2). The relaxation curve itself can then be drawn and fitted with Formula (1) to obtain the relaxation time constants τ and β.

For a more detailed understanding of how the formulas are derived mathematically, the following literature is referred to [17,22,23,43,53,84]. Formula (4) condenses the verbalized process into a concluding mathematical relation.

$$\exp\left[\left(-\frac{\mathrm{t}}{\tau(\mathrm{T})}\right)^{\beta}\right] = \phi_{\mathrm{KWW}}(\mathrm{t},\mathrm{T}) = 1 - \frac{\Delta \mathrm{H_r(t)}}{\Delta \mathrm{H_r}(\infty)} \tag{I.4}$$

To clarify, with this procedure, the relaxation times are measured indirectly. This involves interrupting the relaxation process at a time (t) and measuring to what extent the sample is already relaxed compared to its maximum relaxation ($\Delta H_r(\infty)$). This approach neither shows the real rate of the relaxation process (what happens in between the obtained data points) nor measures the relaxation with certainty due to possible side reactions in the DSC measurements that increase or decrease ΔH_r. Due to these artificial side reactions, ΔH_r, and thus the relaxation energy, are wrongly determined to be higher or lower than their actual value.

With the described procedure, the investigation of relaxation time constants τ and β with DSC applying the KWW function corresponds to a kinetic model. It uses ΔH_r as a function of aging time and thus assumes that the relaxation time τ of a sample is independent of the measurement time (t) [43]. However, the relaxation time τ is actually not a constant and will increase during the aging time [43]. This can be explained quite logically because, over time (t), the formulation approaches its equilibrated state and the energy gradient between the energy excess and the equilibrated state minimizes. Thus, the relaxation process decelerates and the relaxation times rise. In scientific terms, the fictional temperature T_f decreases during storage below T_g [85].

Nevertheless, practically, this method works well, although a few theoretical simplifications have to be made. The determination of relaxation times could be improved by a direct measurement of the relaxation rate, which is not possible with DSC but with IMC, which is explained in the next section.

I.3.3 Isothermal Microcalorimetry (IMC), Direct Measurement of Relaxation

The difficulty in the direct measurement of α-relaxations is the long-time scale of the reaction, which can be up to several months, and also the non-ergodic behavior of the system [16,47]. However, as mentioned before, α-relaxations are dependent on more factors than simply the storage temperature and T_g and thus should be measured directly [47]. To make this possible, a very sensitive instrument with a high resolution and baseline stability is needed, which a DSC cannot provide. An isothermal microcalorimeter is capable of providing these features as it was originally developed to investigate microbiological reactions with very low and latent heat [86,87]. In principle, this instrument works similarly to a DSC. The sample is transferred to a measurement ampoule, which is then, together with a reference ampoule, inserted at the equilibration position of the instrument (Figure I.3). This position is needed to bring the sample to the measurement temperature. Due to the high sensitivity of the instrument, direct insertion into the measuring cup would lead to a signal overshoot connected to disturbing noise. Thus, the sample is held at an elevated position for 10–60 min before it is lowered into the measuring position.

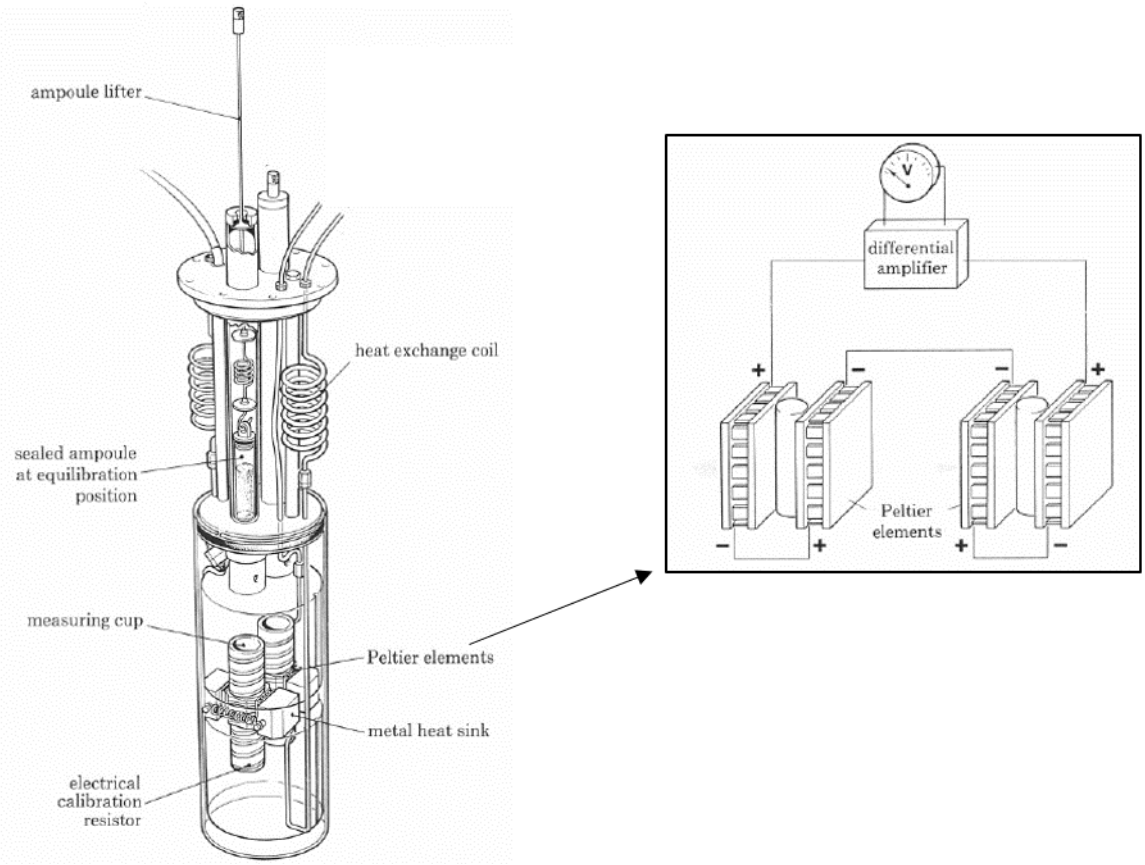

Figure I.3 Measurement cylinder of the isothermal microcalorimeter. The small picture shows a magnified view of the Peltier elements. With courtesy from TA Instruments [88].

The measuring cups are connected with Peltier elements that measure the differential heat signal between the measurement and reference ampoule. In contrast to a DSC, the IMC only takes isothermal measurements at one defined temperature, but the stability of this temperature is much higher than using a DSC in an isothermal mode. This is guaranteed with a large heat sink—in practice, a 25 L water (or oil) bath that controls the temperature within 0.0001 K [86,88]. Thus, the general noise of an IMC can be reduced to ± 10 nW in the short term and to a baseline stability to $\pm 40 \frac{nW}{24\ h}$. As demonstrated in Figure I.4, an isothermal measurement at 25 °C results in a normalized maximum heat signal of approximately 75 $\frac{\mu W}{g}$ for the objective to measure relaxations in freeze-dried products. With a sample weight of around 300 mg, this means an absolute signal of 22.5 $\frac{\mu W}{g}$. A DSC with a baseline flatness of ± 100 µW would not be able to separate such a relaxation signal from noise [87].

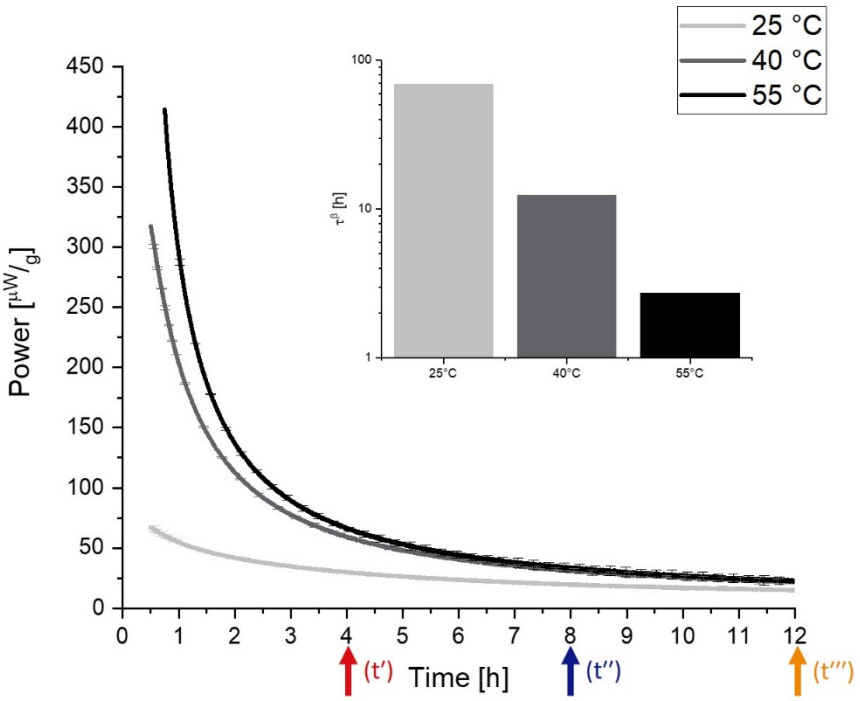

Figure I.4 Relaxation curves of the same trehalose-based formulation as in Figure I.2 obtained by isothermal microcalorimetry at different measurement temperatures. The small diagram represents the respective calculated τ^{β} values. The markers (t′)–(t‴) represent the different relaxation states of the formulation compared to Figure I.1a as a fictive example.

Thus, IMC is able to measure the rate of a relaxation $\left(\frac{\Delta H_r(t)}{\Delta t}\right)$ reaction directly during the tempering process, in contrast to the method with DSC [17]. For this reason, the KWW function in Formula (1) has to be differentiated to bring the power output of the IMC measurement in connection with a relaxation enthalpy (mathematically, power is the derivative of energy).

$$\mathrm{P} = 277.8 \times \Delta \mathrm{H_r}(\infty) \times \frac{\beta}{\tau} \times \left(\frac{\mathrm{t}}{\tau}\right)^{\beta-1} \times \exp\left[-\left(\frac{\mathrm{t}}{\tau}\right)^{\beta}\right] \qquad \text{(I.5)}$$

Formula (5) above presents the differentiation of the KWW function with the number 277.8 being a result of conversion of units and P the normalized power in $\frac{\mu W}{g}$ [17]. This formula has to be improved to avoid errors in the evaluation near $t = 0$ due to the fact that the power P approaches infinity when time approaches zero [17]. For this reason, the formula postulated by Peyron et al. was adopted for the evaluation of IMC data by Liu et al. [17,89].

$$\mathrm{P} = 277.8 \times \frac{\Delta H_r(\infty)}{\tau_0} \times \left(1 + \frac{\beta t}{\tau_1}\right) \times \left(1 + \frac{t}{\tau_1}\right)^{\beta-2} \times exp\left[-\left(\frac{t}{\tau_0}\right) \times \left(1 + \frac{t}{\tau_1}\right)^{\beta-1}\right] \qquad \text{(I.6)}$$

Hence, Formula (6), also called the modified stretch exponential function (MSE), is used to interpret the relaxation data obtained by IMC. With the correction, the time derivative remains

finite near zero and Formula (6) reduces to Formula (1), the KWW equation, at long time scales [17]. To obtain a summarized τ (τ_{MSE}) out of τ_0 and τ_1, as is natively given for the KWW equation (τ_{KWW}), the following formula is used [17].

$$\tau_{\mathrm{MSE}} = \tau_0^{\frac{1}{\beta}} \times \tau_1^{\frac{\beta-1}{\beta}} \tag{I.7}$$

Figure I.4 shows the curves that are measured by IMC at different temperatures and the obtained respective τ^β values. In contrast to the DSC method, according to the KWW function, which measures the relaxation times indirectly, the rate of reaction ("the speed of relaxation") is directly measured by IMC. This leads to manifold advantages of IMC measurement—for instance, increased resolution and exact determination of the α-relaxation times without side reactions.

I.3.4 Comparison of DSC and IMC for α-Relaxation Analysis

As the concept of α-relaxations has now been introduced, a few more terms need to be clarified, to prevent confusion. There are different definitions in the literature for "sample storage below T_g", which would, in the case of an IMC measurement, also correspond to the measurement temperature. The terms are "annealing", "aging", and "tempering". Throughout this review, the term "tempering" is used as it does not interfere with other process steps in freeze-drying. Furthermore, in practical usage and the literature, the τ^β values are almost always given instead of the single parameters τ and β because, in this way, more robust results are generated [17,53]. The possibility to investigate relaxation times with an isothermal microcalorimeter instead of using differential scanning calorimetry was first introduced by Liu et al. [17]. Since then, a few attempts have been made to compare the methods. In the following part, the measurement and evaluation methods are compared. To allow such a comparison, the values determined with DSC and the KWW function are called τ_{KWW}^β, the results of IMC with the MSE function τ_{MSE}^β.

I.3.4.1 The behavior of τ and β

Theoretically, the relaxation determination with DSC and IMC should provide the same results, but both parameters, τ and β, depend strongly on their thermal history, which includes the temperature, composition, pressure, and also the measurement method itself. It must not be forgotten that although the enthalpy relaxation (τ_{MSE}^β) is considered similar to the enthalpy recovery (τ_{KWW}^β), this must not always be the case [23]. Thus, practically, the estimated value of τ^β can be different between both methods. Hancock et al. investigated the relaxations of quench-cooled amorphous systems consisting of polyvinylpyrrolidone (PVP), indomethacin, or

sucrose [48]. The β-values of these single-component systems correlated with the molecule size using τ_{KWW}^{β}. Small molecules had generally higher β-values [48]. This means that small-molecule systems possess a more homogenous distribution of relaxation states compared to larger polymers. Taking into account that calorimetrically investigated α-relaxations depend on the movements of whole molecules, the observation of Hancock et al. is reasonable because small molecules are less sterically impeded than larger ones. Thus, the chance is higher that small molecules such as sucrose can quickly "move" to the same equilibrated energy state, relaxing homogenously from there on, in contrast to polymers such as PVP. Van den Mooter et al. further observed a decrease in the β-values using τ_{KWW}^{β} when the tempering temperature was lowered [90]. These findings were obtained during their studies on pure quench-cooled API triazolam, temazepam, and diazepam [90]. Moreover, this can be explained with molecular movement. At lower temperatures, the molecular movement of the small molecules is decreased, resulting in a prolonged time until the molecules approach an equal relaxation state, and, thus, there is a wide distribution of these relaxation substates. Bhugra et al. stated that the value of β, independent of whether it is determined as β_{KWW} or β_{MSE}, is not coupled to temperature [53]. They support their data with correlating relaxation measurements below and above T_g [53]. For this purpose, single-component systems of amorphous disaccharides were utilized. The obtained β-values remained similar in the applied temperature range [53]. This is the only publication that has reported such a case, which is further in contrast to the theoretical background of the α-relaxation theory. Recent studies investigated relaxation processes also by molecular modeling and tried to fix one of the parameters (τ or β) for more robust results [79]. Wilkinson et al. proposed a model where the temperature dependence of the stretch exponent β is taken into account [79]. Their results indicate an overall temperature dependency of β. It can be considered that near and around T_g, the temperature dependency of β is so small that the impact disappears in the noise of the measurement.

In general, it can be noted that the β-values themselves, as well as the combined τ^{β} results obtained by the MSE equation, are smaller than those measured with the KWW function [17,53]. This could be a numerical error, but it could be that the IMC method captures also some other modes of relaxation that the DSC method is not able to detect [17]. Liu et al. showed that, sometimes, the τ_{KWW}^{β} gives unphysical τ and β values whereas the τ_{MSE}^{β} gives reasonable results [17]. These measurements were performed with freeze-dried or quench-cooled pure sucrose and trehalose formulations [17]. At the moment, there is no valid explanation for this, but it is assumed that the τ_{KWW}^{β} tends to fail when the corresponding change in power during

the IMC of the sample is very fast in the beginning [17]. As mentioned, the generation of one data point for the determination of τ_{KWW}^{β} needs much more effort than measuring τ_{MSE}^{β}. The resolution in τ_{KWW}^{β} is strongly reduced with the consequence that, particularly at short time scales, where the relaxation occurs rapidly and strongly, the data points are not sufficient to calculate τ_{KWW}^{β} correctly and reproducibly. In the direct IMC measurement, a data point is created, e.g., every 2 s, whereas, in the DSC measurement, the gaps between the single points often are around 1800 s. A further advantage of determining τ_{MSE}^{β} is that the calculation is based on three fitting parameters (τ_0, τ_1, and β) instead of only two (τ and β) for the τ_{KWW}^{β}.

It should be noted that Pikal et al. developed a method to determine relaxation times only with the width of T_g [85]. Only three publications were found that compared the $\tau_{\Delta T_g}^{\beta}$ with τ_{MSE}^{β} or τ_{KWW}^{β} [22,42,85]. Chieng et al. support the qualitative relationship between the KWW method and the "width of Tg method" (ΔT_g), although these two methods are not fully quantitatively comparable [22,85,91]. It is concluded that the $\tau_{\Delta T_g}^{\beta}$ is qualitatively operational but more precise results can be achieved with τ_{KWW}^{β}, or even better with τ_{MSE}^{β}.

I.3.4.2 General observations for samples with different thermal history

Shamblin at al. pointed out the difference between the thermal history of samples [16]. In their studies, pure substances (sorbitol, sucrose, trehalose, and indomethacin) were converted into an amorphous solid in different ways, by freeze-drying, melt-quenching, and melt-quenching with subsequent aging [16]. These systems significantly differ in their changes in heat capacity, with lyophilized systems having the highest and aged samples the lowest [16]. This means that, compared to the thermodynamic equilibrated state, which is the heat capacity above T_g, lyophilized samples also differ the most (largest Δc_p), hence having the highest energy excess among the samples. As expected, Liu et al. reported that, above T_g, the differences in heat capacity vanished and all products then had the same heat capacity [16]. To explain this, they emphasized the complex thermal history of freeze-dried samples through the stresses that affect a formulation during the process: the maximum freeze-concentrated state, followed by freezing itself and the removal of water by sublimation and evaporation [16,43]. Once again, the need for more awareness regarding thermodynamic matrix properties during the optimization of freeze-drying processes is strengthened by this point of view.

Furthermore, freeze-dried samples possess a shorter relaxation time (low value of τ^{β}). This means that such samples are less rigid and more mobile [17,23]. Moreover, it is observed that, especially in freeze-dried samples, the relaxation energy is greater than the recovery [17]. This indicates that freeze-dried samples possess another mode of energy excess, which is not recovered at T_g and thus not reversible, in addition to α-relaxation. Both aspects—the higher relaxation energy within shorter times and the faster molecular mobility—emphasize the fact that lyophilizates should be investigated more intensively regarding their τ_{MSE}^{β}. A process that leads to low energy excess combined with a long relaxation time (high τ_{MSE}^{β} value) could strongly improve the long-term stability of freeze-dried drug products.

Obviously, the measurement via IMC is superior compared to the DSC method. It is the only possibility to truly measure the rate of α-relaxations directly. More data points can be generated easily to increase the resolution and the MSE as the fit-function leads to more reliable values of τ and β. In fact, the IMC measurement requires a greater sample mass (300 mg) compared to a single DSC measurement (10 mg), but for each data point of τ_{KWW}^{β}, at least one measurement is needed. Even if the resolution of the τ_{MSE}^{β} measurement is decreased to three data points per hour in a 12 h measurement, measuring τ_{KWW}^{β} with the same resolution would need at least 36 DSC runs, thereby increasing the needed sample mass to 360 mg. However, it has to be kept in mind that a DSC measurement is needed to obtain Δc_p at T_g and the T_g itself, to calculate $\Delta H_r(\infty)$. Furthermore, a DSC instrument is available in most laboratories that deal with freeze-drying, compared to an IMC instrument, which is rare and expensive to acquire. A summary of DSC and IMC methods in the context of relaxation determination is provided in Tables I.A1 and I.A2, respectively.

It should be noted that the calorimetric methods also have their disadvantages compared to other relaxation determining analytics. Side effects such as crystallization or melting can superimpose relevant relaxation phenomena even when the DSC is used in modulated mode. Furthermore, methods such as dielectric spectroscopy are able to determine relaxation parameters above T_g [53]. In IMC measurements, a high sample mass is needed and the measurement time can take even days. The resulting relaxation data of the different methods can of course differ, but, for each purpose, a certain method is more suitable. The reason that this review is strongly focused on the calorimetric methods is that it was shown in the past that the data obtained by calorimetry can be most helpful in the pharmaceutical field.

I.4 Application of α-Relaxation Analysis

In the following, the results and conclusions from the application of α-relaxation analysis from previously published papers are reviewed and completed by our own new data.

I.4.1 Correlation of τ^{β} with Storage Stability of Active Pharmaceutical Ingredients

The idea is that, with increasing relaxation time, i.e., a high value of τ^{β}, molecular movement in the formulation is reduced. For several degradation pathways of biological entities, molecular movement is mandatory and, hence, these degradation processes should be decreased.

In 1994, Duddu et al. performed experiments to correlate the aggregation of a protein drug with α-relaxation times. For their study, lyophilized sucrose and trehalose formulations containing a chimeric monoclonal antibody in the ratio of sugar:protein 12.5:1 were utilized [92]. Although trehalose formulations have a higher T_g, the measured relaxations at 5 °C, far below Tg, were the same as in the sucrose formulations [92]. The mathematical reason for this is simple: the relaxations at different temperatures showed Arrhenius-like behavior for trehalose samples, while sucrose-based formulations possess non-Arrhenius-like kinetics. Thus, the relaxation times matched at a certain temperature, around 5 °C in this case, leading to even shorter relaxation times for trehalose below this temperature. The results thus suggest that, at storage temperatures below 5 °C, the molecular mobility in trehalose-based samples is higher and degradation processes are faster than in sucrose-based glasses. With this, surprisingly, although trehalose has the higher T_g, the better stabilizer might be sucrose at the widely used storage condition of 2–8 °C. On the basis of their results, Duddu et al. normalized the "real" storage time (t) of their aggregation study using the relaxation time (τ) and called it the reduced relaxation time, Rrt (see Formula (8)).

$$\text{Reduced relaxation time (Rrt)} = \frac{\mathrm{t}}{\tau} \tag{I.8}$$

This approach tries to define the protein aggregation in relation to the "real" experiment time and the relaxation process of the respective system. Nevertheless, for both formulations, less than 2% aggregation was predicted when the reduced relaxation time $\left(\frac{t}{\tau}\right)$ was lower than 10. This means that, with the determined relaxation time (τ_{KWW}) of 10^8 h at 5 °C for sucrose and 10^6 h for trehalose, the real storage time until 2% aggregation would occur is in the order of 10^9 h and 10^7 h (several years; see Formula (9)).

$$\text{Rrt} = \frac{\mathrm{t}}{\tau}, \text{with } \tau = 10^6 \text{ h and Rrt} = 10 \rightarrow \mathrm{t} = 10 \times 10^6 \text{ h} = 10^7 \text{h} = 1142 \text{ years} \tag{I.9}$$

Although this was a well-considered work providing first impressions on the α-relaxation times of pharmaceutical products, the results question the relevance of correlating stability with α-relaxations. It appears that the differences between sucrose and trehalose formulations are so small that they do not truly matter at storage temperatures under refrigerated conditions. Furthermore, the predictive calculation in Formula (9) was not proven by real aggregation data. The authors themselves emphasized the need to perform more comparable stability studies in this area, which was done later by, e.g., Shamblin et al., in 2006. The authors were some of the first to publish an investigation on the correlation of the stability of freeze-dried formulations with α-relaxation times [93]. They investigated different lyophilized cephalosporine and ethacrynate sodium mixtures. From their results, it becomes very clear that reactions requiring whole molecule movements (such as dimerization in ethacrynate sodium) are strongly coupled with the relaxation times [93]. This is in contrast to degradation processes, which are more or less independent of molecular movement, or only need a small functional group to move (opening of a β-lactam ring in cephalosporine mixtures) and consequently show only a weak correlation to relaxation times [93]. Shamblin et al. also found out that direct formulation-specific aspects superimpose the effect of α-relaxation. Astonishingly, cefoxitin sodium showed increased stabilization of the β-lactam ring when sucrose was added, although sucrose significantly reduced the global α-relaxation time of the formulation. This occurred due to an unexpected stabilization effect of sucrose on this certain API, which showed that excipients as such can have a much stronger impact on the stability than the relaxation time. Moreover, Wang et al. reported similar results for their studies. They investigated mixtures of five different proteins in sugar matrices with different sugar/protein ratios. With the addition of sucrose to the proteins, τ_{MSE}^{β} increased as well as the protein stability. Up to a sugar:protein ratio of 1:1, τ_{MSE}^{β} correlated perfectly well with long-term stability. However, at ratios beyond 1:1, meaning with more sucrose added, τ_{MSE}^{β} decreased, although the protein stability from this point on further increased [94]. Quite similar studies, presenting an inconsistency between formulation parameters and relaxation, can be found in Abdul-Fattah et al., Chang et al., and Shamblin et al. [21,56,93]. Therefore, it can be concluded that α-relaxation studies are not able to directly help in the selection of the best formulation composition, but more promising results can be found for investigations concerning the connection of process parameters and relaxation.

Luthra et al. were able to detect a correlation of α-relaxation with long-term stability (rpHPLC) in mixtures of aspartam/sucrose and aspartame/trehalose [95]. In their study, subsequent to the lyophilization process, tempering was performed and the samples were kept at different

temperatures below T_g for a certain amount of time. The authors describe that tempered formulations indeed have a higher initial protein degradation compared to freshly prepared samples; however, this initial damage is (over-)compensated during storage. With initial tempering, the degradation kinetics were dramatically slowed down. Hence, tempering leads to higher sample purity in the long term despite the disadvantages at t(0) of this specially treated specimen [95]. The idea behind tempering is that, at elevated temperatures below T_g (e.g., 60 °C for trehalose formulations), more energy excess of the sample is released in a short period of time compared to the subsequent storage conditions (e.g., 4–25 °C for pharmaceutical formulations). With this, α-relaxation time τ^{β} increases throughout the heating process. Hence, the molecular movement and, thus, the degradation process are slowed down. As high temperatures typically accelerate chemical degradation, the rule for tempering must be as high as necessary but as low as possible.

Abdul-Fattah et al. showed results that also emphasize the theory of tempering with moxalactam/mannitol mixtures. As a stability surrogate in their experiments, the decarboxylation rate of freeze-dried moxalactam was utilized. The results of decarboxylation and relaxation correlated over a wide range of tempering times and temperatures [31]. This means that with the increasing time and temperature of the tempering process, the decarboxylation rate was decreased. These observations suggest that if the degrading factor strongly depends on molecular motions, α-relaxations can be used as a stability predicting factor and the stability of the formulation can be increased through this tempering practice. In the most simple fashion, tempering could be conducted by the adaption of the secondary drying time and temperature. In a later study, Abdul-Fattah et al. considered this further and included vacuum-dried formulations in their studies [96]. Compared with freeze-drying and spray-drying, the vacuum-dried formulations were exposed to high temperatures at a longer time range. As expected, the relaxation recovery at T_g of vacuum-dried samples was the highest, because they relaxed the most, as was the stability of the formulation [96].

The disadvantage with tempering in all of these studies was the initial damage of the formulation. The question is whether using more moderate tempering protocols would allow an optimum to be found. Tempering at lower temperatures, perhaps with a longer tempering time, could lead to sufficient structural α-relaxations without affecting the other physical properties of the formulation [70]. Several studies conclude that α-relaxations might be negligible at 50 K below T_g (using DSC methods) [48,90]. Thus, the optimum tempering temperature must be in the range of T_g to $T_g - 50$. However, the fact that different formulations result in relaxation

curves with different slopes at the same $T_g - T$ temperature indicates that different materials react individually, with different responses to temperature variation [48]. Borde et al. suggested that enthalpy relaxation is an interaction of available thermal energy on the one side and the driving force (energetic distance toward equilibrium) on the other side [97]. At T_g, the relaxation times τ_{KWW} should be the same within different formulations, which could be proven in some studies [48]. This idea arises from the thermodynamic consideration that, at T_g, the glass reaches the supercooled, thermodynamically equilibrated, liquid state. However, Luthra et al., as well as Chung et al., found in their DSC studies that there is a maximum in relaxation not at $T = T_g$ but at a temperature of $T_g - T = 20$, which is, at first glimpse, contrary to the consideration stated above. They explained the phenomenon of the mobility maximum as follows [43,84]. If the tempering happens far away from T_g ($T_g - T_a \geq 20$), the process is under kinetic control. This means that the molecular mobility is so slow that, during the aging experiment, only a small enthalpy loss happens. When approaching T_g ($T_g - T_a < 20$), the process is under thermodynamic control. At this point, less enthalpy excess of the glass compared to the equilibrated state remains within the sample. Thus, only limited energy excess is possible and the relaxation time decreases as the tempering temperature increases [43,84]. We developed Figure I.5 to summarize the important consideration of a tempering optimum. It can be seen (as well as in Figure I.1a) that, at temperatures below T_g, the enthalpy excess of the glass increases with increasing distance towards T_g compared to the thermodynamic equilibrated state. Thus, the lower the temperature is, the more energy excess is stored in the samples and the longer are the relaxation processes. When the kinetic border crosses the thermodynamic limit line, it is possible to "fully" relax a sample. From this point on, "always 100%" of the energy excess is released. Even closer to T_g, the measured enthalpy recovery decreases, because thermodynamically less energy excess is stored within the sample. This results again in a decrease in τ_{KWW}^{β}.

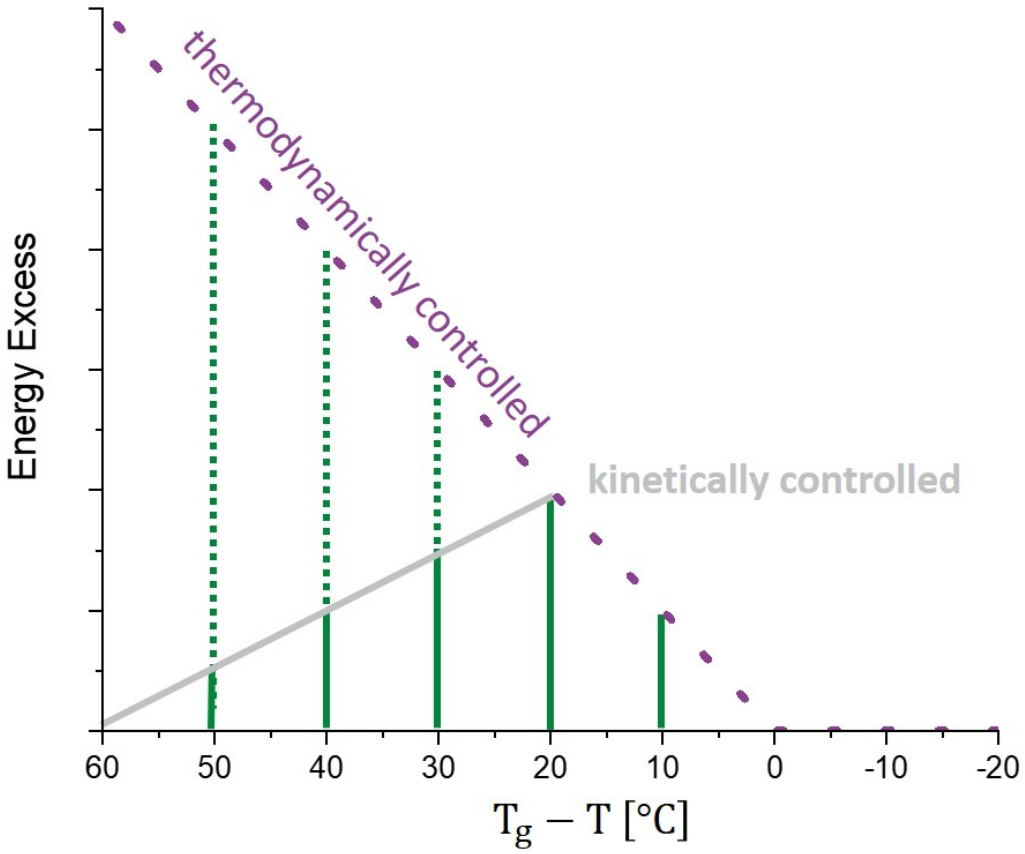

Figure I.5 Model graph to explain the concept of an optimum tempering temperature. The purple line shows the theoretical maximum of energy excess that a sample possesses at a temperature of $T_g - T$ calculated with Formula (3). The grey line represents the kinetic limitation at the time scale of the experiment at the same temperature of $T_g - T$. The green solid lines show the measured relaxation that occurs at the time scale of the experiment, compared with the theoretical maximum, visualized by the green dotted line.

Based on the existing literature, experiments were performed in our group to obtain more insights about the kinetic and thermodynamic factors of the tempering process and the relaxation behavior afterwards. As the former publications mostly use the τ_{KWW}^{β} method to determine the optimum tempering temperature, we decided to re-evaluate the considerations with the τ_{MSE}^{β} method. Directly measuring relaxation times with higher sensitivity should enable us to see whether $T_g - T = 20$ °C is also the optimum tempering temperature for τ_{MSE}^{β} and if the relaxation is in fact fully hindered at $T_g - T > 50\,°C$. Further, it was necessary to investigate whether the kinetic boarder shifts and approaches the thermodynamic limit at higher values of $T_g - T$ with longer time scales of the measurement, or whether, at this energy barrier, at a certain point, relaxation no longer occurs (meaning that the relaxation process slows down to a time scale of several years) although an energy excess is theoretically present. This would

be relevant in the context of industrial processes where the cold chain for lyophilizates is interrupted for many days at room temperature, i.e., up to 25 °C.

Two placebo mixtures containing trehalose and sucrose were studied. Two freeze-drying cycles with different freezing steps were performed: one with random ice nucleation (RN) and one with controlled ice nucleation (CN). The formulations and the processes were used to cover a broad range of different T_g values between 50 °C and 100 °C. In this study, measurement temperatures of 25 °C, 40 °C, and 55 °C were used with the IMC. Thus, measurements far from and near T_g were possible. A tempering time of 7 days was used. Details of the composition and production of the samples can be found in Section 6, the Materials and Methods. Figure I.6 illustrates the measurement procedure.

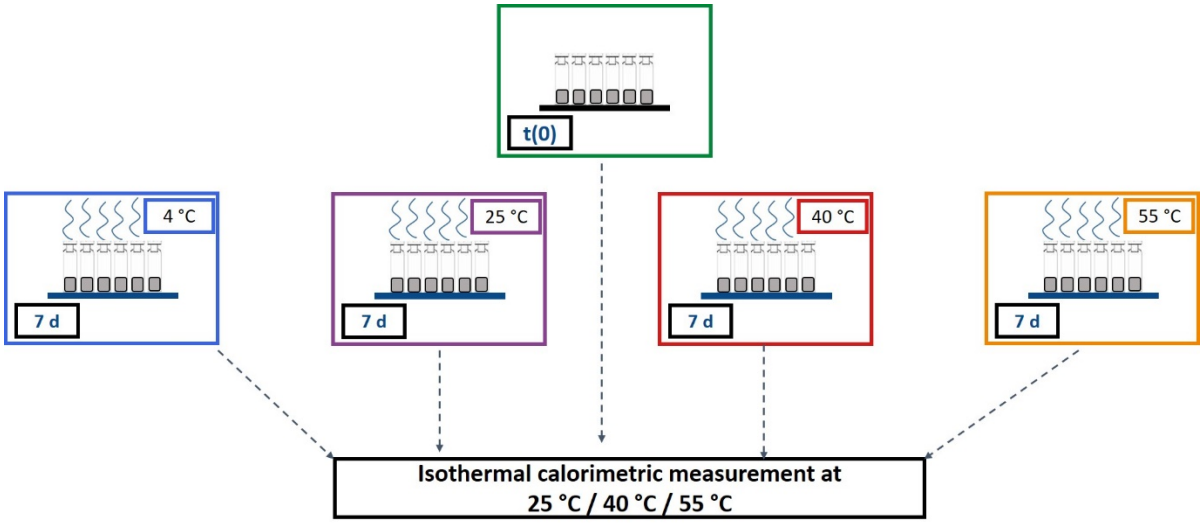

Figure I.6 Overview on the tempering time and temperatures as well as the measurement temperatures in IMC that were used in this study.

When the obtained results are discussed, the following has to be kept in mind. The "t(0) samples" were measured directly after the freeze-drying process; thus, the concept here is that the subsequent tempering process for the temperatures 25 °C, 40 °C, and 55 °C could be tracked in real time. IMC always measures the relaxation process while it happens, so the measurement temperature equals the tempering/storage temperature of a sample. For the samples that were tempered for 7 days at 4 °C, 25 °C, 40 °C, and 55 °C before the measurement, the tempering process belongs to the thermal history/preparation process of the sample. It was investigated how strongly the sample still relaxed after different tempering protocols. The measuring temperatures of the instruments were chosen to cover typical conditions for storage and accelerated stability studies (25 °C, 40 °C) as well as a high temperature to approach T_g (55 °C). Much higher or lower temperatures of the instruments were not possible due to

technical limitations. Figures I.7–I.9 display the resulting curves as well as the calculated τ_{MSE}^{β} values.

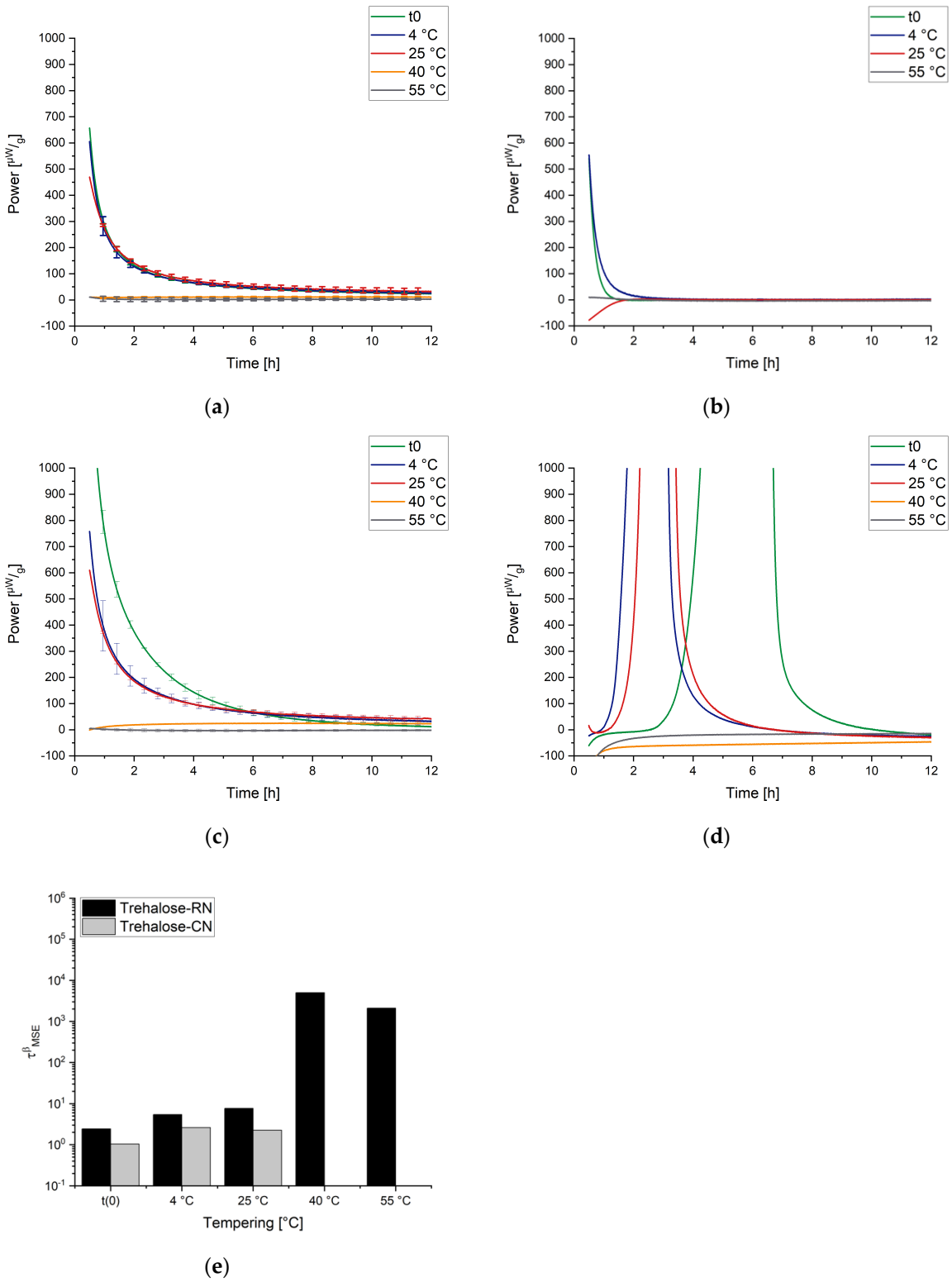

Figure I.7 Isothermal measurements performed at 55 °C. Freshly prepared sample (green), 4 °C tempered sample (blue), 25 °C tempered sample (red), 40 °C tempered sample (orange), 55 °C tempered sample (grey). (**a**) Trehalose-RN, (**b**) Sucrose-RN, (**c**) Trehalose-CN, (**d**) Sucrose-CN, (**e**) calculated values of $\tau^{\beta}[h]$. Missing bars indicate unsuccessful curve fitting. Error bars in sucrose samples not shown for better clarity.

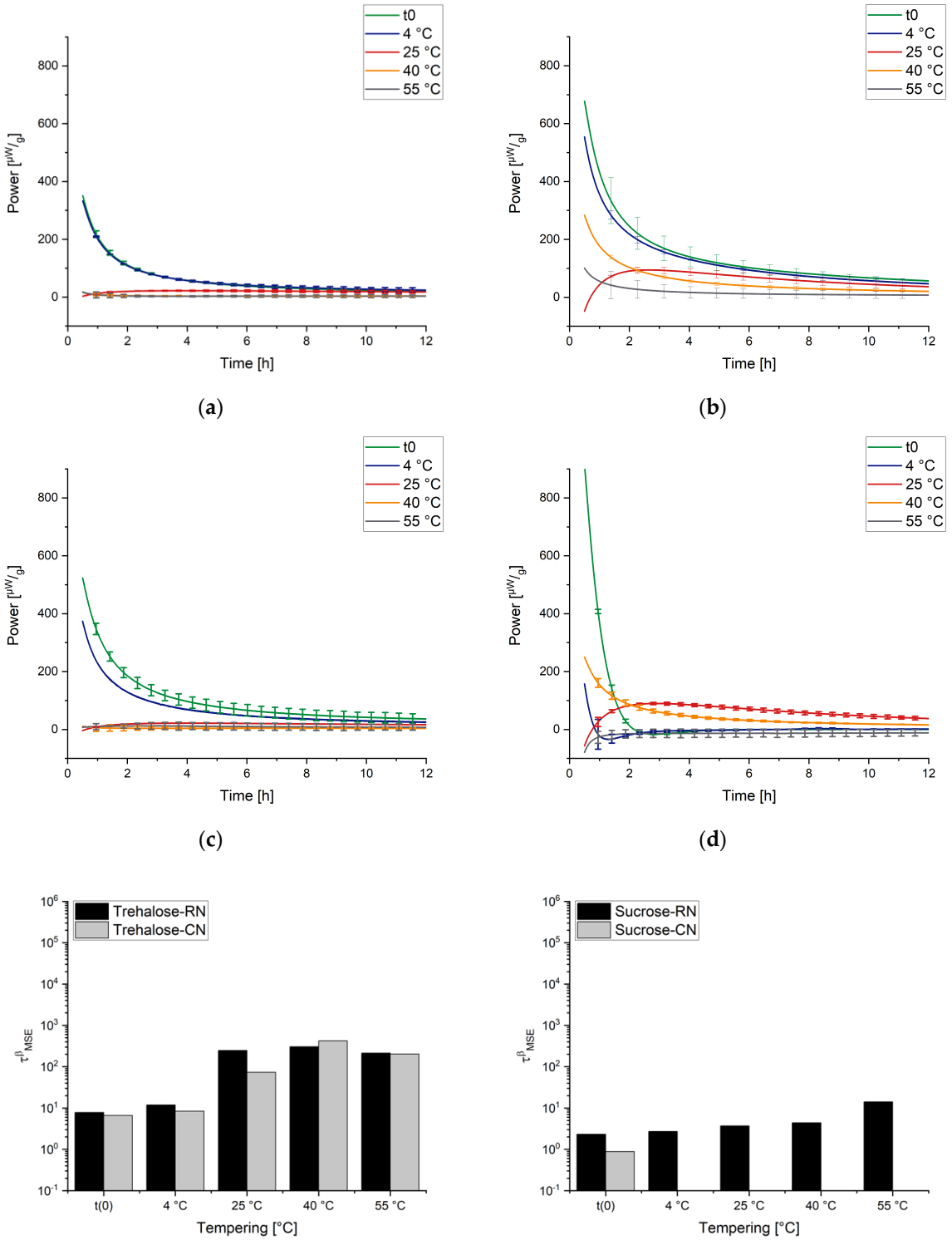

Figure I.8 Isothermal measurements performed at 40 °C. Freshly prepared sample (green), 4 °C tempered sample (blue), 25 °C tempered sample (red), 40 °C tempered sample (orange), 55 °C tempered sample (grey). (**a**) Trehalose-RN, (**b**) Sucrose-RN, (**c**) Trehalose-CN, (**d**) Sucrose-CN, (**e**) and (**f**) calculated values of $\tau^{\beta}[h]$. Missing bars indicate unsuccessful curve fitting.

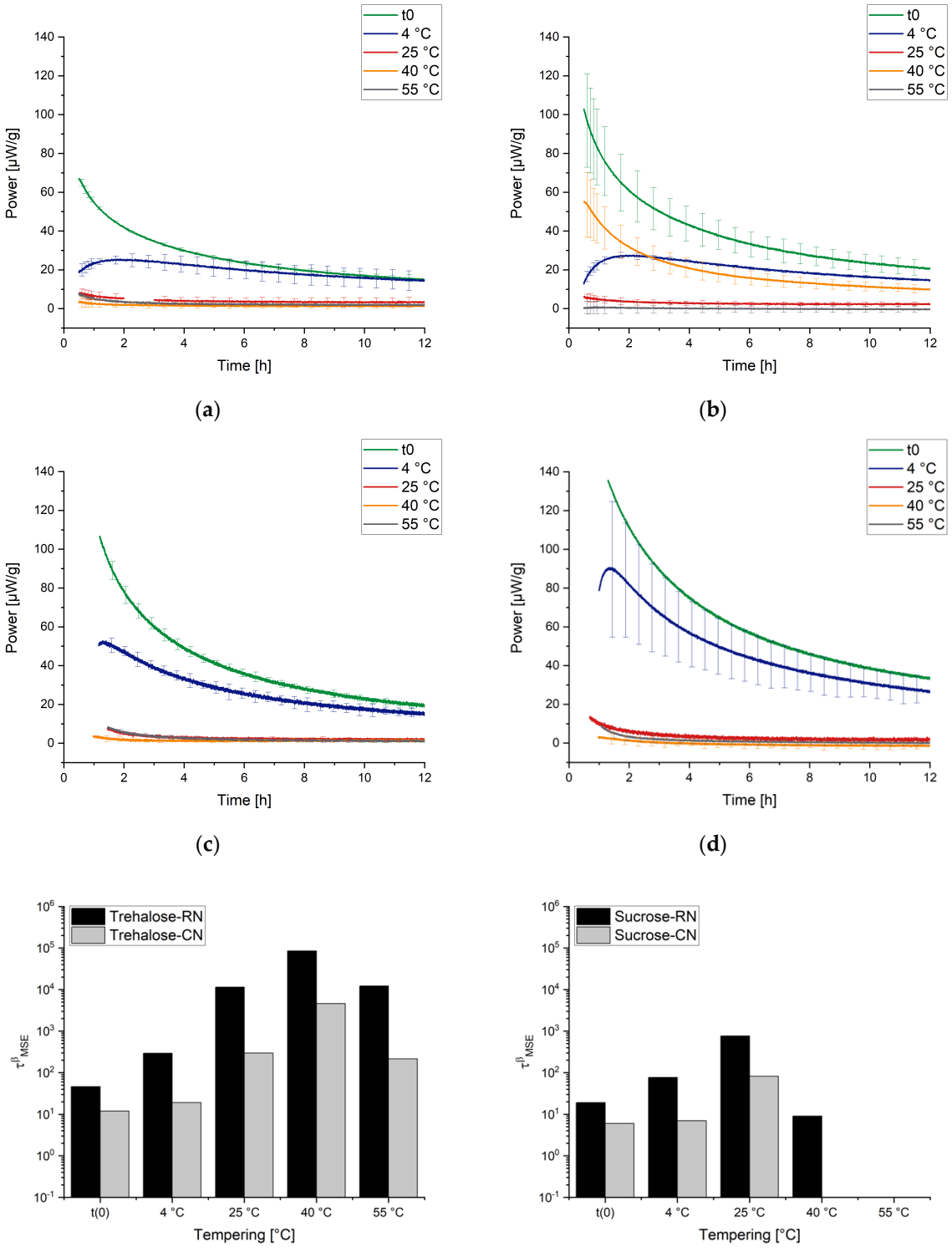

Figure I.9. Isothermal measurements performed at 25 °C. Freshly prepared sample (green), 4 °C tempered sample (blue), 25 °C tempered sample (red), 40 °C tempered sample (orange), 55 °C tempered sample (grey). (**a**) Trehalose-RN, (**b**) Sucrose-RN, (**c**) Trehalose-CN, (d) Sucrose-CN, (**e**) and (**f**) calculated values of $\tau^{\beta}[h]$. Missing bars indicate unsuccessful curve fitting.

In the 55 °C measurement (Figure I.7a), the result for the different tempering conditions of trehalose-based samples generated by a random ice nucleation process (Trehalose-RN) can be

separated into two clusters, one with t(0), 4 °C, and 25 °C and the second with 40 °C and 55 °C. The cluster of t(0)-25 °C suggests that higher tempering process temperatures are needed to relax the formulation adequately. Moreover, the values of τ_{MSE}^{β} are low and all on a similar level (2–8 h), compared to τ_{MSE}^{β} for the 40 °C and 55 °C tempered samples of 5008 h and 2097 h, respectively. Consequently, 40 °C tempering over a period of 7 days seems to be the best method to increase the relaxation times in this formulation. In contrast to the findings of Luthra and Chung [41,84], however, 40 °C is not equal to $T_g - T = 20\,°C$ but rather to $T_g - T = 60\,°C$. This means that the proposed model in Figure I.5 is not correct or that the intersection point of the kinetic border and the thermodynamic energy excess of trehalose formulations is not at $T_g - T = 20\,°C$. To clarify this issue, the fitted t(0) curves of Trehalose-RN and sucrose-based samples generated by the random ice nucleation process (Sucrose-RN) measured at 25 °C, 40 °C, and 55 °C were plotted in the time range of 0–12 h and then integrated. The resulting area under the curve (AUC) was converted to the unit $\frac{J}{g}$. Thus, the model in Figure I.5 could be applied to the samples Trehalose-RN and Sucrose-RN. The results are displayed in Figure I.10. In fact, the theoretical considerations and the model of Figure I.5 seem to work very well. The AUC of Trehalose-RN increases continuously with increased temperature. With 55 °C as the highest measured temperature and a T_g of 100 °C, all observed relaxation times were kinetically controlled. In contrast, the AUC of Sucrose-RN first increased and then decreased again at 55 °C because the intersection point of the kinetic and thermodynamic line was crossed.

The resulting curves of the trehalose-based samples generated by controlled ice nucleation (Trehalose-CN) show three clusters at the measurement temperature of 55 °C, instead of two as with the Trehalose-RN curves. Thus, it seems that 4 °C and 25 °C tempering have an impact on relaxation times compared to t(0) in Trehalose-CN samples but not in Trehalose-RN samples. Due to the different processes (RN vs. CN), both samples possess different T_g temperatures, although they have the same excipient composition. The respective T_g temperatures are 85 °C for Trehalose-CN and 100 °C for Trehalose-RN. These findings clearly show that the ratio between T_g and the measurement temperature (equals storage temperature) is very important. Concerning relaxation times, this could mean that the tempering temperature is a complex issue that cannot be fixed at a specific value such as $T_g - T = 20\,K$ and the planned storage temperature always has to be taken into account. For example, the α-relaxation times of Trehalose-RN tempered at 25 °C and 55 °C are quite similar when measured at 40 °C (Figure I.8a,e) as well as when measured at 25 °C (Figure I.9a,e). After tempering for 1 week at 25 °C, relaxation is the same as for tempering at 55 °C. Consequently, although kinetically

limited (see Figure I.5), tempering for longer times at a lower temperature can compensate for high tempering temperatures. With this consideration, tempering at 55 °C would be unnecessarily high when the samples need to be stored at 25 °C or 40 °C. In the past, tempering temperatures of 50 °C or higher were utilized [31,95]. However, the present results suggest that a tempering protocol of $Storage\ temperature + xK$ is sufficient and would offer better long-term stability with less protein damage in the beginning.

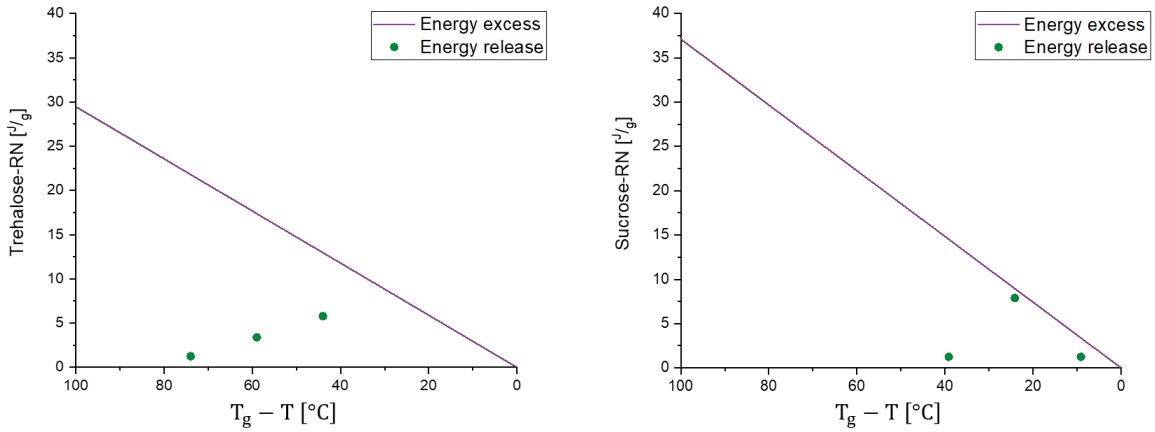

Figure I.10 Model of Figure I.5 applied to the samples Trehalose-RN (a) and Sucrose-RN (b). The purple rectangles show the theoretical maximum of energy excess that the respective sample possesses at a temperature of $T_g - T$ calculated with Formula (3). The green dots show the measured relaxation that occurs in the time scale of the experiment.

With a lower measurement temperature, the absolute power signals decreased in all samples. It is noticeable that some curves show a maximum in the power signal instead of continuously approaching the x-axis. This phenomenon is called the "tempering shoulder" in the following. This tempering shoulder occurs independently of the formulation in the curves of samples that were tempered around 15–20 K below the IMC measurement temperature (e.g., in 4 °C tempered samples measured at 25 °C, 25 °C measured samples at 40 °C, and 40 °C tempered samples at 55 °C). This observation was also made by Abdul-Fattah for foam-dried formulations and they excluded this part of the curve from the calculation of τ_{MSE}^{β} [56]. Kawakami and Pikal stated enthalpy recovery as origin of this phenomenon [23]. They reported that the tempering shoulder cannot be easily explained by classical relaxation theory but could arise from several substates of a formulation. Whereas most parts of such a sample recover energy, there are still some small distributed substates that relax. In the beginning, thus, it is a combined peak of endothermal and exothermal events, with exothermal ones remaining in the end [23]. However, although this phenomenon is not fully explained yet, the samples that showed this tempering shoulder were also the samples with the best API stability according to

Abdul-Fattah et al. [56]. The present results suggest that the obtained tempering shoulder is a phenomenon that is observable at a specific ratio of tempering and measuring temperature.

Moreover, some of the Sucrose-CN samples showed a small endothermal consumption valley after the relaxation decay. At the moment, it cannot be verified where this thermal event arises from. One idea could be that, through the controlled nucleation process, the crystallization tendency is significantly higher than in other formulations, because the residual moisture is the highest and the T_g the lowest among the samples. Thus, this could be the consumption of a small amount of activation energy that a crystallization process needs without crystallization occurring in the timespan of the experiment.

Overall, within the same formulation, α-relaxations can be a suitable predictive tool for long-term stability, but the relevant degradation pathway must include reactions that depend on molecular movements. It has to be understood that the ingredients of the formulation always have a stronger impact on stability than relaxation. Thus, parameters such as τ_{MSE}^{β} are not able to improve formulation recipes but are a tool for process optimization. In the context of freeze-drying, this includes mainly the primary and secondary drying steps. The tempering of samples within a time scale of a few hours increases the long-term stability of the formulation but with slightly increased protein damage at t(0) compared to non-tempered samples. To improve the tempering procedure, experiments with IMC were conducted that showed that relaxation occurs at every temperature, even far below the $T_g - T = 50°C$ region, e.g., for samples that were tempered at 4 °C. The tempering temperature should be chosen according to the planned storage conditions. It should be good practice to temper a product at no higher than 25 °C when it is planned to be ultimately stored at 4 °C. Within a week, the kinetic limitations between samples tempered at 25 °C and 55 °C had already equalized, and with an unnecessarily high tempering temperature, more initial protein damage would occur without a significant improvement in the relaxation time.

I.4.2 Further Applications of α-Relaxation Studies

I.4.2.1 Crystallization.

The stabilization of a protein in a glassy matrix is based on the prerequisite that such an amorphous matrix is present in a sufficient quantity and does not crystallize during the relevant storage period. It is therefore highly desirable to ensure the preservation of the amorphous state and to predict how long it may take until crystallization will start. Zhou et al. found that molecular mobility can be correlated with the tendency for crystallization [98]. They investigated different small-molecule APIs and sucrose. At this point, it must be noted that the APIs were converted to the amorphous state by quench cooling, whereas sucrose was freeze-dried. Among the quench-cooled samples, mobility as well as configurational entropy correlated with crystallization tendencies [98]. To determine the crystallization tendency, DSC was utilized, applying a heating ramp up to temperatures above T_g and not an isothermal approach below T_g. It is suggested that crystallization above T_g is probably not a good marker, because above T_g, the thermal history could be erased. Surana et al. found that a longer annealing time in freeze-dried trehalose below T_g lowered the onset temperature of crystallization above T_g [99,100]. This result confirms that the origin of a glass (freeze-dried vs. quench-dried) has to be considered even for events above T_g. Surana et al. concluded from their results that, through tempering below T_g, crystallization pre-nuclei are built that have no influence on matrix mobility below T_g but accelerate crystallization above T_g [99]. These nuclei are not reversible and thus do not disappear above T_g [99]. Later, Bhugra et al. showed that the relaxation times determined above T_g with dielectric relaxation spectroscopy match the extrapolation of the relaxation times of (τ_{MSE}^{β}), determined by IMC, below T_g [53]. The study was conducted with several small-molecule APIs as model compounds. This would mean that relaxation times below T_g are able to govern or predict processes above T_g. Bhugra et al. thus experimentally showed that coupling between α-relaxation below T_g and crystallization above T_g could be plausible even without the theory of pre-nuclei. In a further study, Bhugra et al. aimed to prove this idea and investigated the onset time of the isothermal crystallization of spray-dried and freeze-dried sucrose above T_g with Formula (10) [101].

$$ln(\theta c) = \left(\frac{M}{\beta}\right) \times ln(\tau^{\beta}) + C \quad \text{(I.10)}$$

In the equation, θ_c is the induction time of crystallization; M is the coupling coefficient, and C is a constant [101]. M has to be divided by β due to mathematical reasons concerning the slope of the curve by using τ^{β} as a mobility parameter. The results showed a coupling coefficient of

around 0.5, suggesting that crystallization and molecular mobility are not simply reciprocal and more factors contribute to the crystallization behavior [101]. It could additionally be noted that crystallization onset times for freeze-dried samples are much shorter than for spray-dried samples [101]. Thermodynamic driving forces, different process durations and temperatures of spray-drying vs. freeze-drying, as well as differences in surface are discussed as reasons to explain this phenomenon [101]. A coupling between relaxation times and crystallization onset below T_g did not work properely [101]. Finally, reference is made to an excellent review by Bhugra and Pikal that deals with crystallization from the amorphous state, as well as to a review from Grzybowska et al. that focuses on relaxation analysis by dielectric techniques [102,103].

In our own set of experiments, we wished to investigate the coupling of crystallization onset with molecular mobility below T_g as this is much more relevant for the storage of pharmaceutical products than the crystallization onset above T_g. Our group reported in 2018 that the crystallization of sucrose in lyophilizates is accelerated by Polysorbate 20 (PS 20) [104]. To check whether this could depend on a measurable increase in molecular mobility with increasing PS 20 concentration, four different formulations containing 2 mg/mL of an IgG_1 antibody and sucrose were investigated. They differed in the concentration of added PS 20 and/or pH. The fresh samples were measured in an isothermal microcalorimeter at 40 °C over the duration of several days. With this method, the crystallization onset of the formulation could be observed easily, in real time, and in detail. Furthermore, the relaxation as well as the onset of crystallization were recorded at once within one sample. In Figure I.11, the results are presented.

It was observed that PS 20 accelerated the crystallization of sucrose, with 1.6 mg/mL PS 20 crystallizing first, followed by 0.8 mg/mL PS 20, with no crystallization during the measurement period in samples without PS 20. This was expected due to the results of Vollrath et al., 2018 [104]. However, interestingly, the values of τ_{MSE}^{β} increased and the curve flattened with increasing PS 20 concentration. With the knowledge that a higher concentration of PS 20 leads to an earlier onset of crystallization and the presented relaxation theory, we would have expected a decrease in the relaxation times τ_{MSE}^{β}. Furthermore, it could be noted that the samples containing 0.8 mg/mL PS 20 possessed the same relaxation time independent of the pH value, but clearly not the same crystallization behavior. This again proves very clearly that the formulation composition has a stronger impact on the sample compared to relaxation parameters.

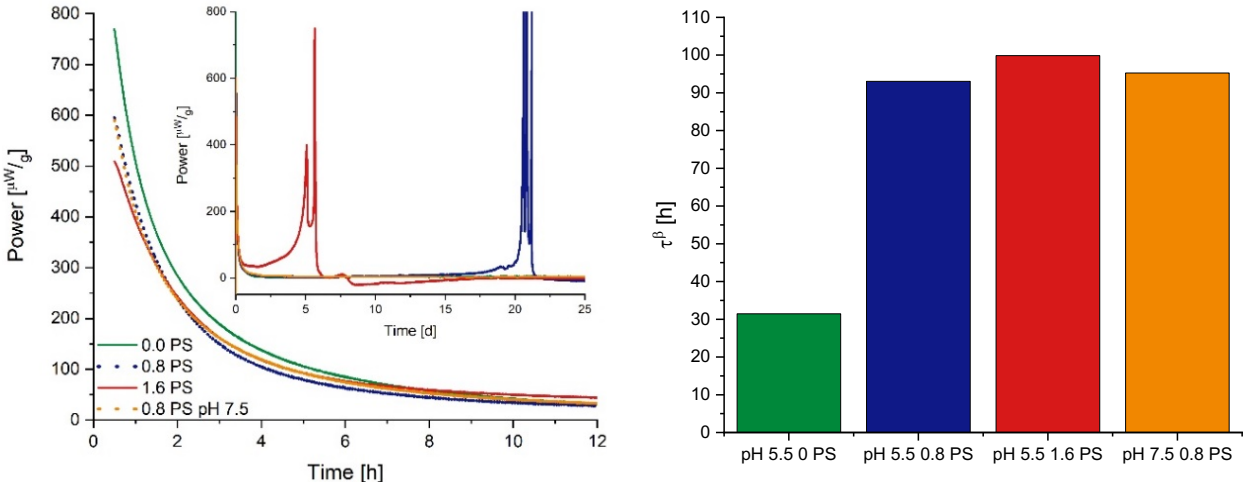

(**a**) (**b**)

Figure I.11 (a) Relaxation behavior of sucrose formulations containing 2 mg/mL IgG$_1$ antibody and a different concentration of polysorbate 20 from a range 0.0 – 1.6 mg/mL. Except one formulation with a pH of 7.5, all other samples had a pH of 5.5. The measurement was performed by isothermal microcalorimetry with a measurement temperature of 40 °C. The small picture shows the complete measurement, which was performed over 25 days. The different crystallization peaks within a formulation most likely result from sample pooling to reach the needed amount of sample for the measurement. (**b**) Calculated values of τ_{MSE}^{β}.

I.4.2.2 Influence of the freezing step on α-relaxation

The impact of primary drying and secondary drying of a freeze-drying cycle on relaxation appears logical. Thermal treatment is executed on a forming glass by the shelves. However, the influence of the freezing step is not as clear and has not been investigated systematically so far. During freezing, a freeze concentrate is built, which itself is a glassy matrix. This glass is then dried and thus the initial glass is converted to another glass in the end.

To investigate the influence of the freezing step on the lyophilized formulation, a sucrose- as well as a trehalose-based formulation containing 2 mg/mL of an IgG$_1$ antibody were prepared and freeze-dried with four different freezing processes. Random nucleation (RN), random nucleation with annealing step (AN), controlled nucleation with ice fog (CN), and quench cooling (QN) were performed and the samples subsequently equilibrated at −45 °C. Primary and secondary drying was then performed in the same freeze-drying process to ensure the same conditions. The resulting products were measured at 40 °C in the IMC, and trehalose-based formulations were additionally measured at 55 °C. The resulting data are displayed in Figure I.12a,c,e. The curves of RN, AN, and QN overlap and show no significant discrepancy, while CN clearly differs. In sucrose-based formulations, samples of the CN process possess a relaxation curve with a smaller absolute heat signal and an endothermal valley after the relaxation decay, ending in a zero power signal. At both measurement temperatures, the

resulting curves for the CN process of the trehalose-based samples exhibit a higher absolute power signal with stronger decay compared to the other curves.

Different freezing steps typically lead to different specific surface areas in the resulting freeze-dried cake and different levels of residual moisture. In particular, CN is used to control ice nucleation and the ice crystal size. After the water sublimates, the remaining pores in samples generated by CN are larger and the sample overall possesses a smaller specific surface area, which often leads to products with higher residual moisture [105].

With its strong influence on the glass transition itself, residual moisture clearly has a strong impact on matrix relaxations. Liu et al. found an increase in the relaxation time τ_{MSE}^{β} by a factor of 6 while residual moisture increased from ca. 0% to 2.7% [17]. On the other hand, Wang et al. reported that effects such as tempering overrule the influence of residual moisture [70]. For a meaningful comparison, it is therefore necessary to normalize dry matrices for residual moisture before one can determine the direct effect of CN on relaxation. Of course, the residual moisture of CN samples can be adapted to the level of the other processes by increasing the secondary drying time or temperature. However, the problem in the experimental scope is that this would cause a change in thermal history. We therefore adapted the re-moisturizing method of Lo Presti et al., to equalize the moisture level of different processes when studying the question of how nucleation affects relaxation [106]. The moisture levels were equalized to the sample with the highest residual moisture (CN samples) of ca. 1.5% and the results are presented in Figure I.12b,d,f. For the ICM measurements performed at 40 °C (Figure I.12b,d), the equalized moisture level led to an increase in the absolute power signal of the processes RN, AN, and QN; however, a significant difference compared to the curve of the CN sample was still observable. In contrast, when measured at 55 °C, the RN and CN curves were equal to each other, resulting in the same τ_{MSE}^{β} value.

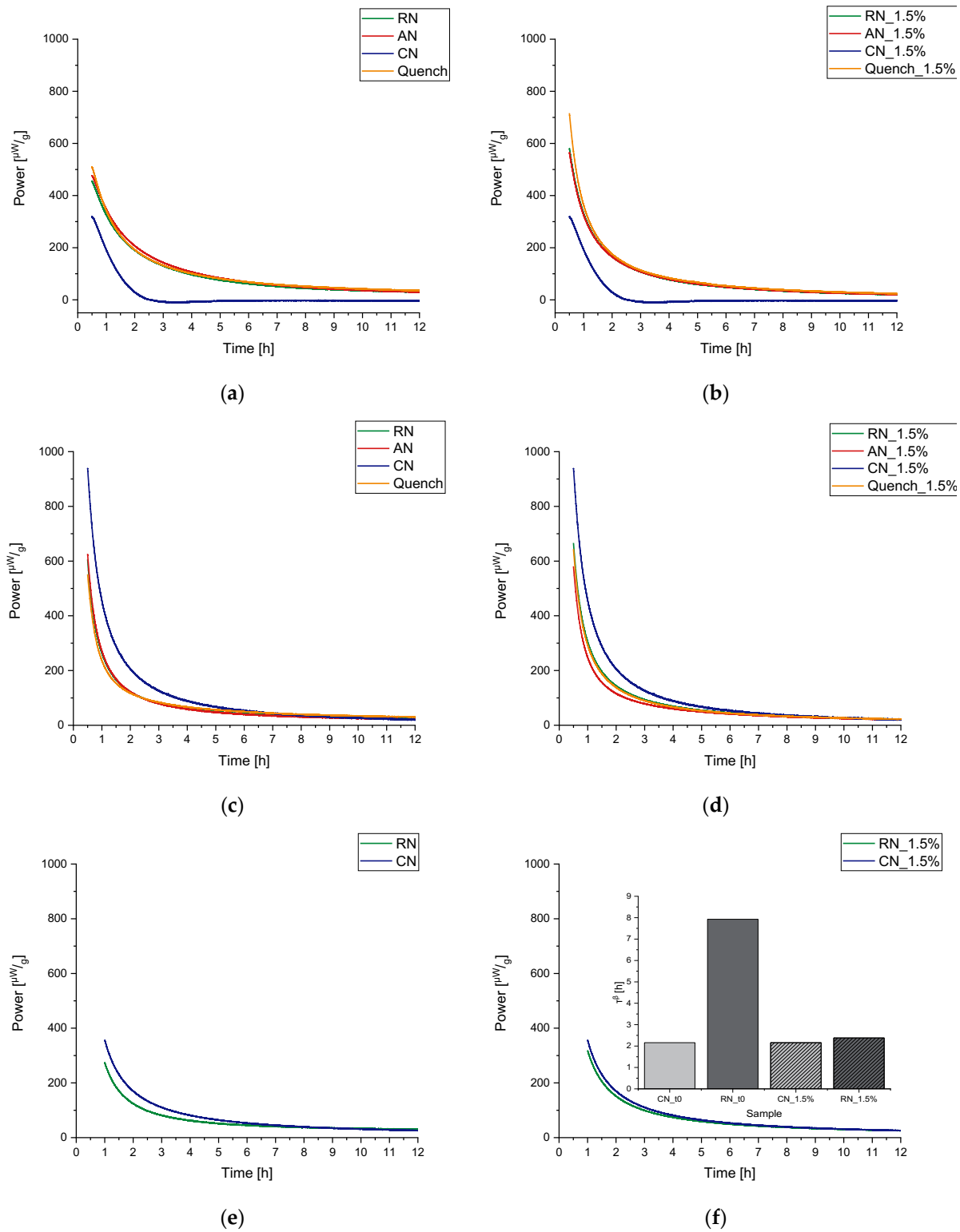

Figure I.12. Relaxation curves of samples with different freezing processes but same compositions. (**a**,**b**) Sucrose-based formulations measured at 40 °C, (**c**,**d**) trehalose-based formulations measured at 40 °C, (**e**,**f**) trehalose-based formulations measured at 55 °C. Samples in (**a**), (**c**), and € were measured at t(0), whereas samples in (**b**), (**d**), and (**f**) were adjusted to the same residual moisture of around 1.5%. The small diagram in (**f**) displays the respective τ_{MSE}^{β} values of the corresponding samples in (**e**,**f**). At 55 °C, only CN and RN processes were compared.

Our results are consistent with those obtained by Abdul-Fattah et al. [96]. In their experiment, AN and RN samples were compared and no difference in α-relaxation times was obtained. In trehalose-based formulations measured at 55 °C, the adjustment of the residual moisture of RN and CN samples resulted in equal relaxation behavior. Further, Chung et al. found that, in the thermodynamically controlled relaxation area (Figure I.5), the slope $\frac{d\Delta H_\infty}{dT_g - T_a}$ was proportional to residual moisture [84]. However, in our case, the adaption of residual moisture should have led to the same α-relaxation times for sucrose formulations and not for trehalose ones, as it seems to be that the former are in the thermodynamically controlled range and the latter in the kinetically controlled range (Figure I.10).

All in all, the results suggest that also the freezing step itself has to be taken into account when the process parameters of freeze-dried formulations are compared. Residual moisture has an impact on the α-relaxation times, which is explainable with the double effect of decreasing the T_g temperature and simultaneously decreasing viscosity, hence increasing molecular mobility. Differences in the freezing step and residual moisture contribute separately to α-relaxation times.

I.4.3 Collapse as a Tempering Process at Relatively Low Temperatures

The basic idea is to combine the tempering process for the relaxation of the matrix within the primary drying of the freeze-drying process. Thus, one can take advantage of the relatively low T_g of the drying matrix and the tempering process can be conducted at moderate temperatures of 25 °C. Considering full collapse drying as a method of choice, the drying is performed continuously above the T_g of the forming glass until it reaches a high T_g, when, finally, only low residual moisture is left. As a result, the formulation does not leave the equilibrated state as it is in thermodynamic equilibrium almost until the end of the process. With this, the loss of macroscopic structure and eventually bubble formation have to be accepted. With well-conducted collapse drying, the same residual moisture as in elegantly dried cakes can be reached [30]. Moreover, in the studies of Schersch et al., protein formulations were collapsed (heated) on purpose during freeze-drying, with the outcome of improved long-term stability for collapsed protein formulations compared to elegantly dried and tempered ones [30,107]. In addition, an increased relaxation time was shown for collapsed products. Figure I.13 shows how a collapsed product of a trehalose-based sample locates between freshly prepared and tempered versions. It can be considered that the tempering process of the sample happens during the collapse freeze-drying cycle and there is no need to subsequently add it afterwards. Thus, the additional heat input to relax the matrix occurs when a high amount of water is present and

the absolute temperatures needed are relatively low and so is the stress for the protein. It is, on the other hand, important to restrict this period of time when a rather highly concentrated protein solution sits at a rather high temperature, as these conditions typically lead to the degradation of the protein, including aggregation.

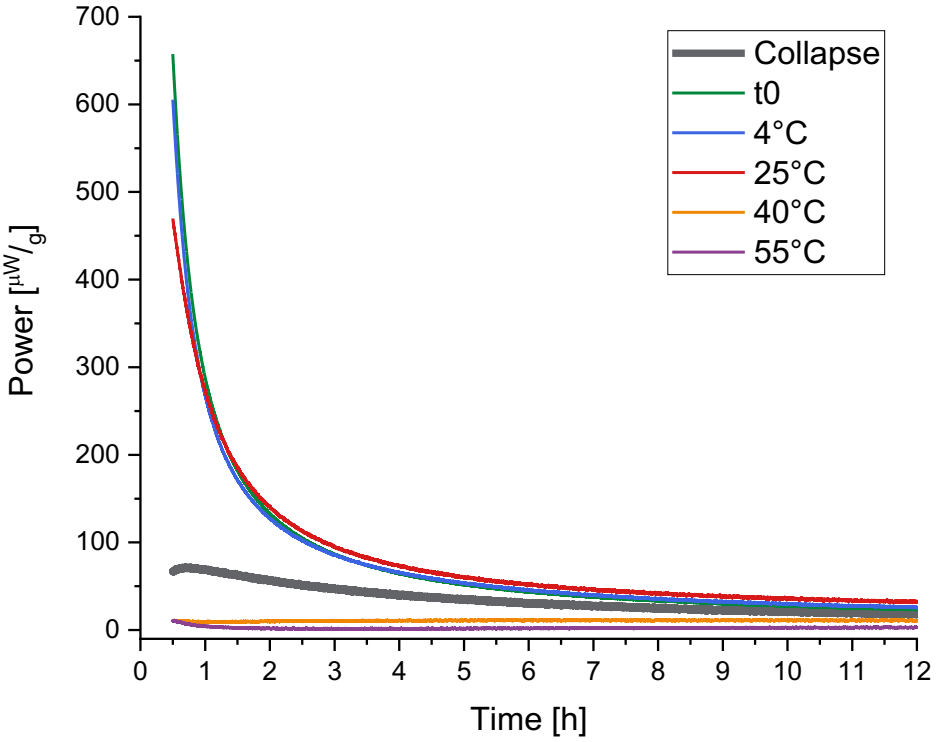

Figure I.13 Comparison of the relaxation curve of the trehalose-based collapsed product with the curves of trehalose-based samples after conventional freeze-drying followed by tempering at different temperatures.

I.5 Conclusions

Molecular mobility, especially in the form of α-relaxations, was explained, and the impact on freeze-dried products was reviewed. Although studying molecular mobility cannot primarily determine an optimal formulation recipe, it can assist in process optimization. The basis of all further considerations is the experience that the tempering of lyophilized solid products to increase the relaxation time leads to less degradation, i.e., higher storage stability. Instead of post-process tempering, we propose to use collapse or aggressive freezing drying as fast, elegant, and particularly gentle methods to remove the energy excess from freeze-dried products already during the primary drying. IMC is able to measure the heat of relaxation directly, whereas with DSC, it is only possible to measure the enthalpy recovery. Without using IMC, certain phenomena would not be detected, e.g., the tempering shoulder or the endothermal energy valley of controlled nucleated samples would be overlooked. The latter shows that

controlled nucleation does more to the structure of a lyo-cake than simply increasing the ice crystal size. Furthermore, IMC leads to a better data resolution and measures modes of relaxations that are not captured with conventional DSC.

I.6 Outlook

In 2010, Wang et al. showed that, in some cases, α-relaxations are more stability determining than β-relaxations [70]. This is one of the last publications found that used IMC in the context of freeze-drying. In the last few years, although liquid protein formulations have been optimized, freeze-drying is still frequently used to produce stable dry solid protein drug products. Furthermore, new freeze-drying techniques such as controlled nucleation and collapse drying have emerged. Therefore, α-relaxation optimization by IMC and other techniques might be revisited for further improvement of product stability after lyophilization, which was neglected in the past decade.

We wish to remind the interested community of this option and we will use such α-relaxation measurements with IMC to answer the question of whether aggressive or collapse drying would be equivalent to or better for the storage stability of proteins compared to standard cycles; compared to a regular tempering practice, according to the Pikal group, IMC could further help to improve secondary drying processes in general [27,63,66,91].

I.7 Materials and Methods

I.7.1 Materials

For the preparation of placebos and monoclonal antibody formulations, the following excipients were used: IgG_1 was in stock at Ludwig-Maximilians-Universität München (LMU), sucrose was obtained from Sigma-Aldrich (Steinheim, Germany), D(+)-Trehalose dihydrate was purchased from VWR chemicals (Leuven, Belgium), L-Methionine, U.S.P. was used from J.T. Baker (Center Valley, Pennsylvania), Histidine from Alfa Aesar (Kandel, Germany) was utilized, and Polysorbate 20 was provided by Croda (Nettetal, Germany).

I.7.2 Preparation of Formulations

The composition of the formulations that were used in the performed experiments can be found in table I.1.

Table I.1 Compositions of formulations used in the different experiments.

Substance $[\frac{g}{l}]$	Sucrose-Placebo	Trehalose-Placebo	Su5.5-2-0PS	Su5.5-2-8PS	Su5.5-2-16PS	Su7.5-2-8PS	Tr.5.5-2-8PS
IgG_1	-	-	2	2	2	2	2
Sucrose	79.45	-	79.45	79.45	79.45	79.45	-
Trehalose	-	79.45	-	-	-	-	79.45
Methionine	1.5	1.5	-	-	-	-	-
Histidine	0.42	0.42	0.42	0.42	0.42	0.42	0.42
Polysorbate 20	0.4	0.4	-	0.8	1.6	0.8	0.8

I.7.3 Freeze-Drying

For the elegant cakes, the primary and secondary drying step were kept the same using a Christ ε2-6D laboratory scale freeze-dryer (Martin Christ, Osterode am Harz, Germany). Primary drying was performed at a pressure of 0.09 mbar and a shelf temperature of −25 °C. Secondary drying was performed at 0.09 mbar applying a 0.15 K/min temperature ramp to 30 °C, which was then held for 4 h. After the drying, samples were immediately cooled to −45 °C and stoppered under a nitrogen atmosphere.

Random nucleated freezing (RN) was performed with equilibration at 5 °C for 1 h followed by ramping down to a setpoint of −45 °C with a cooling rate of 1 K/min. The temperature was then held constant for 2.5 h.

Annealing was performed with the freezing step of RN but followed by a subsequent temperature increase to −20 °C with 1 K/min and a hold time of 1.5 h. Afterwards, the samples were again cooled down to −45 °C with a rate of 1 K/min and an additional hold time of 1.5 h before the primary drying time was started.

Freezing with controlled nucleation (CN) additionally included a further equilibration step at −5 °C for 1 h followed by the introduction of ice crystals using a LyoCoN system (Martin Christ, Osterode am Harz, Germany).

Quench cooling was performed by purging the sample tray with liquid nitrogen. After 2 min, the samples were placed in the freeze-dryer, which was precooled to −45 °C. The samples were then held for 1.5 h at −45 °C before primary drying was conducted.

The freezing step of collapse intended freeze-drying was performed as for randomly nucleated samples. The mixed primary and secondary drying step begun with a pressure of 2 mBar and a

temperature ramp from −45 °C to 45 °C with a heating rate of 0.7 K/min. The conditions were then held for 24 h. The pressure was then decreased to 0.03 mbar and again held at 45 °C for 20 h. After the drying, samples were immediately cooled to −45 °C and stoppered under a nitrogen atmosphere.

I.7.4 Sample Tempering

Sample tempering was performed after the freeze-drying process with crimped and closed samples. Drying cabinets were set to the chosen temperatures and the tempering duration was 7 days.

I.7.5 Differential Scanning Calorimetry

A Mettler Toledo DSC 821e (Gießen, Germany) was used for DSC experiments. For the samples in Figure I.2a, a linear measurement method was used. At first, the sample was cooled and held at −10 °C for 3 min. Subsequently, the first heating cycle was performed with a heating rate of 10 K/min up to 140 °C. Then, the sample was again cooled to −10 °C with a cooling rate of −10 K/min and held at this temperature for 3 min. The second heating cycle was performed similarly to the first heating cycle. Only the two heating cycles are shown in the diagram. For mDSC, a temperature range of −10–180 °C was measured with a heating ramp of 2 K/min, an amplitude of 1 °C, and a period of 120 s. A collection of further DSC methods from the literature can be found in Table I.A1.

I.7.6 Isothermal Microcalorimetry

A LKB 2277 Thermal Activity Monitor (TAM) (ThermoMetric AB, Järfälla, Sweden) equipped with 4 mL ampoule twin cylinders (2277-201) was used to determine the isothermal heatflow. The instrument was electrically calibrated in the 300 µW area as proposed by Shamblin et al., and the function verified with the suggested chemical methods from Beezer et al. [93,108,109]. We experimentally demonstrated that breaking the lyophilized cake into powder and its transfer into the stainless steel ampoules does not disturb the relaxation measurement. This was performed by generating lyophilized samples directly in glass measurement ampoules with subsequent measurement without mechanically dividing the sample (data not shown). However, as presented in the technical note, rubber stoppers on glass vials can generate a significant interfering signal [110]. Thus, stainless steel ampoules were used for further measurements.

The freeze-dried samples were transferred to stainless steel measuring ampoules in a dry air-purged atmosphere. Approximately 150 mg sample was used (if necessary, pooled from several product vials). The reference ampoule stayed empty (in contrast to using crystalline glycine as

in reference [17]). The measurement and reference ampoule were first lowered to the thermal equilibrium position and held for 15 min to allow equilibration (in contrast to 30 min [17]). Both ampoules were then slowly lowered to the measurement position of the TAM. The experiment was performed at 25 °C, 40 °C, and 55 °C, respectively. Data points were collected in intervals of 2 s for the first hour of the measurement and afterwards with 10 s intervals. The duration of the measurement was 12–24 h. In the literature, often, measurement times of 48 h or even more are used [17,21] but the shape of Figure I.4 suggests that the time of the measurement can be strongly reduced to increase the performance of IMC measurements. In particular, the curve determined at a temperature of 55 °C shows that even after 2 h more, the heat power signal is reduced by more than half. This should be adequate for a reproducible fit. To prove the considerations, samples of Trehalose-RN and Sucrose-RN were measured for more than 100 h at 25 °C and different time intervals were used for the fit. Table I.2 displays the results. The determined values of τ_{MSE}^{β} did not change if the fit time exceeded 25 h, or, for Su-PlaM, even 12 h. Of course, a standard procedure cannot be provided here. Variables such as sample formulation, freeze-drying process, and temperature of the calorimeter have to be taken into account. For example, at a measurement temperature of 55 °C, the evaluation time can be even reduced to 12 h (data not shown). It is important to bear in mind that the start of the fit begins at 0.5 h at the earliest, due to the noise of friction through sample insertion in the instrument. A collection of other IMC methods from the literature can be found in Table I.A2 of Appendix B.

Table I.2 Comparison of the calculated τ_{MSE}^{β} values from the same 100 h measurement. End times were chosen between 12 h and 100 h.

Fit time Onset [h]—Endset [h]	Sucrose Formulation $\tau_{MSE}^{\beta}[h]$	Trehalose Formulation $\tau_{MSE}^{\beta}[h]$
0.5–12	11	41
0.5–25	11	37
0.5–50	11	37
0.5–100	11	37

I.7.7 Curve Fitting

The software OriginLab 2019b was used to perform the non-linear curve fitting. An iterative algorithm based on Levenberg–Marquardt was utilized. The start values were chosen as 2 for τ_0, 1 for τ_1, and 0.1 for β. To verify the function of the fit, literature data were plotted, where possible, and the plotted curve refitted with the settings in OriginLab. The obtained τ_{MSE}^{β} values were consistent with the presented data from the literature, e.g., [23,30].

I.7.8 Karl Fischer Titration

For the determination of residual moisture content, Karl Fischer titration was utilized. Approximately 20 mg of sample was transferred into empty 2R vials in a glove box with humidity lower than 10%. A coulometric Karl Fischer titrator Aqua 40.00 (Elektrochemie Halle, Halle, Germany) equipped with an external oven was used. The oven was set at 100 °C to extract the water from the sample. The extracted water was then transported into the calorimetric cell.

Author Contributions: Conceptualization, G.W.; methodology S.G., T.M. and G.W.; investigation, S.G.; resources, G.W.; data curation, S.G.; writing—original draft preparation, S.G.; writing—review and editing, T.M. and G.W.; visualization, S.G.; supervision, T.M. and G.W.; project administration, G.W. All authors have read and agreed to the published version of the manuscript."

Funding: This research received no external funding.

Data Availability Statement: Data are contained within the article

Acknowledgments: The authors wish to thank Jürgen Seidel from the Technical University Bergakademie Freiberg for his helpful technical and physical discussions as well as support with the handling of the instrument. Without his kind help, the measurements would not have been possible.

Conflicts of Interest: The authors declare no conflicts of interest.

I.8 Appendix

I.8.1 Appendix A

Table I.A1. Collection of DSC methods as suggested by different authors. n.a., not available.

Author	Purpose	Sample Weight [mg]	Lid	Heating Rates [K/min]	Hold Temperatures above T_g [K]	Tempering Temperature below T_g [K]
Hancock et al. 1995. [48]	Investigate relaxation times of pure, melt-quenched substances with DSC	2–10	Pierced	20	10–25	16–47
Van den Mooter et al. [90]	Investigate relaxation times of pure, melt-quenched APIs with DSC	2–6	Closed	10	20	16–66
Shamblin et al. [16]	Temperature + enthalpy of fusion of lyophilized substances	±5	Closed	10	n.a.	n.a.
	c_p values of lyophilized substances	±5	n.a.	2 * (60, 0.5)	n.a.	n.a.
	Relaxation times of pure lyophilized substances with mDSC	±5	n.a.	n.a.	15	15
Aso et al. [111]	Correlation of mobile mobility and crystallization of quench-cooled samples	±5	Pierced	20	45	25
Liu et al. [17]	Investigation and comparison of relaxation times of quench-cooled and freeze-dried samples. Additionally to DSC, also IMC was used for determination	5–10	Closed	n.a.	n.a.	n.a.
Zhou et al. [98]	c_p values of lyophilized and quench-cooled substances	±10	Closed	1 * (100, 0.5)	50	20–50
Surana et al. [99,100]	Investigate relaxation times and crystallinity onset of freeze-dried trehalose	4–5	Pierced	10	n.a.	20–60
Chang et al. [21]	T_g and Δc_p determination for IMC	5–10	Closed	1 * (100, 0.5)	n.a.	n.a.
Luthra et al. [41]	Enthalpy recovery and T_g mDSC were used, where enthalpy recovery might be superimposed by T_g	5–10	Closed	10 1 * (80, 0.85)	25	50-15
Wang et al. [70]	T_g and Δc_p determination for IMC	n.a.	n.a.	2 * (120, 1)	30	n.a.

* mDSC (period time [s], amplitude [±K]).

I.8.2 Appendix B

Table I.B1 Collection of performed relaxation measurements by different authors.

Author	τ^{β} Method	Formulation	Outcome
Abdul-Fattah et al. [31]	MSE	Freeze-dried moxalactam mannitol system	Tempering (called annealing in the original literature) increased the structural relaxation time τ^{β}_{MSE} of the samples, leading to improved long-term stability.
Abdul-Fattah et al. [56]	MSE	Mixtures of monoclonal antibodies with increasing sucrose content prepared by freeze-drying, spray-drying, and vacuum drying	"Initial endothermic response" in sucrose-rich vacuum-dried formulations appeared with unclear origin. With increased sucrose fraction, stability of the antibodies increased. Correlation between relaxation times and protein depending of the process was better for fast dynamics (not the topic of this review) than for global α-relaxation times.
Bhugra et al. [53]	KWW and MSE	Pure quench-cooled systems of indomethacin, nifedipin, ketoconazol and flopropione	Relaxation time constants above and below T_g are highly correlated.
Duddu et al. [92]	KWW	Trehalose- or sucrose-based formulations of a monoclonal antibody	Trehalose-based formulations showed Arrhenius-like behavior while sucrose showed non-Arrhenius kinetics. Thus, although sucrose is in general the more fragile glass, at temperatures below 5 °C, trehalose seems to be more fragile.
Hancock et al. [48]	KWW	Pure quench-cooled systems of indomethacin, PVP, and sucrose	Relaxation time at $T_g - 50\ °C$ is up to many years. Relaxations could predict stability of some pharmaceutical products.
Liu et al. [17]	KWW and MSE	Pure quench-cooled or freeze-dried systems of saccharides (sucrose, trehalose, raffinose, lactose, stachyose)	τ^{β}_{MSE} is obtained with less labor, more data points than τ^{β}_{KWW}. τ^{β}_{MSE} is furthermore precise and enables the measurement of samples that relax very slowly with only a minor release of heat. Further, a rational development of peptide and protein formulations should be possible.
Kawakami and Pikal [23]	KWW and MSE	Review	The evaluation with τ^{β}_{MSE} is superior compared to τ^{β}_{KWW}. In general, τ^{β} is suggested as parameter of choice instead of comparing the single parameters τ and β, respectively.
Shamblin et al. [93]	MSE	Freeze-dried amorphous drug mixtures	The correlation of α-relaxation with protein stability is dependent on the rate controlling step of the degradation process. The latter should be coupled to molecular mobility as well as α-relaxation.
Luthra et al. [41,95]	KWW and MSE	Freeze dries sucrose/aspartam and trehalose/aspartame formulations	Tempering (called annealing in the original study) significantly decreases the degradation rate and an optimum temperature for the tempering process was set $T_g - T = 20\ °C$.
Van den Mooter et al. [90]	KWW	Pure quench-cooled systems of diazepam, temazepam, and triazolam	Molecular mobility might be unimportant for temperatures less than $T_g - 50\ °C$. Relaxations could predict stability of some pharmaceutical products.
Wang et al. [94]	KWW and MSE	Sucrose:protein mixtures in different ratios	MSE correlates with protein stability up to a sucrose/protein mass ratio of 1:1 (increase in τ^{β}_{MSE}) as well as FTIR. With higher sucrose concentration beyond 1:1, τ^{β}_{MSE} decreases although protein stability further increases; thus, τ^{β}_{MSE} did not correlate at this ratio anymore.

I.9 References

1. Advancing Health Through Innovation: New Drug Therapy Approvals 2020. Available online: https://fda.report/media/144982/final+FINAL+NewDrugsApprovalReport_Final2020_210108_0948_FINAL.pdf (accessed on 15 September 2021).
2. Peters, C.; Brown, S. Antibody–Drug Conjugates as Novel Anti-Cancer Chemotherapeutics. *Biosci. Rep.* **2015**, *35*, e00225, doi:10.1042/BSR20150089.
3. Schirrmacher, V. Cancer Vaccines and Oncolytic Viruses Exert Profoundly Lower Side Effects in Cancer Patients than Other Systemic Therapies: A Comparative Analysis. *Biomedicines* **2020**, *8*, 61, doi:10.3390/biomedicines8030061.
4. Fritzsching, B. Personalized Medicine in Allergic Asthma: At the Crossroads of Allergen Immunotherapy and "Biologicals". *Front. Pediatr.* **2017**, *5*, 3–6, doi:10.3389/fped.2017.00031.
5. Kis, Z.; Kontoravdi, C.; Shattock, R.; Shah, N. Resources, Production Scales and Time Required for Producing RNA Vaccines for the Global Pandemic Demand. *Vaccines* **2020**, *9*, 3, doi:10.3390/vaccines9010003.
6. Butreddy, A.; Janga, K.Y.; Ajjarapu, S.; Sarabu, S.; Dudhipala, N. Instability of Therapeutic Proteins—An Overview of Stresses, Stabilization Mechanisms and Analytical Techniques Involved in Lyophilized Proteins. *Int. J. Biol. Macromol.* **2021**, *167*, 309–325, doi:10.1016/j.ijbiomac.2020.11.188.
7. Stadtman, E.R. Protein Oxidation and Aging. *Free Radic. Res.* **2006**, *40*, 1250–1258, doi:10.1080/10715760600918142.
8. Adem, Y.T.; Molina, P.; Liu, H.; Patapoff, T.W.; Sreedhara, A.; Esue, O. Hexyl Glucoside and Hexyl Maltoside Inhibit Light-Induced Oxidation of Tryptophan. *J. Pharm. Sci.* **2014**, *103*, 409–416, doi:10.1002/jps.23809.
9. Daugherty, A.L.; Mrsny, R.J. Formulation and Delivery Issues for Monoclonal Antibody Therapeutics. *Adv. Drug Deliv. Rev.* **2006**, *58*, 686–706, doi:10.1016/j.addr.2006.03.011.
10. Bis, R.L.; Mallela, K.M.G. Antimicrobial Preservatives Induce Aggregation of Interferon Alpha-2a: The Order in Which Preservatives Induce Protein Aggregation Is Independent of the Protein. *Int. J. Pharm.* **2014**, *472*, 356–361, doi:10.1016/j.ijpharm.2014.06.044.
11. Chi, E.Y.; Krishnan, S.; Randolph, T.W.; Carpenter, J.F. Physical Stability of Proteins in Aqueous Solution: Mechanism and Driving Forces in Nonnative Protein Aggregation. *Pharm. Res.* **2003**, *20*, 1325–1336, doi:10.1023/A:1025771421906.

12. Wang, W. Lyophilization and Development of Solid Protein Pharmaceuticals. *Int. J. Pharm.* **2000**, *203*, 1–60, doi:10.1016/S0378-5173(00)00423-3.
13. Constantino, H.R. Excipients for Use in Lyophilized Pharmaceutical Peptide, Protein, and other Bioproducts. In *Lyophilization of Biopharmaceuticals*; Constantino, H.R., Pikal, M.J., Eds.; AAPS Press: Arlington, VA, USA, 2004; pp. 139–228, ISBN 0-9711767 6-0.
14. Liu, B.; Zhou, X. Freeze-Drying of Proteins. In *Cryopreservation and Freeze-Drying Protocols*; Wolkers, W.F., Eds.; Springer: New York, NY, USA, 2015; pp. 459–476, ISBN 978-1-4939-2193-5.
15. Emami, F.; Vatanara, A.; Park, E.J.; Na, D.H. Drying Technologies for the Stability and Bioavailability of Biopharmaceuticals. *Pharmaceutics* **2018**, *10*, 131, doi:10.3390/pharmaceutics10030131.
16. Shamblin, S.L.; Tang, X.; Chang, L.; Hancock, B.C.; Pikal, M.J. Characterization of the Time Scales of Molecular Motion in Pharmaceutically Important Glasses. *J. Phys. Chem. B* **1999**, *103*, 4113–4121, doi:10.1021/jp983964+.
17. Liu, J.; Rigsbee, D.R.; Stotz, C.; Pikal, M.J. Dynamics of Pharmaceutical Amorphous Solids: The Study of Enthalpy Relaxation by Isothermal Microcalorimetry. *J. Pharm. Sci.* **2002**, *91*, 1853–1862, doi:10.1002/jps.10181.
18. Pikal, M.J.; Rigsbee, D.R. The Stability of Insulin in Crystalline and Amorphous Solids: Observation of Greater Stability for the Amorphous Form. *Pharm. Res.* **1997**, *14*, 1379–1387, doi:10.1023/a:1012164520429.
19. Cicerone, M.T.; Douglas, J.F. β-Relaxation Governs Protein Stability in Sugar-Glass Matrices. *Soft Matter* **2012**, *8*, 2983–2991, doi:10.1039/c2sm06979b.
20. Allison, S.D.; Chang, B.; Randolph, T.W.; Carpenter, J.F. Hydrogen Bonding between Sugar and Protein Is Responsible for Inhibition of Dehydration-Induced Protein Unfolding. *Arch. Biochem. Biophys.* **1999**, *365*, 289–298, doi:10.1006/abbi.1999.1175.
21. Chang, L.; Shepherd, D.; Sun, J.; Ouellette, D.; Grant, K.L.; Tang, X.; Pikal, M.J. Mechanism of Protein Stabilization by Sugars during Freeze-Drying and Storage: Native Structure Preservation, Specific Interaction, and/or Immobilization in a Glassy Matrix? *J. Pharm. Sci.* **2005**, *94*, 1427–1444, doi:10.1002/jps.20364.
22. Chieng, N.; Teo, X.J.; Cheah, M.H.; Choo, M.L.; Chung, J.; Hew, T.K.; Keng, P.S. Molecular Dynamics and Physical Stability of Pharmaceutical Co-Amorphous Systems: Correlation Between Structural Relaxation Times Measured by Kohlrausch-Williams-Watts With the Width of the Glass Transition Temperature (ΔTg) and the Onset of Crystallization. *J. Pharm. Sci.* **2019**, *108*, 3848–3858, doi:10.1016/j.xphs.2019.09.013.

23. Kawakami, K.; Pikal, M.J. Calorimetric Investigation of the Structural Relaxation of Amorphous Materials: Evaluating Validity of the Methodologies. *J. Pharm. Sci.* **2005**, *94*, 948–965, doi:10.1002/jps.20298.
24. Chang, L.L.; Pikal, M.J. Mechanisms of Protein Stabilization in the Solid State. *J. Pharm. Sci.* **2009**, *98*, 2886–2908, doi:10.1002/jps.
25. Dahan, A.; Beig, A.; Ioffe-Dahan, V.; Agbaria, R.; Miller, J.M. The Twofold Advantage of the Amorphous Form as an Oral Drug Delivery Practice for Lipophilic Compounds: Increased Apparent Solubility and Drug Flux through the Intestinal Membrane. *AAPS J.* **2013**, *15*, 347–353, doi:10.1208/s12248-012-9445-3.
26. Karagianni, A.; Kachrimanis, K.; Nikolakakis, I. Co-Amorphous Solid Dispersions for Solubility and Absorption Improvement of Drugs: Composition, Preparation, Characterization and Formulations for Oral Delivery. *Pharmaceutics* **2018**, *10*, 98, doi:10.3390/pharmaceutics10030098.
27. Löbmann, K.; Laitinen, R.; Strachan, C.; Rades, T.; Grohganz, H. Amino Acids as Co-Amorphous Stabilizers for Poorly Water-Soluble Drugs—Part 2: Molecular Interactions. *Eur. J. Pharm. Biopharm.* **2013**, *85*, 882–888, doi:10.1016/j.ejpb.2013.03.026.
28. Babu, N.J.; Nangia, A. Solubility Advantage of Amorphous Drugs and Pharmaceutical Cocrystals. *Cryst. Growth Des.* **2011**, *11*, 2662–2679, doi:10.1021/cg200492w.
29. Sophocleous, A.M.; Zhang, J.; Topp, E.M. Localized Hydration in Lyophilized Myoglobin by Hydrogen–Deuterium Exchange Mass Spectrometry. 1. Exchange Mapping. *Mol. Pharm.* **2012**, *9*, 718–726, doi:10.1021/mp3000088.
30. Schersch, K. Effect of Collapse on the Stability of Protein Lyophilisates. Ph.D. Thesis, Ludwig Maximilian University of Munich, Munich, Germany, 2009.
31. Abdul-Fattah, A.M.; Dellerman, K.M.; Bogner, R.H.; Pikal, M.J. The Effect of Annealing on the Stability of Amorphous Solids: Chemical Stability of Freeze-Dried Moxalactam. *J. Pharm. Sci.* **2007**, *96*, 1237–1250, doi:10.1002/jps.20947.
32. Andronis, V.; Zografi, G. Molecular Mobility of Supercooled Amorphous Indomethacin, Determined by Dynamic Mechanical Analysis. *Pharm. Res.* **1997**, *14*, 410–414, doi:10.1023/A:1012026911459.
33. Oksanen, C.A.; Zografi, G. Molecular Mobility in Mixtures of Absorbed Water and Solid Poly(Vinylpyrrolidone). *Pharm. Res.* **1993**, *10*, 791–799, doi:10.1023/A:1018988506336.
34. Andronis, V.; Zografi, G. The Molecular Mobility of Supercooled Amorphous Indomethacin as a Function of Temperature and Relative Humidity. *Pharm. Res.* **1998**, *15*, 835–842, doi.org/10.1023/A:1011960112116.

35. Sibik, J.; Zeitler, J.A. Direct Measurement of Molecular Mobility and Crystallisation of Amorphous Pharmaceuticals Using Terahertz Spectroscopy. *Adv. Drug Deliv. Rev.* **2016**, *100*, 147–157, doi:10.1016/j.addr.2015.12.021.
36. Correia, N.T.; Ramos, J.J.M.; Descamps, M.; Collins, G. Molecular Mobility and Fragility in Indomethacin: A Thermally Stimulated Depolarization Current Study. *Pharm. Res.* **2001**, *18*, 1767–1774, doi:10.1023/A:1013339017070.
37. Bhugra, C.; Shmeis, R.; Krill, S.L.; Pikal, M.J. Different Measures of Molecular Mobility: Comparison between Calorimetric and Thermally Stimulated Current Relaxation Times Below Tg and Correlation with Dielectric Relaxation Times Above Tg. *J. Pharm. Sci.* **2008**, *97*, 4498–4515, doi:10.1002/jps.21324.
38. Roozen, M.J.G.W.; Hemminga, M.A.; Walstra, P. Molecular Motion in Glassy Water-Malto-Oligosaccharide (Maltodextrin) Mixtures as Studied by Conventional and Saturation-Transfer Spin-Probe e.s.r. Spectroscopy. *Carbohydr. Res.* **1991**, *215*, 229–237, doi:10.1016/0008-6215(91)84023-8.
39. Cicerone, M.T.; Soles, C.L. Fast Dynamics and Stabilization of Proteins: Binary Glasses of Trehalose and Glycerol. *Biophys. J.* **2004**, *86*, 3836–3845, doi:10.1529/biophysj.103.035519.
40. Cicerone, M.T.; Soles, C.L.; Chowdhuri, Z.; Pikal, M.J.; Chang, L. Fast Dynamics as a Diagnostic for Excipients in Preservation of Dried Proteins. *Am. Pharm. Rev.* **2005**, *8*, 22–27.
41. Luthra, S.A.; Hodge, I.M.; Pikal, M.J. Investigation of the Impact of Annealing on Global Molecular Mobility in Glasses: Optimization for Stabilization of Amorphous Pharmaceuticals. *J. Pharm. Sci.* **2008**, *97*, 3865–3882, doi:10.1002/jps.21255.
42. Chieng, N.; Mizuno, M.; Pikal, M. Characterization of Dynamics in Complex Lyophilized Formulations: I. Comparison of Relaxation Times Measured by Isothermal Calorimetry with Data Estimated from the Width of the Glass Transition Temperature Region. *Eur. J. Pharm. Biopharm.* **2013**, *85*, 189–196, doi:10.1016/j.ejpb.2013.04.003.
43. Luthra, S. Impact of Optimum Annealing on Chemical Stabilization of Model Amorphous Pharmaceuticals. Ph.D. Thesis, University of Connecticut, Storrs, CT, USA, 2007.
44. Ediger, M.D.; Angell, C.A.; Nagel, S.R. Supercooled Liquids and Glasses. *J. Phys. Chem.* **1996**, *100*, 13200–13212, doi:10.1021/jp953538d.
45. Hodge, I.M. Physical Aging in Polymer Glasses. *Science* **1995**, *267*, 1945–1947, doi:10.1126/science.267.5206.1945.

46. Miller, D.P.; Shalaev, E.; Barnard, J. The Roles of Acid–Base Relationships, Interfaces, and Molecular Mobility in Stabilization During Drying and in the Solid State. In *Drying Technologies for Biotechnology and Pharmaceutical Applications*; Ohtake, S., Izutsu, K., Lechuga-Ballesteros, D., Eds.; Wiley: Weilheim,Germany, 2020; pp. 317–346, ISBN 978-3-527-34112-2.
47. Cicerone, M.T.; Tellington, A.; Trost, L.; Sokolov, A. Substantially Improved Stability of Biological Agents in Dried Form: The Role of Glassy Dynamics in Preservation of Biopharmaceuticals. *Bioprocess Int.* **2003**, *1*, 36–47.
48. Hancock, B.C.; Shamblin, S.L.; Zografi, G. Molecular Mobility of Amorphous Pharmaceutical Solids Below Their Glass-Transition Temperatures. *Pharm. Res.* **1995**, *12*, 799–806, doi:10.1023/A:1016292416526.
49. Johari, C.P.; Goldstein, M. Viscous Liquids and the Glass Transition. II. Secondary Relaxations in Glasses of Rigid Molecules. *J. Chem. Phys.* **1970**, *53*, 2372–2388, doi:10.1063/1.1674335.
50. Cicerone, M.T.; Pikal, M.J.; Qian, K.K. Stabilization of Proteins in Solid Form. *Adv. Drug Deliv. Rev.* **2015**, *93*, 14–24, doi:10.1016/j.addr.2015.05.006.
51. Ngai, K.L. The Origin of the Faster Mechanism of Partial Enthalpy Recovery Deep in the Glassy State of Polymers. *Phys. Chem. Chem. Phys.* **2021**, *23*, 13468–13472, doi:10.1039/d1cp01445e.
52. Vyazovkin, S.; Dranca, I. Probing Beta Relaxation in Pharmaceutically Relevant Glasses by Using DSC. *Pharm. Res.* **2006**, *23*, 422–428, doi:10.1007/s11095-005-9044-4.
53. Bhugra, C.; Shmeis, R.; Krill, S.L.; Pikal, M.J. Predictions of Onset of Crystallization from Experimental Relaxation Times I-Correlation of Molecular Mobility from Temperatures Above the Glass Transition to Temperatures Below the Glass Transition. *Pharm. Res.* **2006**, *23*, 2277–2290, doi:10.1007/s11095-006-9079-1.
54. Abdul-Fattah, A.M.; Lechuga-Ballesteros, D.; Kalonia, D.S.; Pikal, M.J. The Impact of Drying Method and Formulation on the Physical Properties and Stability of Methionyl Human Growth Hormone in the Amorphous Solid State. *J. Pharm. Sci.* **2007**, *97*, 163–184, doi:10.1002/jps.21085.
55. Duddu, S.D.; Dal Monte, P.R. Effect of Glass Transition Temperature on the Stability of Lyophilized Formulations Containing a Chimeric Therapeutic Monoclonal Antibody. *Pharm. Res.* **1997**, *14*, 591–595.
56. Abdul-Fattah, A.M.; Truong-Le, V.; Yee, L.; Nguyen, L.; Kalonia, D.S.; Cicerone, M.T.; Pikal, M.J. Drying-Induced Variations in Physico-Chemical Properties of Amorphous

Pharmaceuticals and Their Impact on Stability (I): Stability of a Monoclonal Antibody. *J. Pharm. Sci.* **2007**, *96*, 1983–2008, doi:10.1002/jps.20859.

57. Zografi, G.; Newman, A. Interrelationships Between Structure and the Properties of Amorphous Solids of Pharmaceutical Interest. *J. Pharm. Sci.* **2017**, *106*, 5–27, doi:10.1016/j.xphs.2016.05.001.
58. Pikal, M.J.; Rigsbee, D.R.; Roy, M.L. Solid State Chemistry of Proteins: I. Glass Transition Behavior in Freeze Dried Disaccharide Formulations of Human Growth Hormone (HGH). *J. Pharm. Sci.* **2007**, *96*, 2765–2776, doi:10.1002/jps.20960.
59. Haeuser, C.; Goldbach, P.; Huwyler, J.; Friess, W.; Allmendinger, A. Impact of Dextran on Thermal Properties, Product Quality Attributes, and Monoclonal Antibody Stability in Freeze-Dried Formulations. *Eur. J. Pharm. Biopharm.* **2020**, *147*, 45–56, doi:10.1016/j.ejpb.2019.12.010.
60. Pyne, A.; Surana, R.; Suryanarayanan, R. Crystallization of Mannitol below Tg′ during Freeze-Drying in Binary and Ternary Aqueous Systems. *Pharm. Res.* **2002**, *19*, 901–908, doi:10.1023/A:1016129521485.
61. Newman, A.; Zografi, G. Commentary: Considerations in the Measurement of Glass Transition Temperatures of Pharmaceutical Amorphous Solids. *AAPS PharmSciTech* **2020**, *21*, 1–13, doi:10.1208/s12249-019-1562-1.
62. Sundaramurthi, P.; Suryanarayanan, R. Calorimetry and Complementary Techniques to Characterize Frozen and Freeze-Dried Systems. *Adv. Drug Deliv. Rev.* **2012**, *64*, 384–395, doi:10.1016/j.addr.2011.12.004.
63. Höhne, G.; Hemminger, W.F.; Flammersheim, H.-J. *Differential Scanning Calorimetry*, 2nd ed.; Springer: Berlin/Heidelberg, Germany, 2003; ISBN 978-3-662-06710-9.
64. Simperler, A.; Kornherr, A.; Chopra, R.; Bonnet, P.A.; Jones, W.; Motherwell, W.D.S.; Zifferer, G. Glass Transition Temperature of Glucose, Sucrose, and Trehalose: An Experimental and in Silico Study. *J. Phys. Chem. B* **2006**, *110*, 19678–19684, doi:10.1021/jp063134t.
65. Richardson, M.J.; Savill, N.G. Derivation of Accurate Glass Transition Temperatures By Differential Scanning Calorimetry. *Rubber Chem. Technol.* **1976**, *49*, 224–232, doi:10.5254/1.3534959.
66. Hancock, B.C.; Zografi, G. The Relationship Between the Glass Transition Temperature and the Water Content of Amorphous Pharmaceutical Solids. *Pharm. Res.* **1994**, *11*, 471–477.

67. Luthra, S.A.; Hodge, I.M.; Pikal, M.J. Effects of Annealing on Enthalpy Relaxation in Lyophilized Disaccharide Formulations: Mathematical Modeling of DSC Curves. *J. Pharm. Sci.* **2008**, *97*, 3084–3099, doi:10.1002/jps.21186.
68. Mizuno, M.; Pikal, M.J. Is the Pre-Tg DSC Endotherm Observed with Solid State Proteins Associated with the Protein Internal Dynamics? Investigation of Bovine Serum Albumin by Solid State Hydrogen/Deuterium Exchange. *Eur. J. Pharm. Biopharm.* **2013**, *85*, 170–176, doi:10.1016/j.ejpb.2013.04.019.
69. Shultz, A.R.; Young, A.L. DSC on Freeze-Dried Poly(Methyl Methacrylate)-Polystyrene Blends. *Macromolecules* **1980**, *13*, 663–668, doi:10.1021/ma60075a034.
70. Wang, B.; Cicerone, M.T.; Aso, Y.; Pikal, M.J. The Impact of Thermal Treatment on the Stability of Freeze-Dried Amorphous Pharmaceuticals: II. Aggregation in an IgG1 Fusion Protein. *J. Pharm. Sci.* **2010**, *99*, 683–700, doi:10.1002/jps.21960.
71. Angell, C. Relaxation in Liquids, Polymers and Plastic Crystals—Strong/Fragile Patterns and Problems. *J. Non. Cryst. Solids* **1991**, *131–133*, 13–31, doi:10.1016/0022-3093(91)90266-9.
72. Reddy, R.; Chang, L.L.; Luthra, S.; Collins, G.; Lopez, C.; Shamblin, S.L.; Pikal, M.J.; Gatlin, L.A.; Shalaev, E. The Glass Transition and Sub-Tg-Relaxation in Pharmaceutical Powders and Dried Proteins by Thermally Stimulated Current. *J. Pharm. Sci.* **2009**, *98*, 81–93.
73. Hodge, I.M.; Berens, A.R. Effects of Annealing and Prior History on Enthalpy Relaxation in Glassy Polymers. 2. Mathematical Modeling. *Macromolecules* **1982**, *15*, 762–770.
74. Thiewes, H.J.; Steeneken, P.A.M. The Glass Transition and the Sub-Tg Endotherm of Amorphous and Native Potato Starch at Low Moisture Content. *Carbohydr. Polym.* **1997**, *32*, 123–130, doi:10.1016/S0144-8617(96)00133-6.
75. Chang, L.; Milton, N.; Rigsbee, D.; Mishra, D.S.; Tang, X.; Thomas, L.C.; Pikal, M.J. Using Modulated DSC to Investigate the Origin of Multiple Thermal Transitions in Frozen 10% Sucrose Solutions. *Thermochim. Acta* **2006**, *444*, 141–147, doi:10.1016/j.tca.2006.03.006.
76. Artiaga, R.; López-Beceiro, J.; Tarrío-Saavedra, J.; Gracia-Fernández, C.; Naya, S.; Mier, J.L. Estimating the Reversing and Non-Reversing Heat Flow from Standard DSC Curves in the Glass Transition Region. *J. Chemom.* **2011**, *25*, 287–294, doi:10.1002/cem.1347.
77. Gill, P.S.; Sauerbrunn, S.R.; Reading, M. Modulated Differential Scanning Calorimetry. *J. Therm. Anal.* **1993**, *40*, 931–939, doi:10.1007/BF02546852.

78. MODULATED DSC® (MDSC®): How Does It Work?. Available online: http://www.tainstruments.com/pdf/literature/MDSC.pdf (accessed on 15 September 2021).
79. Wilkinson, C.J.; Doss, K.; Gulbiten, O.; Allan, D.C.; Mauro, J.C. Fragility and Temperature Dependence of Stretched Exponential Relaxation in Glass-Forming Systems. *J. Am. Ceram. Soc.* **2021**, *104*, 4559–4567, doi:10.1111/jace.17885.
80. Williams, G.; Watts, D.C. Non-Symmetrical Dielectric Relaxation Behaviour Arising from a Simple Empirical Decay Function. *Trans. Faraday Soc.* **1970**, *66*, 80–85, doi:10.1039/TF9706600080.
81. Kohlrausch, R. Theorie Des Elektrischen Rückstandes in Der Leidener Flasche. *Ann. Phys.* **1854**, *167*, 179–214, https://doi.org/10.1002/andp.18541670203.
82. Phillips, J.C. Microscopic Theory of the Kohlrausch Relaxation Constant BK. *J. Non. Cryst. Solids* **1994**, *172–174*, 98–103, doi:10.1016/0022-3093(94)90421-9.
83. Drogoń, A.; Skotnicki, M.; Skotnicka, A.; Pyda, M. Physical Ageing of Amorphous Indapamide Characterised by Differential Scanning Calorimetry. *Pharmaceutics* **2020**, *12*, 800, doi:10.3390/pharmaceutics12090800.
84. Chung, H.-J.; Lim, S.-T. Physical Aging of Glassy Normal and Waxy Rice Starches: Effect of Aging Temperature on Glass Transition and Enthalpy Relaxation. *Carbohydr. Polym.* **2003**, *53*, 205–211, doi:10.1016/S0144-8617(03)00077-8.
85. Pikal, M.J.; Chang, L.; Tang, X. Evaluation of Glassy-State Dynamics from the Width of the Glass Transition: Results from Theoretical Simulation of Differential Scanning Calorimetry and Comparisons with Experiment. *J. Pharm. Sci.* **2004**, *93*, 981–994, doi:10.1002/jps.10582.
86. *Thermometric 2277 Thermal Activity Monitor Instruction Manual*; TA Instruments: New Castle, Dellaware, US, 2008.
87. TAM IV Isothermal Microcalorimeter. Available online: https://www.tainstruments.com/wp-content/uploads/BROCH-TAM-lV.pdf (accessed on 15 September 2021).
88. *Thermometric 2277 Thermal Activity Monitor Service Manual*; TA Instruments: New Castle, Dellaware, US, 2006.
89. Peyron, M.; Pierens, G.K.; Lucas, A.J.; Hall, L.D.; Stewart, R.C. The Modified Stretched-Exponential Model for Characterization of NMR Relaxation in Porous Media. *J. Magn. Reson. Ser. A* **1996**, *118*, 214–220, doi:10.1006/jmra.1996.0029.
90. Van den Mooter, G.; Augustijns, P.; Kinget, R. Stability Prediction of Amorphous Benzodiazepines by Calculation of the Mean Relaxation Time Constant Using the

Williams-Watts Decay Function. *Eur. J. Pharm. Biopharm.* **1999**, *48*, 43–48, doi:10.1016/S0939-6411(99)00013-2.

91. Chieng, N.; Cicerone, M.T.; Zhong, Q.; Liu, M.; Pikal, M.J. Characterization of Dynamics in Complex Lyophilized Formulations: II. Analysis of Density Variations in Terms of Glass Dynamics and Comparisons with Global Mobility, Fast Dynamics, and Positron Annihilation Lifetime Spectroscopy (PALS). *Eur. J. Pharm. Biopharm.* **2013**, *85*, 197–206, doi:10.1016/j.ejpb.2013.03.036.
92. Duddu, S.P.; Zhang, G.; del Monte, P.R. The Relationship Between Protein Aggregation and Molecular Mobility Below the Glass Transition Temperature of Lyophilized Formulations Containing a Monoclonal Antibody. *Pharm. Res.* **1997**, *14*, 596–600, https://doi.org/10.1023/A:1012196826905.
93. Shamblin, S.L.; Hancock, B.C.; Pikal, M.J. Coupling between Chemical Reactivity and Structural Relaxation in Pharmaceutical Glasses. *Pharm. Res.* **2006**, *23*, 2254–2268, doi:10.1007/s11095-006-9080-8.
94. Wang, B.; Tchessalov, S.; Cicerone, M.T.; Warne, N.W.; Pikal, M.J. Impact of Sucrose Level on Storage Stability of Proteins in Freeze-Dried Solids: II. Correlation of Aggregation Rate with Protein Structure and Molecular Mobility. *J. Pharm. Sci.* **2009**, *98*, 3145–3166, doi:10.1002/jps.21622.
95. Luthra, S.A.; Hodge, I.M.; Utz, M.; Pikal, M.J. Correlation of Annealing with Chemical Stability in Lyophilized Pharmaceutical Glasses. *J. Pharm. Sci.* **2008**, *97*, 5240–5251, doi:10.1002/jps.21391.
96. Abdul-Fattah, A.M.; Truong-Le, V.; Yee, L.; Pan, E.; Ao, Y.; Kalonia, D.S.; Pikal, M.J. Drying-Induced Variations in Physico-Chemical Properties of Amorphous Pharmaceuticals and Their Impact on Stability II: Stability of a Vaccine. *Pharm. Res.* **2007**, *24*, 715–727, doi:10.1007/s11095-006-9191-2.
97. Borde, B.; Bizot, H.; Vigier, G.; Buléon, A. Calorimetric Analysis of the Structural Relaxation in Partially Hydrated Amorphous Polysaccharides. II. Phenomenological Study of Physical Ageing. *Carbohydr. Polym.* **2002**, *48*, 111–123, doi:10.1016/S0144-8617(01)00218-1.
98. Zhou, D.; Zhang, G.G.Z.; Law, D.; Grant, D.J.W.; Schmitt, E.A. Physical Stability of Amorphous Pharmaceuticals: Importance of Configurational Thermodynamic Quantities and Molecular Mobility. *J. Pharm. Sci.* **2002**, *91*, 1863–1872, doi:10.1002/jps.10169.

99. Surana, R.; Pyne, A.; Suryanarayanan, R. Effect of Aging on the Physical Properties of Amorphous Trehalose. *Pharm. Res.* **2004**, *21*, 867–874, doi:10.1023/B:PHAM.0000026441.77567.75.
100. Surana, R.; Pyne, A.; Suryanarayanan, R. Effect of Preparation Method on Physical Properties of Amorphous Trehalose. *Pharm. Res.* **2004**, *21*, 1167–1176, doi:10.1023/B:PHAM.0000033003.17251.c3.
101. Bhugra, C.; Rambhatla, S.; Bakri, A.; Duddu, S.P.; Miller, D.P.; Pikal, M.J.; Lechuga-Ballesteros, D. Prediction of the Onset of Crystallization of Amorphous Sucrose Below the Calorimetric Glass Transition Temperature from Correlations with Mobility. *J. Pharm. Sci.* **2007**, *96*, 1258–1269, doi:10.1002/jps.20918.
102. Bhugra, C.; Pikal, M.J. Role of Thermodynamic, Molecular, and Kinetic Factors in Crystallization From the Amorphous State. *J. Pharm. Sci.* **2008**, *97*, 1329–1349, doi:10.1002/jps.21138.
103. Grzybowska, K.; Capaccioli, S.; Paluch, M. Recent Developments in the Experimental Investigations of Relaxations in Pharmaceuticals by Dielectric Techniques at Ambient and Elevated Pressure. *Adv. Drug Deliv. Rev.* **2016**, *100*, 158–182, doi:10.1016/j.addr.2015.12.008.
104. Vollrath, I. Controlled Nucleation and Heat Flux Measurements as Innovative Technologies for Freeze-Drying. Ph.D. Thesis, Ludwig Maximilian University of Munich, Munich, Germany, 2018.
105. Gitter, J.H.; Geidobler, R.; Presser, I.; Winter, G. A Comparison of Controlled Ice Nucleation Techniques for Freeze-Drying of a Therapeutic Antibody. *J. Pharm. Sci.* **2018**, *107*, 2748–2754, doi:10.1016/j.xphs.2018.07.019.
106. Lo Presti, K.; Friess, W. Adjustment of Specific Residual Moisture Levels in Completely Freeze-Dried Protein Formulations by Controlled Spiking of Small Water Volumes. *Eur. J. Pharm. Biopharm.* **2021**, (under review).
107. Schersch, K.; Betz, O.; Garidel, P.; Muehlau, S.; Bassarab, S.; Winter, G. Systematic Investigation of the Effect of Lyophilizate Collapse on Pharmaceutically Relevant Proteins, Part 2: Stability During Storage at Elevated Temperatures. *J. Pharm. Sci.* **2012**, *101*, 2288–2306, doi:10.1002/jps.23121.
108. Beezer, A.E.; Hills, A.K.; O'Neill, M.A.A.; Morris, A.C.; Kierstan, K.T.E.; Deal, R.M.; Waters, L.J.; Hadgraft, J.; Mitchell, J.C.; Connor, J.A.; et al. The Imidazole Catalysed Hydrolysis of Triacetin: An Inter- and Intra-Laboratory Development of a Test Reaction for Isothermal Heat Conduction Microcalorimeters Used for Determination of Both

Thermodynamic and Kinetic Parameters. *Thermochim. Acta* **2001**, *380*, 13–17, doi:10.1016/S0040-6031(01)00629-3.

109. Hills, A.K.; Beezer, A.E.; Connor, J.A.; Mitchell, J.C.; Wolf, G.; Baitalow, F. Microcalorimetric Study of a Proposed Test Reaction—The Imidazole Catalysed Hydrolysis of Triacetin. Temperature and Imidazole Concentration Dependence. *Thermochim. Acta* **2002**, *386*, 139–142, doi:10.1016/S0040-6031(01)00773-0.
110. Angberg, M.; Nyström, C.; Castensson, S. Evaluation of Heat-Conduction Microcalorimetry in Pharmaceutical Stability Studies (1) Precission and Accuracy for Static Experiments in Glass Vials. Available online: http://www.tainstruments.com/pdf/M142.pdf. (accessed on 15 September 2021).
111. Aso, Y.; Yoshioka, S.; Kojima, S. Relationship between the Crystallization Rates of Amorphous Nifedipine, Phenobarbital, and Flopropione, and Their Molecular Mobility as Measured by Their Enthalpy Relaxation and 1H NMR Relaxation Times. *J. Pharm. Sci.* **2000**, *89*, 408–416, doi:10.1002/(sici)1520-6017(200003)89:3<408::aid-jps11>3.0.co;2-%23.

Chapter II Aim and objective of the thesis

As introduced in Chapter I, calorimetric investigations of the amorphous matrix and its α-relaxations were presented as a useful tool to investigate and predict long-term stability of pharmaceutical products in the past. However, most of the investigations were performed with small molecules or pure API formulations. Only a few publications report data concerning multi-component systems and even less data dealt with freeze-dried protein formulations. With the rising number of biological formulations in form of proteins, mRNA or viruses that need to be lyophilized, there is an urgent need to understand amorphous protein containing matrices more deeply and how their stability can be controlled. The correlation of formulation stability with α-relaxations at an early state after the lyophilization process can help to predict the long-term product behavior without the need of time-consuming stability studies. With this knowledge, the development of freeze-drying cycles could be improved to achieve lyophilization protocols that result in short process times to save time and costs but also lead to long-term stable protein formulations. More detailed, the main objectives of the studies in this dissertation are:

1. We want to achieve more knowledge about the factors influencing relaxation in the context of freeze-drying. The relaxation behavior of the freeze-dried matrix can e.g. be controlled by the freezing-step, a quite different factor than temperature to change α-relaxations. The effect of variations in the freezing step has been studied experimentally in chapter III. In freeze-drying processes more parameters can be controlled like pressure, ice morphology and residual moisture. Variations in pressure were used in chapter IV to induce structural collapse, ice morphology was investigated as a factor in chapter III and residual moisture in chapter I.

2. We want to correlate α-relaxation times with unwanted events that can happen in a freeze-dried product. Crystallization during storage is one of these events. Every amorphous matrix will sooner or later crystallize because the crystal, in contrast to the amorphous state, is in a thermodynamic equilibrium. Thus, it is expectable that α-relaxations, releasing energy excess of the amorphous state, correlate with crystallization phenomena and this is investigated more deeply in chapter III. By using different freezing protocols, a different relaxation and crystallization behavior of sucrose and trehalose based formulations was achieved. Furthermore, different amounts of polysorbate 20 were utilized to accelerate crystallization in sucrose based formulations. The crystallization times were then correlated with the relaxation times.

3. Tempering of already dried matrices is the common way to increase α-relaxation times. Thereby, unwanted phenomena like protein aggregation or matrix crystallization should be reduced. In chapter IV we included such tempering processes already in the freeze-drying cycles. This should reduce time and energy consumption of the process. Above all, tempering the matrix with these gentle conditions should reduce the initial amount of protein aggregates at t(0). Harsh freeze-drying protocols up to structural collapse of the solid matrix were utilized and in comparison with two "classical" tempering protocols the long-term stability of an IgG_1-antibody against aggregation was investigated. To determine the correlation of aggregation rates with α-relaxation times graphical plots were created.

4. To verify the relevance of correlating α-relaxations with the aggregation rate of an IgG_1-antibody we furthermore study in chapter IV if the correlations that can be drawn in the laboratory scale would be transferable to industrial processes. Very stable and practically relevant formulations of the IgG_1-antibody are used and shall show whether even small differences in the protein aggregation rate can be predicted with α-relaxation times.

5. Besides the main research questions a number of pre-experiments shall be presented in chapter V. Here, the behavior of semi-crystalline matrices is investigated, microwave radiation as possible alternative tempering method is studied and the effect of polymers on the quality of formulation matrix relaxation and their correlations with stability should be investigated.

Chapter III Prediction of Unwanted Crystallization of Freeze-Dried Protein Formulations Using α-Relaxation Measurements

This chapter is published as: Groël, S.; Menzen, T.; Winter, G. (2023). Prediction of Unwanted Crystallization of Freeze-Dried Protein Formulations Using α-Relaxation Measurements. *Pharmaceutics* 2023, 15, 703.

This article belongs to the Special Issue Amorphous Drug Formulations: Progress, Challenges and Perspectives.

Note from the authors: To establish a coherent numbering and pagination within this document the numbers of references, figures and tables were adapted. Apart the minor changes, the version included in this thesis is identical with the published article.

The published article can be accessed online via:

https://doi.org/10.3390/pharmaceutics15020703

III.1 Abstract

There is a lack of methods to predict the isothermal crystallization behavior of amorphous freeze-dried formulations stored below the glass transition temperature. This study applies isothermal microcalorimetry to predict long-term crystallization during product storage time. The relaxation curve of a fresh sample recorded within 12 h after lyophilization is correlated with the long-term crystallization time at the same temperature. Storage conditions of 25 °C and 40 °C are examined and five model formulations containing either sucrose or trehalose with different concentrations of an IgG_1 antibody are investigated. The amorphous formulations were created by different freeze-drying processes only differing in their freezing step (random nucleation; additional annealing step of 1.5 h and 3 h, controlled nucleation; quench cooling). Samples that crystallized during the study time of 12 months showed a promising correlation between their relaxation time and crystallization behavior upon storage. Furthermore, the study shows that polysorbate 20 strongly accelerates crystallization of sucrose and that the freezing step itself has a strong impact on the relaxation phenomena that is not levelled out by primary and secondary drying.

Keywords: amorphous pharmaceuticals; crystallization; differential scanning calorimetry (DSC); freeze-drying; isothermal microcalorimetry (IMC); molecular mobility

III.2 Introduction

The amount of biological therapeutics has strongly increased in recent years [1]. Those entities face degradation problems during shipment and long-term storage when kept in their liquid formulation [2]. Thus, freeze- or spray-drying can be used to achieve long-term stability of these products upon removal of water [3,4]. To successfully freeze-dry those materials, sugars, such as sucrose or trehalose, are used as bulking agents and lyoprotectants [5]. Those excipients are able to protect and sustain the structure of biotherapeutics, including antibodies [6]. In particular, sugars can mimic water with their hydroxyl groups, thereby supporting the native conformation of the antibody upon lyophilization based on the water replacement theory [7,8]. To fulfil this stabilizing effect, the sugar has to stay amorphous during the storage time of the product [9,10]. However, during storage, crystallization of sugars can occur, even if the storage temperature is significantly below the glass transition temperature (T_g) [11]. Therefore, it is important to avoid crystallization of the excipients during the lifetime of the pharmaceutical formulation [12]. Consequently, methods that predict crystallization in the early stage of development are needed to dis- cover formulations and process conditions that are prone to result in crystallization upon storage, which frequently lasts up to 2 years or more [11,13,14].

Differential scanning calorimetry (DSC) is one method to estimate the crystallization tendency of a formulation [15]. With this method, the T_g and its onset as well as the energy of crystallization above T_g can be determined [16]. Of course, the onset of crystallization measured above T_g can be used as a surrogate for isothermal crystallization tendencies, but dominant reactions at high temperatures, especially above T_g, are not always the leading reactions at lower temperatures below T_g [17]. Particularly in glasses where Arrhenius kinetics cannot be applied, this could lead to incorrect predictions [18].

Another method is X-ray Powder Diffraction (XRD), where an X-ray diffractogram of the freeze-dried product is recorded. An absence of clear reflection peaks is proof for a fully amorphous sample, as an ordered structure, such as a crystal, is necessary to diffract the beam in a well-defined angle [19]. This method is the standard approach to monitor the recent status of a sample, but has no predictive potential [20–23].

Below T_g, structural relaxation phenomena are successfully used as general stabil- ity predicting factors for amorphous formulations [24,25]. One possibility to quantify relaxation processes is isothermal microcalorimetry (IMC) [26]. Here, α-relaxations can be estimated from a measured curve decay of a freshly prepared glass within a few days [27]. The curve shape can be fitted with equation III.1 (see below) and expressed as the relaxation time τ^{β} [h]. The higher the

energy excess is, the smaller the relaxation time τ^{β} [h] will be and the more degradation reactions, including crystallization, can happen [25]. Thus, the theory is to create amorphous formulations with as little energy excess as possible, which results in a high value of τ^{β}. A detailed explanation and derivation of τ^{β} can be found elsewhere [25,28]. It should be pointed out that relaxation measurements are only suitable for process optimization with the same formulation. The excipients have a strong impact on product behavior, affecting multiple properties, and thus cannot be captured by α-relaxation measurements alone [28].

In earlier crystallization studies considering α-relaxations, single-component systems with either sucrose as the excipient [18,24] or non-protein active pharmaceutical ingredients (APIs), such as nifedipine [18,29], were utilized. Furthermore, most of the studies attempt to predict the onset of crystallization at the temperature of interest with relaxation measurements at other temperatures. In this study, in a first step, protein-free multi-component placebo formulations created by freeze-drying are investigated to verify that the prediction of crystallization in mixed formulations is possible at all. In a second step, an IgG_1 antibody as API is added to the formulations. In both concepts, the systems were studied with IMC and after long-term storage.

In addition, a second question is targeted by this study. Most of the changes in the relaxation behavior of amorphous samples are explained with their different thermal history compared to a reference sample [30–32]. To investigate this, if the freezing step of a lyophilization process has an impact on the relaxation behavior of the final product, different freeze-drying protocols that only differ in their freezing step are applied (random nucleation; additional annealing step of 1.5 h and 3 h, controlled nucleation; quench cooling). Although the freezing step itself could be considered a thermal treatment, as the amorphous phase is shielded by the frozen water and no drying process is happening, it is possible that these effects are levelled off later by the thermal history introduced by primary and secondary drying.

Five different formulations are used to investigate if and how the prediction of isothermal crystallization is possible. Three formulations with a low antibody content of 2 mg/mL with different polysorbate 20 (PS20) concentrations ranging from 0–1.6 mg/mL, a formulation with a high antibody content of 50 mg/mL, and a formulation containing trehalose are studied. The different amounts of PS20 in the first three samples are considered to accelerate crystallization despite a low residual moisture content [33]. A high protein concentration of 50 mg/mL is used to investigate if the model is applicable for more challenging protein/sugar ratios and trehalose is utilized as another sugar with a higher T_g compared to sucrose.

III.3 Materials and Methods

III.3.1 Preparations of Formulations

An IgG1 antibody (LMU1) was utilized as a model protein. It was purified with a Sepharose HiTrap SP column (Cytiva, Marlborough, MA, USA) with an ÄKTA protein purification system (Cytiva, Marlborough, MA, USA) to remove polysorbate 20 (PS20) from the bulk starting material. The elution buffer was exchanged with a cross-flow filtration unit MinimateTM TFF capsule with an omega polyethersulfone (PES) membrane (MW 30,000 Da; Pall Corporation, New York, NY, USA) by using a 7-fold excess of 20 mM histidine buffer pH 5.5 (Alfa Aesar, Ward Hill, MA, USA). After the process, the concentration of LMU1 was determined with a NanoDropTM 2000 UV photometer (Thermo Fisher Scientific, Waltham, MA, USA). Stock solutions of the further excipients, D-(+)-trehalose dihydrate (VWR International, Radnor, PA, USA), sucrose (Sigma-Aldrich, Steinheim, Germany), and polysorbate 20 (PS20) (Croda, Edison, NJ, USA), were created and mixed with the LMU1 solution to produce the formulations according to Table III.1. Finally, the formulations were filtered using a 0.22-µm PES Sartolab®RF vacuum filter unit (Sartorius AG, Goettingen, Germany) before filling 1 mL solution in 2 R vials (MGlas AG, Muennerstadt, Germany). The vials were semi-stoppered with West 13-mm Lyo Nova Pure RS 1356 4023/50 G stoppers (West Pharmaceutical Services, Inc., Exton, PA, USA) and placed on a freeze-drying tray with two rows of placebo-filled vials as the outer radiation shield.

Table III.1 Used formulations. Concentrations given in mg/mL.

Excipient	2 mg/mL 00PS_Suc	2 mg/mL 04PS_Suc	2 mg/mL 16PS_Suc	50 mg/mL 16PS_Suc	2 mg/mL 04PS_Tre
LMU1	2	2	2	50	2
sucrose	79.45	79.45	79.45	79.45	-
trehalose	-	-	-	-	79.45
PS20	-	0.4	1.6	1.6	0.4

III.3.2 Freeze-Drying Protocols

Five freeze-drying processes only differing in their freezing steps are applied. The freezing protocols are presented in Table III.2 and Figure III.1.

Table III.2 Applied freezing protocols during the lyophilization process.

Process	Step Number [#]	Shelf Temperature [°C]	Hold Time [h]	Ramp Rate of the Shelf towards the Next Step [K/min]
RN	1	20	-	−1
	2	−5	1.00	−1
	3	−45	1.50	*
AN1.5	1	20	-	−1
	2	−5	1.00	−1
	3	−45	1.50	+1
	4	−20	1.50	−1
	5	−45	1.50	*
AN3.0	1	20	-	−1
	2	−5	1.00	−1
	3	−45	1.50	+1
	4	−20	3.00	−1
	5	−45	1.50	*
CN	1	20	-	−1
	2	−5	1.00	†
	3	−5	2.00	−1
	4	−45	1.50	*
QN	1	20	-	quenching
	2	−196 ‡	0.03	-
	3	−45	1.500	*

* indicates the start of primary drying.† Indicates the controlled nucleation process by introduction of ice fog. ‡ estimated temperature of a liquid nitrogen bath [34].

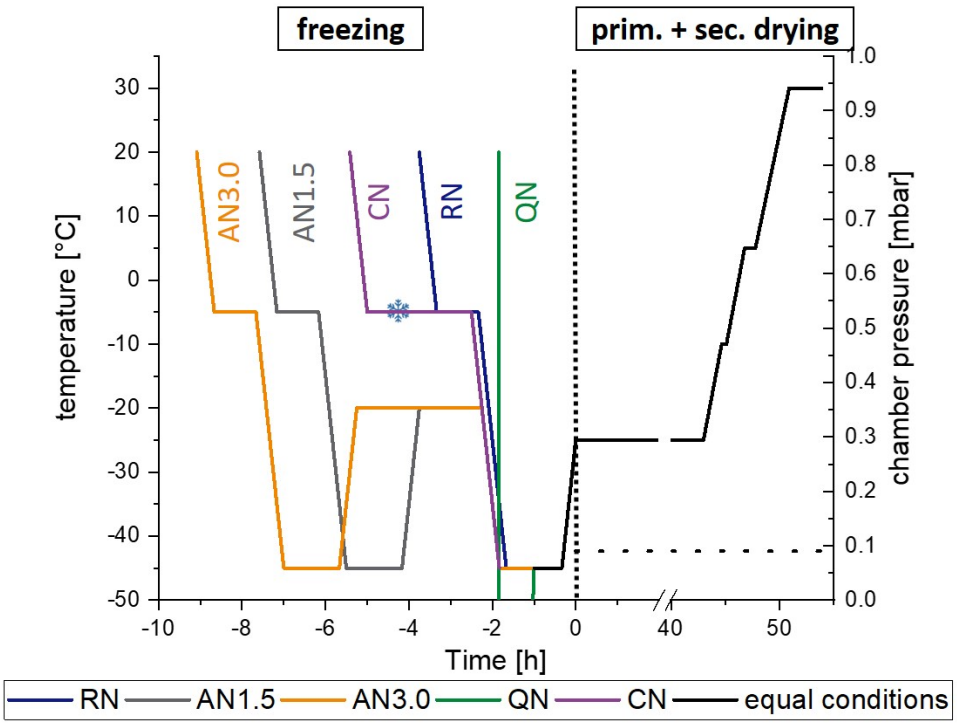

Figure III.1 Graphical scheme of the different freezing processes. The snowflake in the CN curve indicates the introduction of ice crystals in the chamber after equilibration at −5 °C. The dotted line separates the freezing step from the drying process. RN, random nucleation; AN1.5, additional annealing step of 1.5 h; AN3.0, additional annealing step of 3.0 h; CN, controlled nucleation; QN, quench cooling. Solid lines represent the temperature in °C and the dashed line the chamber pressure.

To initiate primary drying, the temperature was ramped with 1 K/min from −45 °C to −25 °C and a pressure of 0.09 mbar was set. Primary drying was conducted for 48 h. For secondary drying, the shelves were ramped to 30 °C with a rate of 0.15 K/min including a holding time at −10 °C for 0.5 h and at 5 °C for 1 h. The final temperature of 30 °C was held for 4 h before the vials were stoppered under a nitrogen atmosphere. The freeze-drying was performed with a Christ ε2-6D laboratory-scale freeze-dryer (Martin Christ Gefriertrocknungsanlagen GmbH, Osterode am Harz, Germany) and a LyoCoN system (Martin Christ Gefriertrocknungsanlagen GmbH, Osterode am Harz, Germany) was utilized for a controlled nucleation process via ice fog. The complete freeze-drying protocols are displayed in Figure III.1.

III.3.3 Residual Moisture Content

The residual moisture content in [% (*w/w*)] was determined by coulometric Karl Fischer Titration. The samples were ground with a spatula under a controlled atmosphere with a humidity <10% and 10–30 mg was transferred to a new 2 R Vial. The vials were heated in an oven to 100 °C, which allows the water to evaporate and be transferred by a dry gas stream into

the measurement cell. The residual moisture content was calculated by dividing the measured mass of water by the transferred sample mass.

III.3.4 Differential Scanning Calorimetry

To determine the T_g [°C] and the $\Delta H_r(\infty)$ [J/g], a Mettler Toledo DSC 821e (Mettler Toledo, Gießen, Germany) differential scanning calorimeter was used. The values are obtained by using a modulated scanning mode with a heating rate of 2 K/min, a period of 2 min, and an amplitude of 1 K. To extract the data, the resulting signal was transformed in a reversing, non-reversing, and total curve. The reversing curve was used to define the values for the relaxation calculation whereas the total curve was used to investigate the crystallization peak. Sample preparation was conducted in a controlled atmosphere with a humidity <10%. In total, 5–15 mg sample were transferred to an aluminum crucible and hermetically sealed. An empty reference pan was prepared that stayed in the instrument for all measurements.

III.3.5 Isothermal Microcalorimetry (To Determine τ^{β})

A LKB 2277 Thermal Activity Monitor (TAM) equipped with 4 mL ampoule twin cylinders (2277-201) (TA Instruments, New Castle, DE, USA) was used to determine the α-relaxation times of the lyophilizates. The samples were transferred to stainless steel measuring ampoules in a controlled atmosphere with a humidity <10%. Approximately 150 mg pooled (from more than one glass vial to reach the required amount) samples were used. The reference ampoule remained empty. The measurement and reference ampoule were first lowered to the thermal equilibrium position and held for 15 min to allow equilibration. Both ampoules were then slowly lowered to the measurement position of the TAM. The experiments were performed at 25 °C and 40 °C. Data points were collected with an interval of 2 s for the first hour of the measurement and afterwards in a 10 s interval. The duration of the measurement was 12 h. The obtained curve was fitted in OriginPro 2019b with the modified stretch exponential function as suggested by Pikal and Kawakami (Equation (III.1)) [25]. The start parameters are set to $\tau_0 = 2$, $\tau_1 = 1$, and $\beta = 0.1$ and further conditions are $\tau_0 > \tau_1$ as well as $0 < \beta \leq 1$.

$$P = 277.8 \times \frac{\Delta H_r(\infty)}{\tau_0} \times \left(1 + \frac{\beta t}{\tau_1}\right) \times \left(1 + \frac{t}{\tau_1}\right)^{\beta-2} \times \exp\left[-\left(\frac{t}{\tau_0}\right) \times \left(1 + \frac{t}{\tau_1}\right)^{\beta-1}\right] \quad \text{(III.1)}$$

$$\text{with } \Delta H_r(\infty) = \left(T - T_g\right) \times c_p$$

III.3.6 Specific Surface Area

With a Brunauer-Emmet-Teller (BET) krypton gas adsorption instrument (Autosorb 1; 3P-Instruments, Odelzhausen, Germany), the specific surface area of the samples (SSA) was determined. The samples were ground with a spatula in a controlled atmosphere with a humidity

<10% and 80–100 mg sample were transferred to measurement glass tubes. Outgassing was performed at room temperature for at least 2 h and the measured curve was fitted by the Autosorb 1 software.

III.3.7 2.7. X-ray Powder Diffraction

The absence of crystals in the freshly prepared samples was verified with a Rigaku MiniFlex benchtop XRD instrument (Rigaku Corporation, Tokyo, Japan). A copper anode at 40 kV and 15 mA was used to generate CuKα radiation (λ = 0.15417 nm). The freeze-dried samples were ground with a spatula under a controlled atmosphere with a humidity <10% and transferred to a silica sample holder. Powder diffraction was measured ranging from 3° to 60° 2θ in 0.02° measurement intervals with a speed of 10°/min.

III.3.8 Procedure to Correlate Crystallization with Relaxation Time τ^{β}

To correlate the crystallization of the samples at 25 °C and 40 °C, the relaxation time τ^{β} [h] is plotted with the crystallization time during storage in [h]. To determine the latter, two procedures were carried out. For fast crystallizing samples (placebo formulations and 2 mg/mL_1.6PS_Suc at 40 °C), the samples were left in the IMC instrument until a crystallization peak occurred. The peak was confirmed as a crystallization event by subsequent DSC and XRD measurements. Here, the peak maximum was used as the crystallization time.

For all other samples that would block the IMC instrument too long, weekly DSC measurements of sample aliquots were performed. The changes in the crystallization peak above T_g (onset and enthalpy) were tracked and compared with the measurements performed the weeks before. The onset temperature of this peak was recorded and plotted. The reduction of the onset temperature above T_g also indicates an ongoing crystallization at the storage temperature of 25 °C below T_g.

III.4 Results

III.4.1 Macroscopic and Microscopic Appearance

Macroscopic and microscopic pictures of the 2 mg/mL_16PS_Suc are presented in Figure III.2. They are representative for all formulations.

(**a**)

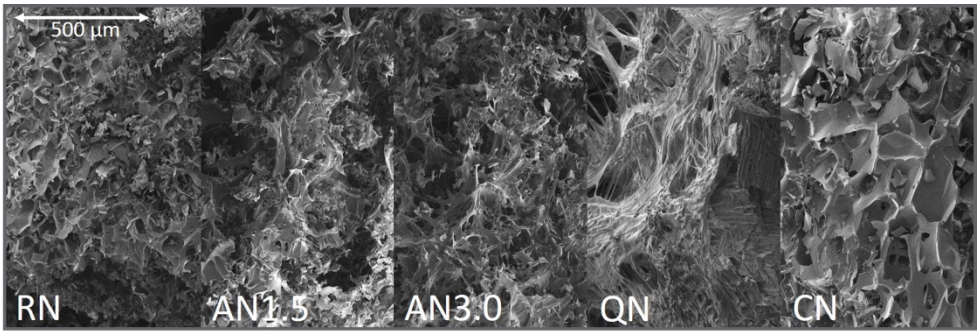

(**b**)

Figure III.2. Representative optical appearance of 2 mg/mL_1.6PS_Suc samples: (**a**) macroscopic appearance and (**b**) scanning electron microscopy. Processes from left to right: RN, random nucleation; AN1.5, additional annealing step of 1.5 h; AN3.0, additional annealing step of 3.0 h; CN, controlled nucleation; QN, quench cooling.

III.4.2 Residual Moisture

The residual moisture levels of the products are presented in Table III.3. Additionally, the RN, QN, and CN processes from the 2 mg/mL_1.6PS_Suc formulation were equalized in their residual moisture content, as described by Lo Presti and Frieß [35]. The comparison with the untreated samples is presented in Table III.4. Overall, the CN process leads to the highest residual moisture content whereas the QN process leads to products with the lowest level of residual moisture. The processes RN, AN1.5, and AN3.0 only slightly differ in their water content and no clear trend can be found. For the formulations containing sucrose and 2 mg/mL IgG_1, no effect of the amount of PS20 on residual moisture can be observed. The 50 mg/mL_1.6PS_Suc and 2 mg/mL_0.4PS_Tre samples are drier after the RN, AN1.5, AN3.0, and QN processes compared to the other samples. Only after CN do they retain a water content comparable to the other formulations.

Table III.3 Residual moisture levels of the freeze-dried formulations in [% *w/w*]. $n = 2$, values represent the mean value and the corresponding standard deviation.

Excipient	2 mg/mL 00PS_Suc	2 mg/mL 04PS_Suc	2 mg/mL 16PS_Suc	50 mg/mL 16PS_Suc	2 mg/mL 04PS_Tre
RN	1.04 ± 0.03	0.84 ± 0.06	0.70 ± 0.06	0.31 ± 0.02	0.28 ± 0.05
AN1.5	0.90 ± 0.02	0.77 ± 0.07	0.85 ± 0.13	0.39 ± 0.04	0.36 ± 0.02
AN3.0	0.85 ± 0.00	0.93 ± 0.04	0.85 ± 0.01	0.35 ± 0.02	0.33 ± 0.03
QN	0.41 ± 0.04	0.49 ± 0.14	0.55 ± 0.02	0.17 ± 0.06	0.13 ± 0.01
CN	1.45 ± 0.10	1.42 ± 0.12	1.35 ± 0.02	1.34 ± 0.01	1.59 ± 0.22

Table III.4 Comparison of residual moisture levels of the original and moisture equilibrated 2 mg/mL_1.6PS_Suc samples in [% *w/w*]. $n = 2$, values represent the mean value and the corresponding standard deviation.

Process	Original	Moisture Equilibrated
RN	0.70 ± 0.06	1.30 ± 0.14
QN	0.55 ± 0.02	1.15 ± 0.16
CN	1.35 ± 0.02	1.36 ± 0.12

III.4.3 Specific Surface Area (SSA)

The values for the SSA of the samples can be found in Table III.5. The results are similarly clustered as for residual moisture. The biggest differences between processes are obtained between CN and QN, with CN having the lowest and QN the highest SSA. The other processes result in quite similar surfaces. Between formulations, the biggest differences can be found comparing the 2 mg/mL_0.4PS_Tre formulation and the 50 mg/mL_1.6PS_Suc formulation with the remaining formulations, with all 2 mg/mL_Suc samples having lower SSA values for the RN, AN1.5, and AN3.0 process. Additionally, the SSA for 50 m/mL_1.6PS_Suc formulations were significantly higher in QN and lower in CN than all other formulations.

Table III.5 Specific surface area of the created formulations in [m^2g^{-1}]. $n = 1$, two samples were pooled in one measuring tube to reach the needed sample mass.

Excipient	2 mg/mL 00PS_Suc	2 mg/mL 04PS_Suc	2 mg/mL 16PS_Suc	50 mg/mL 16PS_Suc	2 mg/mL 04PS_Tre
RN	0.455	0.552	0.563	0.714	0.665
AN1.5	0.404	0.594	0.549	0.747	0.739
AN3.0	0.528	0.574	0.506	0.726	0.616
QN	1.080	0.982	0.914	2.270	0.982
CN	0.328	0.313	0.241	0.157	0.389

III.4.4 Differential Scanning Calorimetry Results

Table III.6 shows the T_g values of the freeze-dried formulations. The complete DSC results with Δc_p, $\Delta H_r(\infty)$ at 25 °C and 40 °C as well as the onset and enthalpy of crystallization are not presented. They are considered in the calculation of the relaxation data and are presented in Appendix A to improve the clarity of the publication.

Table III.6 Glass transition temperatures of the freeze-dried formulations [°C]. n = 2, values represent the mean value and the corresponding standard deviation.

Excipient	2 mg/mL 00PS_Suc	2 mg/mL 04PS_Suc	2 mg/mL 16PS_Suc	50 mg/mL 16PS_Suc	2 mg/mL 04PS_Tre
RN	60.21 ± 0.04	62.26 ± 2.73	62.27 ± 2.93	80.32 ± 0.04	104.46 ± 0.09
AN1.5	60.09 ± 0.03	64.10 ± 1.41	60.19 ± 1.74	84.14 ± 0.24	104.09 ± 0.04
AN3.0	60.16 ± 0.04	62.09 ± 2.74	60.01 ± 2.47	80.31 ± 0.42	104.08 ± 0.16
QN	72.03 ± 0.06	66.20 ± 3.19	64.05 ± 3.06	84.14 ± 0.42	106.51 ± 0.23
CN	48.98 ± 0.08	50.45 ± 2.67	48.29 ± 3.11	63.82 ± 0.70	100.11 ± 0.11

III.4.5 X-ray Powder Diffraction

Absence of crystallinity was shown by XRD for all freshly freeze-dried formulations. The onset of crystallization estimated by IMC and DSC was reviewed by XRD measurements.

III.4.6 Isothermal Microcalorimetry

The measured relaxation curves as well as the calculated τ^{β}- values are shown in Figures III.3 and III.4 for 40 °C and 25 °C, respectively. The CN-samples show the shortest relaxation time in all samples over all tested temperatures. The order of relaxation times of the remaining samples varies depending on temperature and formulation with the QN process having, in most cases, the longest relaxation time.

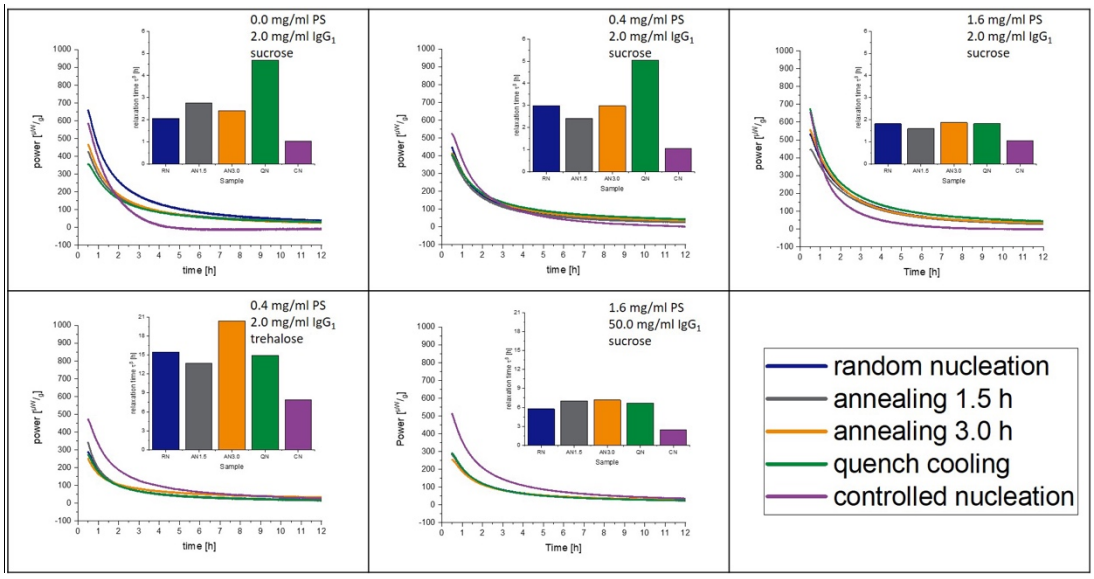

Figure III.3 Relaxation curves obtained from IMC at 40 °C over 12 h.

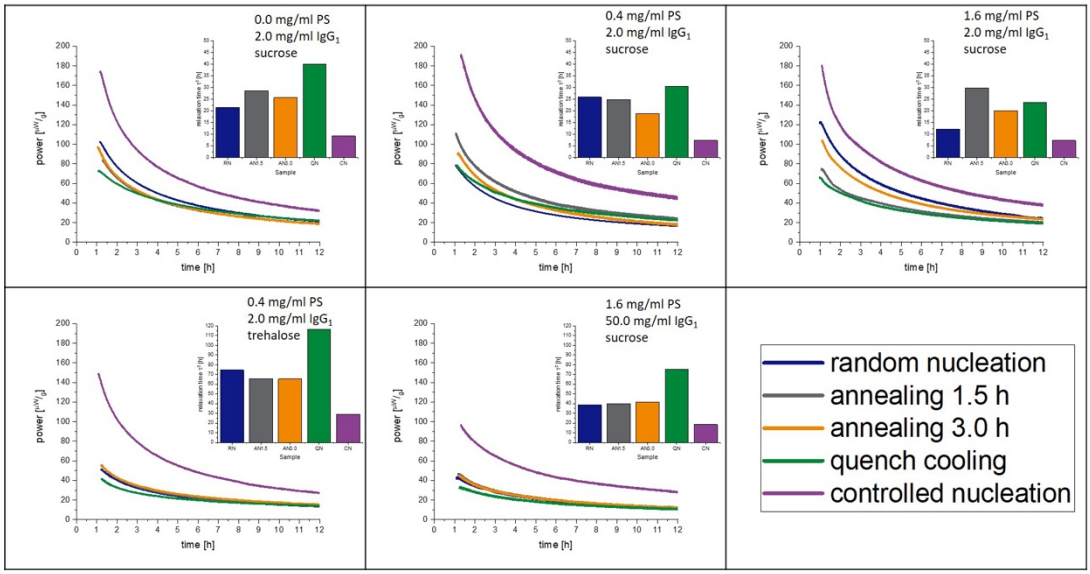

Figure III.4 Relaxation curves obtained from IMC at 25 °C over 12 h.

III.5 Discussion

All freeze-drying processes with the different freezing steps resulted in acceptable dry products. Results from product temperature monitoring can be found in Appendix B. The microscopic and macroscopic appearance, as well as the SSA, indicated that the freezing steps resulted in products with different morphology, as desired. It was expected for the controlled nucleation (CN) samples to have the largest pores (Figure III.2), but lower overall surface area [36,37]. During drying, bigger pores remain, which lead to faster primary drying, but to less effective secondary drying as the SSA is relatively low [38,39]. In the QN process, on the other hand, plenty of very small ice nuclei arise [40]. Thus, the QN process leads to very small pores and an overall high SSA (Table III.5). The RN process can be considered as in-between and ends up with an intermediate SSA. The AN1.5 and AN3.0 processes increase the time for ice nuclei to grow but this trend was not observed in our samples [41,42]. The reason might be that the annealing conditions of −20 °C with a time of only 1.5 or 3.0 h were too short and not high enough in temperature to allow stronger effects. Recent trends in the community are suggesting more “aggressive” annealing conditions close to the eutectic temperature at −4 °C over more than 5 h [43], but were not yet applied in our study.

The trends seen for the structure of the cakes are clearly connected with the residual moisture content of the samples. After primary drying, about 10–15% bound water remains in the amorphous phase of the formulation, which is then removed in secondary drying [44,45]. Here, formulations with a higher SSA will dry much faster. Therefore, applying the same secondary drying conditions leads to a higher residual moisture level in the CN samples compared to the QN samples. The differences in residual moisture impact α-relaxations [31] as well as

crystallization [46]. When searching for a correlation of α-relaxation with crystallization, differences in residual moisture should not matter as both effects should be equally influenced if a correlation exists. However, to answer the question what impact the freezing step has on α-relaxations is a challenge. Water, as a plasticizer, strongly affects the T_g [31] of the freeze-dried cake and, with this, also α–relaxations. For this reason, it is not possible, without further intervention, to separate the effects of the freezing step and residual moisture. Thus, the changes in measured α-relaxations could emerge from the changes in residual moisture alone. To overcome this challenge, two approaches can be applied. The secondary drying for samples with a lower SSA could be prolonged or an equalizing procedure by moisture adaption (as described by Lo Presti & Frieß) could be applied [35]. The first option would change the thermal history and can therefore not be utilized. The second option is too time-consuming to be applied for an entire 12-month stability study sample set. Therefore, a pre-test study was performed on the 1.6PS_Suc placebo formulation without protein, considered as a sample with a high and fast crystallization tendency. This approach shall give insight whether the correlation of α-relaxation with crystallization is possible.

III.5.1 Placebo Formulation Pre-Test

Figure III.5 shows the result of this pre-test. A similar approach had already been published but had not been evaluated concerning the crystallization tendency [28]. The residual moisture of the samples is around 1.3 ± 0.2% after moisture equalization and is considered as equal [28,31]. It can be seen in Figure III.5 that the freezing step has a clear influence on the relaxation, with CN having the shortest relaxation time and QN the longest. RN and AN1.5 are in between. The annealing time of 1.5 h at −20 °C was not long enough to introduce stronger effects. Thus, in the following main study, an annealing step of 3.0 h was added. Nevertheless, the crystallization of the samples occurs qualitatively exactly in the order of the relaxation times, with CN being the first sample to crystallize, followed by AN1.5, RN, and with QN being the last. A reasonable linear correlation between relaxation times and onset of crystallization with $r^2 = 0.88$ can be found. Moreover, it is remarkable that the relaxation curve of CN samples shows a different shape than the other curves. In the beginning, besides the expected crystallization peak, a second exothermal peak maximum is obtained at 0.58 h followed by an endothermal valley lasting from 2–5 days of measurement. A similar observation was made for foam-dried [30] samples as well as for tempered and CN samples [28]. The use of controlled ice nucleation seems to introduce similar effects in the lyophilized matrix as a tempering procedure or the heat applied during foam drying.

Overall, the freezing step itself and residual moisture are two separate factors influencing the relaxation behavior and the impact of the freezing step is not levelled off by the drying step. Importantly, a correlation of α-relaxation with crystallization was observed and shall now be investigated more deeply in protein-containing samples.

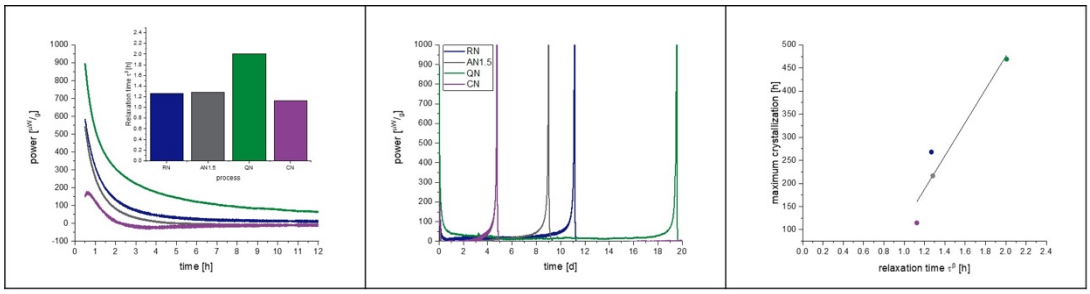

Figure III.5 Placebo pre-tests at 40 °C to examine the correlation of crystallization with α-relaxation and the effect of the freezing step on the latter. The left picture presents a zoomed in area of the IMC measurement to focus on the relaxation curves, which are converted to a τ^{β}-value. The middle graph shows the full view of the measurement including the crystallization of the samples. On the right, the correlation of relaxation time with crystallization maximum of the IMC curves is presented. The correlation coefficient of the fit is $r^2 = 0.88$. Random nucleation (blue), additional annealing step of 1.5 h (grey), quench cooling (green), controlled nucleation (purple).

III.5.2 Protein-Containing Samples Equalized for Residual Moisture

Based on the data in section 4.1, the residual moisture was only adapted for a small group of samples to see if a correlation between relaxation and crystallization also exists in protein-containing matrices. The moisture adapted samples are 2.0 mg/mL_1.6PS_Suc processed by freeze-drying with RN, CN, and QN. Table III.4 shows the residual moisture data of these samples before and after adaption.

With protein formulations, a correlation coefficient of $r^2 = 0.92$ can be obtained by a linear fit of relaxation with crystallization time. With moisture adaption, the correlation coefficient increased to a value of $r^2 = 0.96$ (Figure III.6). We are aware of the fact that a linear correlation with three data points is statistically not robust. However, the pre-tests with placebo and protein-containing samples with moisture adaption were performed to generate a first insight into the relation of relaxation, crystallization, freezing step, and residual moisture (Figure III.7). For this purpose, a limited number of samples was sufficient and justified to set up a bigger study with more processes and formulations. Before we delve into the findings of the main study, we want to summarize what has been found so far:

- The freezing step influences the residual moisture directly by determining the pore size of the formulation [36,37]. Furthermore, the freezing step influences α-relaxation directly by changes in the amorphous phase as well as indirectly by the residual moisture. Both effects are independent from each other.
- The residual moisture influences the α-relaxation and crystallization directly by plastization of the solid phase [31]. The effect on α-relaxation and crystallization is proportional.
- α-relaxation and crystallization below T_g correlate not only in single-component but also in multi-component systems. The addition of 2 mg/mL of protein changes the crystallization behavior of the product (Figures III.5 and III.6), but the correlation of α-relaxation and crystallization remains.

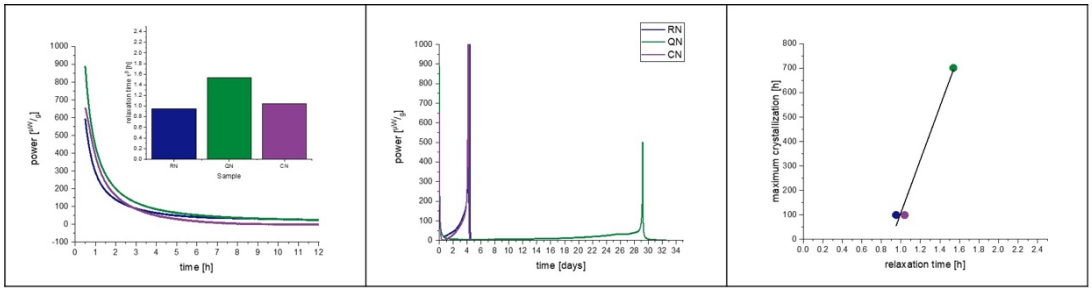

Figure III.6 Moisture equalized samples from the 2 mg/mL_1.6PS_Suc formulation at 40 °C, correlation of crystallization with α-relaxation, and the effect of the freezing step. The left picture presents a zoomed in area of the IMC measurement to focus on the relaxation curves, which are converted to a τ^{β}-value. The middle graph shows the full view of the measurement including the crystallization of the samples. On the right, the correlation of relaxation time with crystallization maximum of the IMC curves is presented. The correlation coefficient of the fit is $r^2 = 0.96$. Random nucleation (blue), quench cooling (green), controlled nucleation (purple).

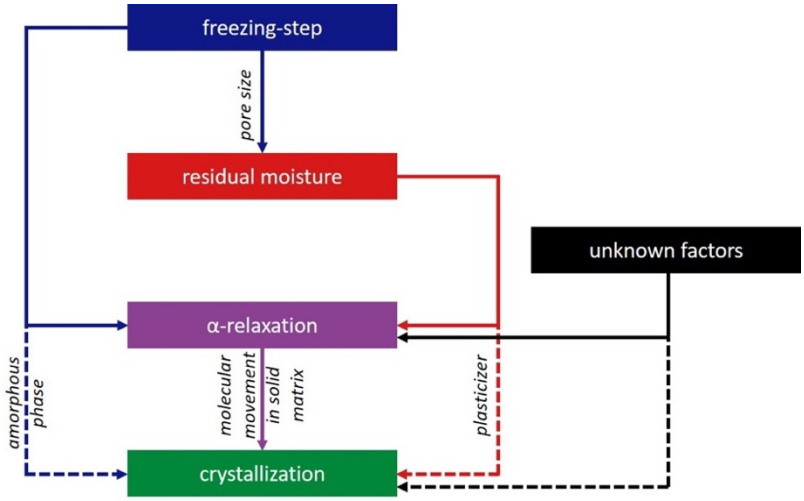

Figure III.7 Graphical scheme of the correlation of the investigated parameters. Solid lines were verified by the pre-tests; dashed lines are effects that seem to be proportional to the connected solid line according to the pre-tests.

All in all, several effects that influence the crystallization tendency of a dry amorphous cake below T_g also influence the α-relaxation in a proportional way. Thus, to determine the crystallization tendency of a formulation, it appears suitable to use α-relaxation as the leading parameter. The hypothesis is that α-relaxation is the only factor that is changed by all factors that affect crystallization and can display those changes introduced by a freeze-drying process in a predictive measurement.

III.5.3 Protein-Containing Samples

Although the correlation of α-relaxations with crystallinity is the focus of the study, three further functional aspects can be observed from the investigations of the protein samples. One is the effect of PS20 on the crystallization of sucrose in lyophilized solids, which can be analyzed by the 2gl_Suc formulations with the different amounts of PS20. Next, the effect of protein concentration on α-relaxations can be attained by comparing 2gl_1.6PS_Suc with 50gl_1.6PS_Suc. Last, the influence of the sugar itself on τ^{β} and the T_g by comparing the 2gl_0.4_Suc with 2gl_0.4PS_Tre can be obtained.

During the investigation period of 12 months, the 2 mg/mL_1.6PS_Suc samples crystallized isothermally at 25 °C and 40 °C, respectively. The 2 mg/mL_0.4PS_Suc formulation from the CN process crystallized at 40 °C, but not at 25 °C. All other process/formulation combinations led to samples that stayed amorphous (Table III.7).

Table III.7 Sample status after 12 months. X = crystallized during storage; - = still amorphous after 12 months.

Process	2 mg/mL 00PS_Suc		2 mg/mL 04PS_Suc		2 mg/mL 16PS_Suc		50 mg/mL 16PS_Suc		2 mg/mL 04PS_Tre	
	25 °C	40 °C	25 °C	40 °C	25 °C	40 °C	25 °C	40 °C	25 °C	40 °C
RN	-	-	-	-	X	X	-	-	-	-
AN1.5	-	-	-	-	X	X	-	-	-	-
AN3.0	-	-	-	-	X	X	-	-	-	-
QN	-	-	-	-	X	X	-	-	-	-
CN	-	-	-	X	X	X	-	-	-	-

From these observations we conclude the following. First, PS20 accelerates crystallization of sucrose. All samples with 2 mg/mL protein and 1.6 mg/mL PS20 crystallized. The only sample with a PS20 concentration below 1.6 mg/mL that crystallized was the 2 mg/mL_0.4PS_Suc formulation from the CN process at 40 °C storage. Here, the significantly higher residual moisture resulting from the CN process was the reason (Table III.3). In contrast, the corresponding sample without PS20 was still amorphous. The mechanism behind the acceleration of crystallization itself is not clear. Factors such as T_g, SSA, and residual moisture were ruled out as they are approximately the same within all the respective samples. The PS20 concentrations of 0.4 mg/mL and 1.6 mg/mL are both far above the critical micelle

concentration (CMC) of PS20 [47–49]. It is possible that micelles of PS20 could act as crystallization nuclei for sucrose. More micelles present in the 1.6 mg/mL PS20 formulation could consequently lead to faster crystallization.

Second, even small changes in excipient composition can change the physical properties of the matrix and some are not detectable with α-relaxation measurements. Concerning the relaxation time τ^{β}, the 2 mg/mL_0.0PS_Suc sample and the 2 mg/mL_1.6_PS_Suc sample are very similar (relaxation time of 1.03 h and 1.04 h, respectively), but evidently, they crystallize at different timepoints upon storage.

Third, a high protein concentration prevents crystallization of the matrix. Whether proteins act as a "binding partner" to PS20 and inhibit the crystallization accelerating effect of the surfactant or whether it is a result of the higher T_g (Table III.6, approx. + 20 °C for 50 mg/mL compared to 2 mg/mL) cannot be answered.

Figure III.8 shows the correlation of α-relaxation and crystallization of the 2 mg/mL_1.6PS_Suc samples at 40 °C. In all formulations, except CN, the rise of the crystallization peak started very slowly, and two peaks are observed. The double peaks (maxima 29.0 d and 32.3 d for RN; 21.8 d and 25.9 d for AN1.5; 19.0 d and 21.2 d for AN3.0; 18.3 d and 20.8 d for QN) arise through the pooling of samples from different vials to reach the minimum amount of 150 mg for IMC measurement. There are certain differences of 2 to 5 days between single vials regarding crystallization time. It is assumed that such differences between samples always exist, but in this case, were carved out through the slow crystallization. The crystallization in Section 4.2 was fast and differences within the pooled samples were so small that they were not observed. In long-term stability studies with drawing times of 1 and 3 months, a crystallization time difference of 5 days would of course not be detectable.

As the onset of crystallization is not directly detectable in the IMC, the maximum crystallization is used to correlate relaxation with crystallization. With $r^2 = 0.58$, the quality of the fit is not as good as in the pre-test, but still indicates a strong correlation. The relaxation times τ^{β} are very close to each other, ranging from approximately 1–5 h. Within the sample set of 2 mg/mL_1.6PS_Suc, this means a 1 h difference in relaxation time τ^{β} corresponds to a shift of 601.35 h (25 days) in crystallization.

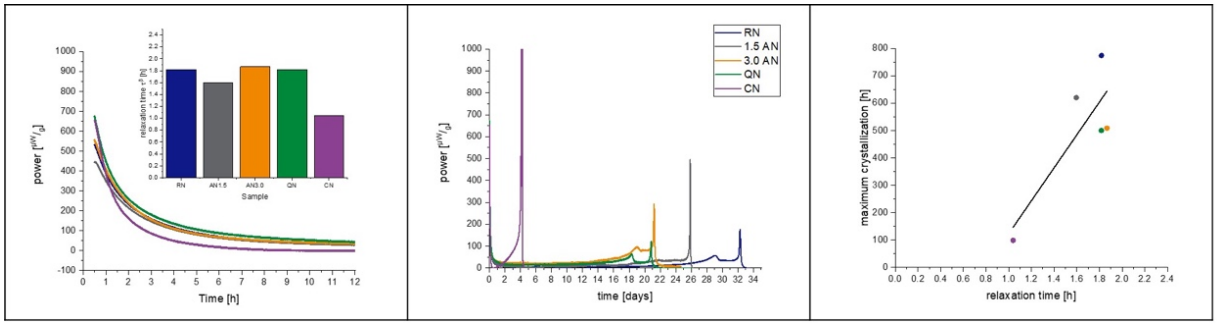

Figure III.8 Samples from the 2 mgmL_1.6PS_Suc formulation at 40 °C; correlation of crystallization with α-relaxation, and the effect of the freezing step. The left picture presents a zoomed in area of the IMC measurement to focus on the relaxation curves, which are converted to a τ^{β}-value. The middle graph shows the full view of the measurement including the crystallization of the samples. On the right, the correlation of relaxation time with crystallization maximum of the IMC curves is presented. The correlation coefficient of the fit is $r^2 = 0.58$. Random nucleation (blue), additional annealing step of 1.5 h (grey), additional annealing step of 3.0 h (orange), quench cooling (green), controlled nucleation (purple).

Nevertheless, at least a qualitative correlation was found, which is very useful if samples from different processes shall be compared for maintaining their amorphous state during long-term storage.

Taking the same samples at a 25 °C storage temperature into account, the order of sample crystallization changed (Figure III.9).

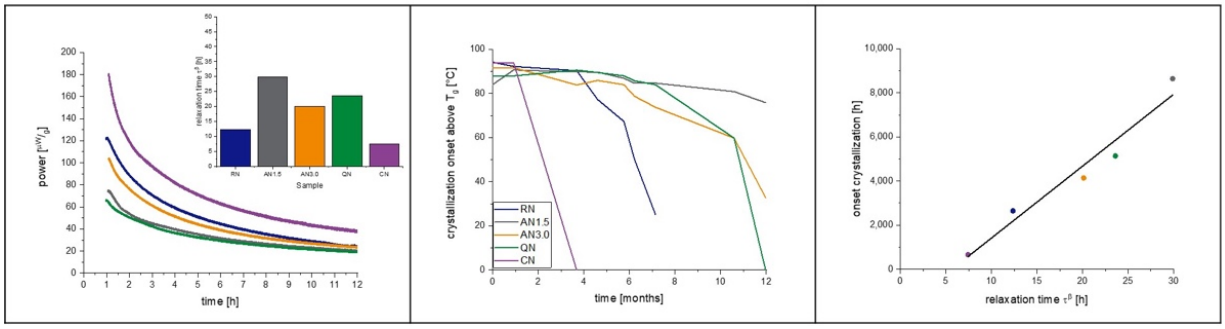

Figure III.9 Samples from the 2 mgmL_1.6PS_Suc formulation at 25 °C; correlation of crystallization with α-relaxation, and the effect of the freezing step. The left picture presents a zoomed in area of the IMC measurement to focus on the relaxation curves, which are converted to a τ^{β}-value. The middle graph shows the crystallization onset of the samples at 25 °C determined with DSC measurement using the onset of crystallization above T_g. On the right, the correlation of relaxation time with crystallization onset is presented. The correlation coefficient of the fit is $r^2 = 0.94$. Random nucleation (blue), additional annealing step of 1.5 h (grey), additional annealing step of 3.0 h (orange), quench cooling (green), controlled nucleation (purple).

Comparing the prediction performance of the IMC with the relaxation time τ^{β} method at 25 °C with 40 °C qualitatively, it must be noted that at 40 °C, only one sample was correctly predicted. In contrast, at 25 °C, all five samples were correctly predicted in the order of crystallization with a correlation coefficient of $r^2 = 0.94$.

In summary, at 40 °C, relaxation times are so close to each other that despite good resolution of the instrument, discrimination between the very small differences in relaxation of the samples is at its limits. At 25 °C, the resolution is high enough to measure the differences.

III.5.4 Comparison of IMC and DSC as Methods for Crystallization Prediction

Comparing the results of the IMC and the DSC, the following can be concluded. At 25 °C, the IMC data has a much better performance than the DSC-based methods. Through the theory of global α-relaxations, it is understood that the IMC method detects more factors that influence crystallization than DSC measurements do. Furthermore, the behavior of glasses significantly changes at T_g making correlations and predictions from experiments above T_g with crystallization below T_g difficult [11,17]. As presented, the order of crystallization of the different samples changed from the 40 °C storage to 25 °C storage temperature. Simultaneously, the order of relaxation times also changed within the corresponding samples. The relaxation method is hence able to detect these changes whereas DSC, in contrast, shows the same; one DSC curve must be used for predictions at 25 °C and 40 °C storage (Figure III.10). Isothermal microcalorimetry and α-relaxation determination is therefore a useful tool to predict crystallization under different storage conditions. It must be kept in mind, though, that for the calculation of τ^{β}-values, T_g values from DSC measurements are necessary.

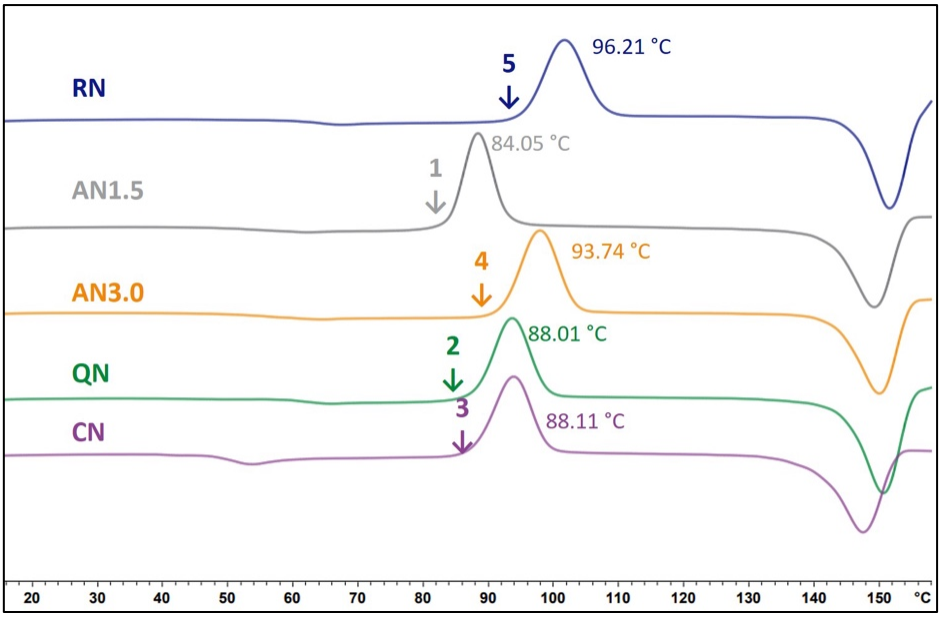

Figure III.10 DSC thermograms of the 2 mg/mLg_1.6PS_Suc formulations. Processes as indicated at the corresponding curve. The temperature in °C displays the onset of crystallization temperature. The numbers rank the order of crystallization onset, starting with the first sample that starts to crystallize.

III.5.5 Influence of PS20 on Relaxation and Crystallization

The present study supports the observation of Vollrath et al. [33]. That PS20 accelerates the crystallization of lyophilized amorphous sucrose matrices. Reasons for this phenomenon were already discussed above. Moreover, an influence of PS20 on the relaxation behavior had been observed in earlier studies [28]. Figures III.11 and III.12 show the change in relaxation times depending on the PS20 concentration. An increase in the PS20 concentration led to a reduction in relaxation time τ^{β}. This effect is more prone in the QN samples and least in the CN samples. From the aspect that PS20 is surface active, a connection with surface effects is very plausible, as QN samples have the highest and CN samples the lowest SSA. As seen in Table III.6, the T_g temperatures of the formulation did not significantly change with change in PS20 concentration, but the relaxation time did. Thus, it can be concluded that PS20 has a matrix effect on the formulation that is not captured in the T_g.

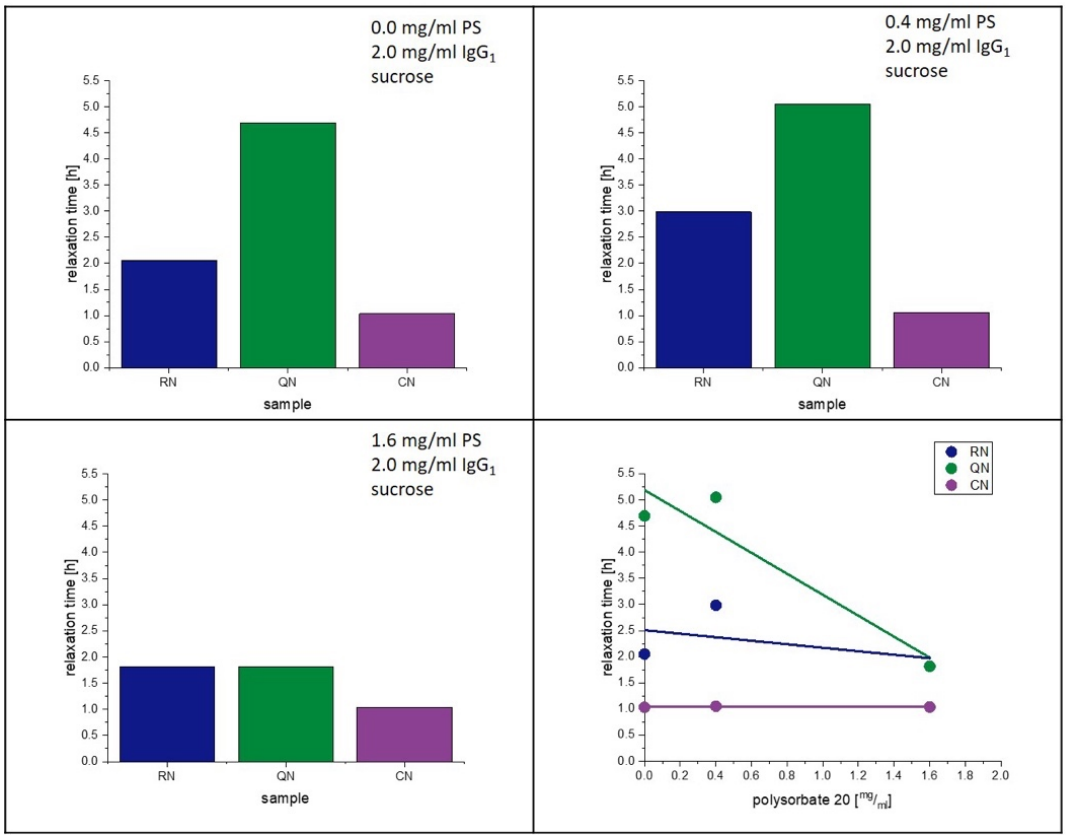

Figure III.11 Influence of polysorbate on relaxation at 40 °C.

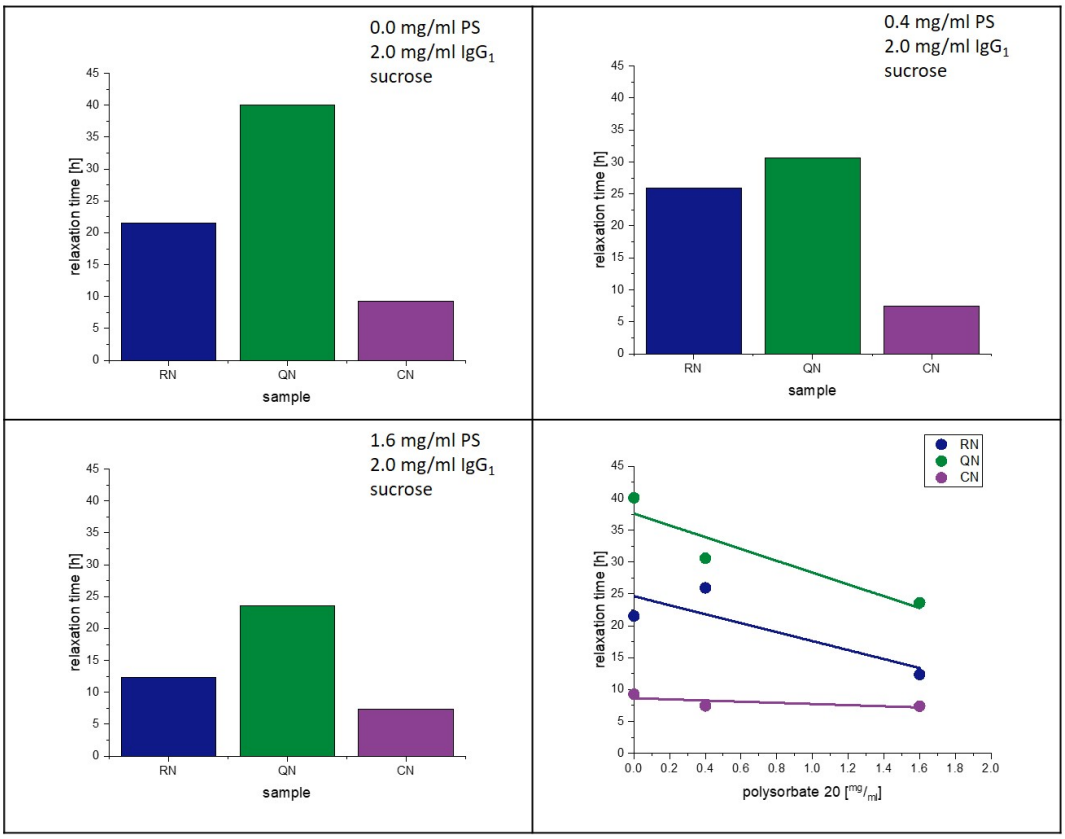

Figure III.12 Influence of polysorbate on relaxation at 25 °C.

III.6 Conclusions

It is possible to predict the isothermal crystallization of protein-containing freeze-dried formulations below T_g by measuring the α-relaxation time, τ^{β}, when certain conditions are fulfilled. Only different processes of the same formulation can be compared. A comparison of different formulations is not possible because the impact of formulation compositions overpowers the impact of the process on the matrix's relaxation behavior. PS20 accelerates the crystallization of sucrose-based lyophilizates. The mechanism was not part of the study; however, it is important to emphasize that higher amounts of PS20 should be used with care. The presented method is not intended to replace DSC measurements and shall be used as an add-on. IMC could predict, at an early development stage, whether a certain lyophilization process would lead to a more or less stable product concerning crystallization over months. The standard analytics of DSC or XRD used during real-time stability studies are unable to deliver such predictive information.

Author Contributions: Conceptualization, G.W. and S.G.; methodology, S.G., T.M. and G.W.; investigation, S.G.; resources, G.W.; data curation, S.G.; writing—original draft preparation, S.G.; writing—review and editing, T.M. and G.W.; visualization, S.G.;

supervision, T.M. and G.W.; project administration, G.W. All authors have read and agreed to the published version of the manuscript.

Funding: This research received no external funding.

Data Availability Statement: Data are contained within the article.

Acknowledgments: The authors would like to thank Elena Richert for checking the manuscript for language and comprehensibility.

Conflicts of Interest: Tim Menzen is employed at Coriolis Pharma Research GmbH and has no financial interest to disclaim. The other authors declare no conflict of interest.

III.7 Appendix

III.7.1 Appendix A

The following Tables III.A1–III.A5 display the further calorimetric results that were left out in the main section of the publication due to clarity.

Table III.A1 Calorimetric data of the 2gl_0.0PS_Suc [°C]. *n* = 2, values represent the mean value and the corresponding standard deviation.

	RN	AN1.5	AN3.0	QN	CN
T_g [°C]	60.21 ± 0.04	60.09 ± 0.03	60.16 ± 0.04	72.03 ± 0.06	48.98 ± 0.08
Δc_p [$Jg^{-1}K^{-1}$]	0.55 ± 0.02	0.42 ± 0.05	0.52 ± 0.08	0.46 ± 0.04	0.51 ± 0.06
$\Delta H_\infty(25°C)$ [Jg^{-1}]	19.21 ± 0.72	14.81 ± 1.76	18.18 ± 2.82	21.45 ± 1.90	12.33 ± 1.46
$\Delta H_\infty(40°C)$ [Jg^{-1}]	11.02 ± 0.41	8.48 ± 1.01	10.42 ± 1.62	14.61 ± 1.29	4.62 ± 0.55
crystallization onset [°C]	97.20 ± 2.57	100.10 ± 0.42	101.65 ± 0.25	119.90 ± 0.28	91.96 ± 1.10
crystallization energy [Jg^{-1}]	70.48 ± 0.95	66.47 ± 0.30	71.20 ± 7.71	62.66 ± 2.31	64.15 ± 1.09

Table III.A. Calorimetric data of the 2gl_0.4PS_Suc [°C]. n = 2, values represent the mean value and the corresponding standard deviation.

	RN	AN1.5	AN3.0	QN	CN
T_g [°C]	62.26 ± 2.73	64.10 ± 1.41	62.09 ± 2.74	66.20 ± 3.19	50.45 ± 2.67
Δc_p [$Jg^{-1}K^{-1}$]	0.52 ± 0.12	0.62 ± 0.02	0.560 ± 0.03	0.48 ± 0.07	0.52 ± 0.10
$\Delta H_\infty(25°C)$ [Jg^{-1}]	19.23 ± 5.21	24.04 ± 0.95	20.73 ± 2.07	19.92 ± 3.79	13.14 ± 3.31
$\Delta H_\infty(40°C)$ [Jg^{-1}]	11.49 ± 3.12	14.82 ± 0.58	12.35 ± 1.23	12.67 ± 2.41	5.40 ± 1.36
crystallization onset [°C]	103.87 ± 5.53	106.15 ± 2.84	96.80 ± 1.31	99.23 ± 6.61	87.15 ± 1.10
crystallization energy [Jg^{-1}]	66.75 ± 1.54	74.32 ± 0.29	69.41 ± 1.00	68.74 ± 1.10	62.69 ± 1.10

Table III.A3 Calorimetric data of the 2gl_1.6PS_Suc [°C]. *n* = 2, values represent the mean value and the corresponding standard deviation.

	RN	AN1.5	AN3.0	QN	CN
T_g [°C]	62.27 ± 2.93	60.19 ± 1.74	60.01 ± 2.47	64.05 ± 3.06	48.29 ± 3.11
Δc_P [$Jg^{-1}K^{-1}$]	0.54 ± 0.02	0.47 ± 0.03	0.57 ± 0.01	0.29 ± 0.01	0.44 ± 0.01
$\Delta H_\infty(25°C)$ [Jg^{-1}]	20.20 ± 1.85	16.64 ± 1.54	20.04 ± 0.90	11.13 ± 0.92	10.14 ± 0.93
$\Delta H_\infty(40°C)$ [Jg^{-1}]	12.07 ± 1.10	9.55 ± 0.88	11.45 ± 0.51	6.85 ± 0.57	3.61 ± 0.33
crystallization onset [°C]	96.21 ± 2.83	84.05 ± 1.16	93.74 ± 0.26	88.01 ± 1.54	88.11 ± 2.86
crystallization energy [Jg^{-1}]	64.79 ± 0.04	57.62 ± 1.23	62.42 ± 1.23	60.85 ± 0.98	63.68 ± 3.02

Table III.A4 Calorimetric data of the 50gl_1.6PS_Suc [°C]. *n* = 2, values represent the mean value and the corresponding standard deviation.

	RN	AN1.5	AN3.0	QN	CN
T_g [°C]	80.32 ± 0.04	84.14 ± 0.24	80.31 ± 0.42	84.14 ± 0.42	63.82 ± 0.70
Δc_P [$Jg^{-1}K^{-1}$]	0.30 ± 0.01	0.34 ± 0.10	0.31 ± 0.02	0.33 ± 0.02	0.40 ± 0.02
$\Delta H_\infty(25°C)$ [Jg^{-1}]	16.71 ± 0.63	20.05 ± 5.97	16.76 ± 1.10	19.58 ± 1.28	15.37 ± 0.72
$\Delta H_\infty(40°C)$ [Jg^{-1}]	12.18 ± 0.46	14.96 ± 4.46	12.21 ± 0.80	14.61 ± 0.96	9.43 ± 0.44
crystallization onset [°C]	†	†	†	†	†
crystallization energy [Jg^{-1}]	†	†	†	†	†

† No crystallization observed in the range of the measurement

Table III.A5 Calorimetric data of the 2gl_0.4PS_Tre [°C]. *n* = 2, values represent the mean value and the corresponding standard deviation.

	RN	AN1.5	AN3.0	QN	CN
T_g [°C]	104.46 ± 0.09	104.09 ± 0.04	104.08 ± 0.16	106.51 ± 0.23	100.11 ± 0.11
Δc_p [$Jg^{-1}K^{-1}$]	0.46 ± 0.07	0.47 ± 0.01	0.41 ± 0.01	0.41 ± 0.02	0.52 ± 0.01
$\Delta H_\infty(25°C)$ [Jg^{-1}]	36.59 ± 5.37	36.82 ± 0.97	32.06 ± 0.89	33.66 ± 1.70	39.36 ± 0.79
$\Delta H_\infty(40°C)$ [Jg^{-1}]	29.68 ± 4.36	29.83 ± 0.78	25.98 ± 0.72	27.47 ± 1.39	31.50 ± 0.64
crystallization onset [°C]	†	†	†	†	†
crystallization energy [Jg^{-1}]	†	†	†	†	†

† No crystallization observed in the range of the measurement

III.7.2 Appendix B

The freezing steps conducted in the freeze-dryer were monitored by pressure and temperature sensors. Figure III.B1 displays the first 10 h of the RN and CN process, respectively. The freezing of the products is proven by the rise of temperature, which is caused from the heat of the ice nucleation process and emphasized in the figure by grey arrows. Absence of a second temperature peak is evidence that the samples were kept frozen after the ice nucleation without incomplete freezing or intermediate melting. Furthermore, the position of the peak demonstrates that the products of the RN process did not freeze during the equilibration step whereas the products of the CN process started to freeze immediately after the pressure drop and rise at approximately 1.5 h which introduces the ice fog in the chamber. The freezing step of the AN1.5 and AN3.0 process are equal to the RN process. The nucleation of the QN samples were not monitored due to practical reasons and safety during the freezing procedure. An absence of an ice nucleation in the freeze dryer indicates a successful freezing of the sample.

The actual cooling rate of the products themselves after freezing were determined by a linear fit during the ramp after nucleation resulting in a cooling rate of − 0.85 K/min for RN, AN1.5 as well as AN3.0 and − 0.75 K/min for CN samples.

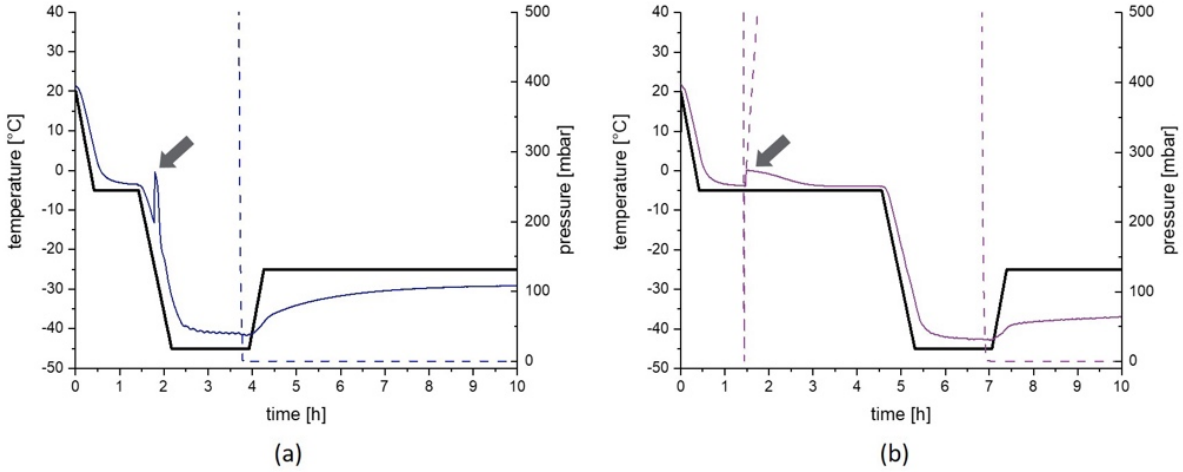

Figure III.B1. Monitoring of freezing of the products. The first 10 h of the random nucleation process (a) and the controlled nucleation process (b) are presented. The black line represents the temperature set point for the shelfs, the colored solid lines the actual product temperature and the dashed line the chamber pressure. Arrows demonstrate the ice nucleation process. The pressure drop and rise at approximately 1.5 h in the controlled nucleation is needed to introduce the ice fog in the chamber.

III.8 Reference

1. Mullard, A. 2020 FDA drug approvals. *Nat. Rev. Drug Discov.* **2021**, *20*, 85–90. https://doi.org/10.1038/d41573-021-00002-0.
2. Chi, E.Y.; Krishnan, S.; Randolph, T.W.; Carpenter, J.F. Physical stability of proteins in aqueous solution: Mechanism and driving forces in nonnative protein aggregation. *Pharm. Res.* **2003**, *20*, 1325–1336. https://doi.org/10.1023/A:1025771421906.
3. Carpenter, J.F.; Pikal, M.J.; Chang, B.S.; Randolph, T.W. Rational design of stable lyophilized protein formulations: Some practical advice. *Pharm. Res.* **1997**, *14*, 969–975. https://doi.org/10.1023/a:1012180707283.
4. Carpenter, J.F.; Chang, B.S.; Garzon-Rodriguez, W.; Randolph, T.W. Rational design of stable lyophilized protein formulations: Theory and practice. *Pharm. Biotechnol.* **2002**, *13*, 109–133. https://doi.org/10.1007/978-1-4615-0557-0_5.
5. Pyne, A.; Surana, R.; Suryanarayanan, R. Crystallization of mannitol below Tg' during freeze-drying in binary and ternary aqueous systems. *Pharm. Res.* **2002**, *19*, 901–908. https://doi.org/10.1023/A:1016129521485.
6. Costantino, H.R. Excipients for Use in Lyophilized Pharmaceutical Peptide, Protein and other Bioproducts. In *Lyophilization of Biopharmaceuticals*; AAPS Press: Arlington, VA, USA, 2004; pp. 139–228, ISBN 0971176760.

7. Allison, S.D.; Chang, B.; Randolph, T.W.; Carpenter, J.F. Hydrogen bonding between sugar and protein is responsible for inhibition of dehydration-induced protein unfolding. *Arch. Biochem. Biophys.* **1999**, *365*, 289–298. https://doi.org/10.1006/abbi.1999.1175.
8. Cicerone, M.T.; Douglas, J.F. β-Relaxation governs protein stability in sugar-glass matrices. *Soft Matter* **2012**, *8*, 2983. https://doi.org/10.1039/c2sm06979b.
9. Liu, J.; Rigsbee, D.R.; Stotz, C.; Pikal, M.J. Dynamics of pharmaceutical amorphous solids: The study of enthalpy relaxation by isothermal microcalorimetry. *J. Pharm. Sci.* **2002**, *91*, 1853–1862. https://doi.org/10.1002/jps.10181.
10. Pikal, M.J.; Rigsbee, D.R. The stability of insulin in crystalline and amorphous solids: Observation of greater stability for the amorphous form. *Pharm. Res.* **1997**, *14*, 1379–1387. https://doi.org/10.1023/a:1012164520429.
11. Shamblin, S.L.; Tang, X.; Chang, L.; Hancock, B.C.; Pikal, M.J. Characterization of the Time Scales of Molecular Motion in Pharmaceutically Important Glasses. *J. Phys. Chem. B* **1999**, *103*, 4113–4121. https://doi.org/10.1021/jp983964%2B.
12. Cicerone, M.T.; Tellington, A.; Trost, L.; Sokolov, A. Substantially Improved Stability of Biological Agents in Dried Form. *BioProcess Int.*, **2003**, *1, 36-47.*
13. Liu, J. Physical characterization of pharmaceutical formulations in frozen and freeze-dried solid states: Techniques and applications in freeze-drying development. *Pharm. Dev. Technol.* **2006**, *11*, 3–28. https://doi.org/10.1080/10837450500463729.
14. Cleland, J.L.; Lam, X.; Kendrick, B.; Yang, J.; Yang, T.; Overcashier, D.; Brooks, D.; Hsu, C.; Carpenter, J.F. A specific molar ratio of stabilizer to protein is required for storage stability of a lyophilized monoclonal antibody. *J. Pharm. Sci.* **2001**, *90*, 310–321. https://doi.org/10.1002/1520-6017(200103)90:3<310:AID-JPS6>3.0.CO;2-R.
15. Kedward, C.J.; MacNaughtan, W.; Blanshard, J.M.V.; Mitchell, J.R. Crystallization Kinetics of Lactose and Sucrose Based On Isothermal Differential Scanning Calorimetry. *J. Food Sci.* **1998**, *63*, 192–197.
16. Chieng, N.; Teo, X.; Cheah, M.H.; Choo, M.L.; Chung, J.; Hew, T.K.; Keng, P.S. Molecular Dynamics and Physical Stability of Pharmaceutical Co-amorphous Systems: Correlation Between Structural Relaxation Times Measured by Kohlrausch-Williams-Watts With the Width of the Glass Transition Temperature (ΔTg) and the Onset of Crystallization. *J. Pharm. Sci.* **2019**, *108*, 3848–3858. https://doi.org/10.1016/j.xphs.2019.09.013.

17. Pikal, M.J.; Dellerman, K.M. Stability testing of pharmaceuticals by high-sensitivity isothermal calorimetry at 25 °C: Cephalosporins in the solid and aqueous solution states. *Int. J. Pharm.* **1989**, *50*, 233–252. https://doi.org/10.1016/0378-5173(89)90127-0.
18. Bhugra, C.; Shmeis, R.; Krill, S.L.; Pikal, M.J. Predictions of onset of crystallization from experimental relaxation times I-correlation of molecular mobility from temperatures above the glass transition to temperatures below the glass transition. *Pharm. Res.* **2006**, *23*, 2277–2290. https://doi.org/10.1007/s11095-006-9079-1.
19. Surana, R.; Suryanarayanan, R. Quantitation of crystallinity in substantially amorphous pharmaceuticals and study of crystallization kinetics by X-ray powder diffractometry. *Powder Diffr.* **2000**, *15*, 2–6. https://doi.org/10.1017/S0885715600010757.
20. Kim, A.I.; Akers, M.J.; Nail, S.L. The physical state of mannitol after freeze-drying: Effects of mannitol concentration, freezing rate, and a noncrystallizing cosolute. *J. Pharm. Sci.* **1998**, *87*, 931–935. https://doi.org/10.1021/js980001d.
21. Iurian, S.; Bogdan, C.; Tomuță, I.; Szabó-Révész, P.; Chvatal, A.; Leucuța, S.E.; Moldovan, M.; Ambrus, R. Development of oral lyophilisates containing meloxicam nanocrystals using QbD approach. *Eur. J. Pharm. Sci.* **2017**, *104*, 356–365. https://doi.org/10.1016/j.ejps.2017.04.011.
22. Haque, M.K.; Roos, Y.H. Crystallization and X-ray Diffraction of Crystals Formed in Water-Plasticized Amorphous Spray-dried and Freeze-dried Lactose/Protein Mixtures. *J. Food Sci.* **2005**, *70*, E359–E366. https://doi.org/10.1111/j.1365-2621.2005.tb09977.x.
23. Haque, M.K.; Roos, Y.H. Crystallization and X-ray diffraction of spray-dried and freeze-dried amorphous lactose. *Carbohydr. Res.* **2005**, *340*, 293–301. https://doi.org/10.1016/j.carres.2004.11.026.
24. Bhugra, C.; Rambhatla, S.; Bakri, A.; Duddu, S.P.; Miller, D.P.; Pikal, M.J.; Lechuga-Ballesteros, D. Prediction of the onset of crystallization of amorphous sucrose below the calorimetric glass transition temperature from correlations with mobility. *J. Pharm. Sci.* **2007**, *96*, 1258–1269. https://doi.org/10.1002/jps.20918.
25. Kawakami, K.; Pikal, M.J. Calorimetric investigation of the structural relaxation of amorphous materials: Evaluating validity of the methodologies. *J. Pharm. Sci.* **2005**, *94*, 948–965. https://doi.org/10.1002/jps.20298.
26. Bhugra, C.; Shmeis, R.; Krill, S.L.; Pikal, M.J. Different measures of molecular mobility: Comparison between calorimetric and thermally stimulated current relaxation times below Tg and correlation with dielectric relaxation times above Tg. *J. Pharm. Sci.* **2008**, *97*, 4498–4515. https://doi.org/10.1002/jps.21324.

27. Shamblin, S.L.; Hancock, B.C.; Pikal, M.J. Coupling between chemical reactivity and structural relaxation in pharmaceutical glasses. *Pharm. Res.* **2006**, *23*, 2254–2268. https://doi.org/10.1007/s11095-006-9080-8.
28. Groël, S.; Menzen, T.; Winter, G. Calorimetric Investigation of the Relaxation Phenomena in Amorphous Lyophilized Solids. *Pharmaceutics* **2021**, *13*, 1735. https://doi.org/10.3390/pharmaceutics13101735.
29. Bhugra, C.; Shmeis, R.; Krill, S.L.; Pikal, M.J. Prediction of onset of crystallization from experimental relaxation times. II. Comparison between predicted and experimental onset times. *J. Pharm. Sci.* **2008**, *97*, 455–472. https://doi.org/10.1002/jps.21162.
30. Abdul-Fattah, A.M.; Truong-Le, V.; Yee, L.; Nguyen, L.; Kalonia, D.S.; Cicerone, M.T.; Pikal, M.J. Drying-induced variations in physico-chemical properties of amorphous pharmaceuticals and their impact on stability (I): Stability of a monoclonal antibody. *J. Pharm. Sci.* **2007**, *96*, 1983–2008. https://doi.org/10.1002/jps.20859.
31. Abdul-Fattah, A.M.; Dellerman, K.M.; Bogner, R.H.; Pikal, M.J. The effect of annealing on the stability of amorphous solids: Chemical stability of freeze-dried moxalactam. *J. Pharm. Sci.* **2007**, *96*, 1237–1250. https://doi.org/10.1002/jps.20947.
32. Luthra, S.A.; Hodge, I.M.; Utz, M.; Pikal, M.J. Correlation of annealing with chemical stability in lyophilized pharmaceutical glasses. *J. Pharm. Sci.* **2008**, *97*, 5240–5251. https://doi.org/10.1002/jps.21391.
33. Vollrath, I. Controlled nucleation and heat flux measurements as innovative technologies for freeze-drying. Ph.D. Thesis, Ludwig Maximilian University of Munich, Munich, Germany, **2018**.
34. NITROGEN|Air Liquide. Available online: https://mygas.airliquide.de/catalog-gas-products/stickstoff-technisch?language=en-DE (accessed on 2 February 2023).
35. Lo Presti, K.; Frieß, W. Adjustment of specific residual moisture levels in completely freeze-dried protein formulations by controlled spiking of small water volumes. *Eur. J. Pharm. Biopharm.* **2021**, *169*, 292–296. https://doi.org/10.1016/j.ejpb.2021.10.011.
36. Konstantinidis, A.K.; Kuu, W.; Otten, L.; Nail, S.L.; Sever, R.R. Controlled nucleation in freeze-drying: Effects on pore size in the dried product layer, mass transfer resistance, and primary drying rate. *J. Pharm. Sci.* **2011**, *100*, 3453–3470. https://doi.org/10.1002/jps.22561.
37. Geidobler, R.; Winter, G. Controlled ice nucleation in the field of freeze-drying: Fundamentals and technology review. *Eur. J. Pharm. Biopharm.* **2013**, *85*, 214–222. https://doi.org/10.1016/j.ejpb.2013.04.014.

38. Hottot, A.; Vessot, S.; Andrieu, J. Freeze drying of pharmaceuticals in vials: Influence of freezing protocol and sample configuration on ice morphology and freeze-dried cake texture. *Chem. Eng. Process. Process Intensif.* **2007**, *46*, 666–674. https://doi.org/10.1016/j.cep.2006.09.003.
39. Rambhatla, S.; Ramot, R.; Bhugra, C.; Pikal, M.J. Heat and mass transfer scale-up issues during freeze drying: II. Control and characterization of the degree of supercooling. *AAPS PharmSciTech* **2004**, *5*, e58. https://doi.org/10.1208/pt050458.
40. Chang, B.S.; Kendrick, B.S.; Carpenter, J.F. Surface-induced denaturation of proteins during freezing and its inhibition by surfactants. *J. Pharm. Sci.* **1996**, *85*, 1325–1330. https://doi.org/10.1021/js960080y.
41. Searles, J.A.; Carpenter, J.F.; Randolph, T.W. Annealing to optimize the primary drying rate, reduce freezing-induced drying rate heterogeneity, and determine T(g)' in pharmaceutical lyophilization. *J. Pharm. Sci.* **2001**, *90*, 872–887. https://doi.org/10.1002/jps.1040.
42. Searles, J.A.; Carpenter, J.F.; Randolph, T.W. The ice nucleation temperature determines the primary drying rate of lyophilization for samples frozen on a temperature-controlled shelf. *J. Pharm. Sci.* **2001**, *90*, 860–871. https://doi.org/10.1002/jps.1039.
43. Kharatyan, T.; Gopireddy, S.R.; Ogawa, T.; Kodama, T.; Nishimoto, N.; Osada, S.; Scherließ, R.; Urbanetz, N.A. Quantitative Analysis of Glassy State Relaxation and Ostwald Ripening during Annealing Using Freeze-Drying Microscopy. *Pharmaceutics* **2022**, *14*, 1176. https://doi.org/10.3390/pharmaceutics14061176.
44. Patel, S.M.; Doen, T.; Pikal, M.J. Determination of end point of primary drying in freeze-drying process control. *AAPS PharmSciTech* **2010**, *11*, 73–84. https://doi.org/10.1208/s12249-009-9362-7.
45. Ehlers, S.; Schroeder, R.; Friess, W. Trouble with the Neighbor during Freeze-Drying: Rivalry About Energy. *J. Pharm. Sci.* **2021**, *110*, 1219–1226. https://doi.org/10.1016/j.xphs.2020.10.024.
46. Makower, B.; Dye, W.B. Sugar Crystallization, Equilibrium Moisture Content and Crystallization of Amorphous Sucrose and Glucose. *J. Agric. Food Chem.* **1956**, *4*, 72–77. https://doi.org/10.1021/jf60059a010.
47. Tomlinson, A.; Zarraga, I.E.; Demeule, B. Characterization of Polysorbate Ester Fractions and Implications in Protein Drug Product Stability. *Mol. Pharm.* **2020**, *17*, 2345–2353. https://doi.org/10.1021/acs.molpharmaceut.0c00093.

48. Kerwin, B.A. Polysorbates 20 and 80 used in the formulation of protein biotherapeutics: Structure and degradation pathways. *J. Pharm. Sci.* **2008**, *97*, 2924–2935. https://doi.org/10.1002/jps.21190.
49. Mittal, K.L. Determination of CMC of polysorbate 20 in aqueous solution by surface tension method. *J. Pharm. Sci.* **1972**, *61*, 1334–1335. https://doi.org/10.1002/jps.2600610842.

Chapter IV Can α-relaxation data of amorphous freeze-dried cakes predict long term IgG1 antibody stability?

This chapter is published as: Groël, S.; Menzen, T.; Winter, G. (2023). Possibilities and limitations of α-relaxation data of amorphous freeze-dried cakes to predict long term IgG_1 antibody stability. *International Journal of Pharmaceutics* 2023, 123445.

Note from the authors: To establish a coherent numbering and pagination within this document the numbers of references, figures and tables were adapted. The finalized version of the article can be found as referenced above.

The final version of the published article can be accessed online via:

https://doi.org/10.1016/j.ijpharm.2023.123445

IV.1 Abstract

The value of correlating global α-relaxations with long term protein stability after freeze-drying is inconsistently reported. This study aims to clarify whether and to what extend the long term stability of a freeze-dried protein formulation can be predicted with this method. For this purpose, the α-relaxation parameter τ^{β} [h] of freshly prepared freeze-dried products is obtained by isothermal microcalorimetry. The concept is, that molecular movements in the amorphous matrix are strongly reduced in cakes with longer relaxation time and the product should therefore be more resistant against aggregation. To increase τ^{β} in comparison to a conventional freeze-drying cycle, aggressive drying cycles including structural collapse of the product as well as tempering protocols after freeze-drying are applied. The τ^{β} values are correlated with the aggregation rate of a freeze-dried IgG_1 monoclonal antibody measured with high performance size exclusion chromatography. The antibody was used in its market formulation and 6 further compositions. A weak correlation between α-relaxation times and IgG_1 aggregation was found. A higher mobility level through increased residual moisture helped to improve the correlation.

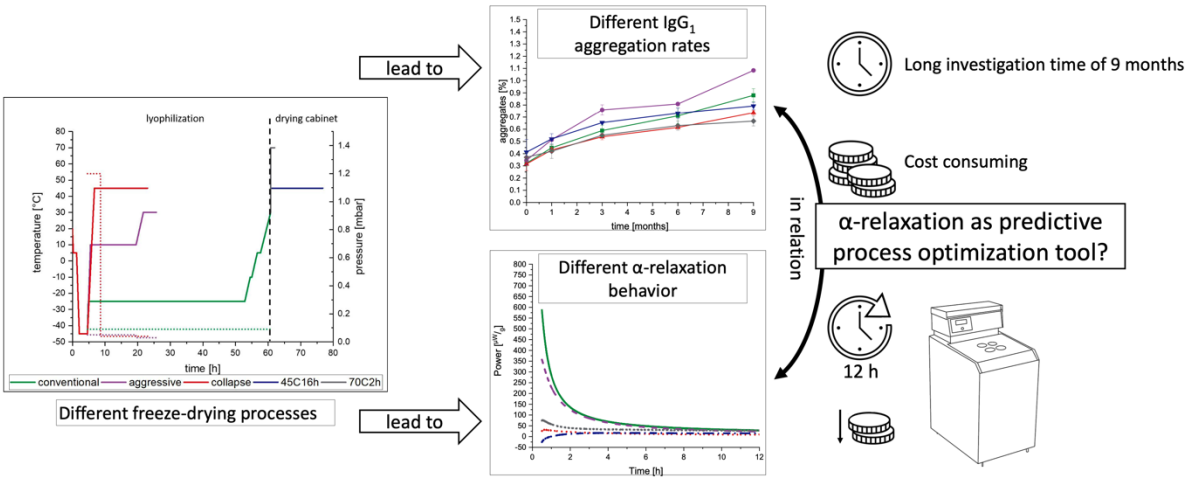

Keywords: aggressive-drying, amorphous, calorimetry, collapse-drying, freeze-drying, isothermal microcalorimetry, lyophilization, mAb, protein formulation, relaxation

IV.2 Introduction

The need for stable formulations of biological therapeutics rapidly increased in the last years [1]. However, the most biological entities like proteins, viruses and RNA, face degradation problems during shipment and storage when they are kept in liquid formulations [2–5]. To freeze-dry those products is a suitable method to stabilize them by gently removing the water [6,7]. Especially for biopharmaceutics like proteins, an amorphous form of the dried formulation is desired as a crystalline state often leads to a high loss of therapeutic activity over time [6]. However, the amorphous form is not thermodynamically stable as it possesses an energy excess and thus will relax towards a crystalline equilibrated state over time, typically during storage [8]. In general, relaxation processes are distinguished in α-, β-, and γ-relaxations and detailed definitions can be found in other publications [9]. The present study focuses on α-relaxations. This relaxation process involves molecular movement, which allows protein degradation even in the solid matrix [10–13]. In particular, degradation processes that require movements of large functional groups or whole molecules like the formation of protein aggregates are driven by the relaxation process [14,15]. Protein aggregates are debated to potentially cause adverse effects including immunoreactions after administration [16–19]. For this reason, several studies investigated α-relaxations and aggregation for their potential correlation [14,20,21]. The relaxation time τ^{β} [h] can be measured with calorimetric methods[22]. The concept is, that with higher values of τ^{β}, the time needed for relaxation or (if correlated) aggregation is prolonged [23]. One parameter that influences the α-relaxation time τ^{β} [h] is the energy excess of the matrix compared to the equilibrated state [24]. A high energy excess leads to a short α-relaxation time. In other words, less energy excess (longer τ^{β} [h]) in

the matrix may allow better long-term stability of the protein formulation. A more detailed theoretical derivation can be found in the publication of Kawakami & Pikal [22] and in a review on the topic that was published recently [25].

The outcome of previous studies was heterogeneous. Some studies, where predominantly small molecule drugs were used and only a minimal amount of excipients was added, showed a good correlation between the stability of the amorphous active pharmaceutical ingredient (API) and the α-relaxation processes in the matrix [14,21,26,27]. In contrast, studies that try to compare different formulation parameters or drying techniques of biopharmaceutics showed limitations in correlation of stability with global α-relaxations [16,23]. One study reports a good correlation of global α-relaxations with the stability of an IgG_1 fusion protein against aggregation [28]. There, τ^{β} is controlled by a thermal treatment, tempering, of the amorphous matrix. Exposing the dried products to an elevated temperature below the glass transition (T_g) leads to a higher value of τ^{β}, as desired [12,29]. In case of a freeze-drying process this would need an additional step including transfer of the product into a drying cabinet [30].

The present study tries to address open questions regarding the stability of freeze-dried proteins and its correlation with α-relaxations: First, is the correlation between global α-relaxations (τ^{β}) and long-term protein aggregation valid for a range of 7 formulation variants? Second, are the effects in relaxation strong enough to see differences in process optimization runs applied to a rather stable market formulation? Third, is it possible to include the tempering step as proposed by Pikal et al. [14,21,26–28] into the freeze-drying process to save time and costs?

Seven formulations were freeze-dried with 5 different processes and then analyzed with respect to stability of an IgG_1 antibody against aggregation over time. A market relevant IgG_1 monoclonal antibody was used as API in a low concentration of 2 g/l and a high concentration of 50 g/l. With this, the question whether the α-relaxation of the sugar or the whole matrix is more relevant was targeted. The formulations were composed with or without polysorbate 20 (PS20), with the expectation that lack of surfactant promotes more aggregation. Either sucrose or trehalose was used to get formulations with different T_g values. 3 freeze-drying processes were defined: a) a conventional cycle resulting in elegant looking cakes, b) an aggressive cycle with harsher conditions and c) a collapse cycle accepting structural collapse of the product. Former studies of our group showed that structural collapse during the freeze-drying process does not necessarily degrade the protein and could even lead to more stable products [31,32]. Moreover, the samples from the conventional cycle were separated and one third went into storage without further treatment, one third was tempered at 70 °C for 2 h and the rest was

tempered at 45 °C for 16 h. The latter represents the temperature conditions of the collapse drying cycle and the 70 °C 2 h process should roughly possess the same energy entry on the product when the mathematical product of time and absolute temperature is taken as reference. But the 70 °C 2 h process is carried out at a higher absolute temperature. Overall, the 5 processes were optimized in a way that products with about the similar residual moisture (r.m.) level were obtained, in order to remove r.m. from the list of variables.

IV.3 Material & Methods

IV.3.1 Preparation of formulations

An IgG_1 monoclonal antibody was purified from its stock solution with an ÄKTA protein purification system (Cytiva, Marlborough, MA, USA) using a Sepharose HiTrap SP column (Cytiva, Marlborough, MA, USA). The eluted buffer was exchanged with a 20 mM histidine buffer pH 5.5 (Alfa Aesar, Ward Hill, MA, USA) using a cross-flow filtration unit Minimate™ TFF capsule with omega polyethersulfone (PES) membrane (MW 30,000 Da; Pall Corporation, New York, NY, USA). To determine the protein concentration after buffer exchange a NanoDrop™ 2000 UV photometer (Thermo Fisher Scientific, Waltham, MA, USA) was utilized. Stock solutions of the other excipients were prepared in the same histidine buffer and spiked to the protein solution to achieve the formulations according to Table IV.1. D-(+)-trehalose dihydrate was obtained from VWR International, Radnor, PA, USA, sucrose from Sigma-Aldrich, Steinheim, Germany and polysorbate 20 (PS20) from Croda, Edison, NJ, USA. Before filling 1 ml solution in 2 R vials (MGlas AG, Muennerstadt, Germany) the final solutions were filtered using a 0.22-µm PES Sartolab® RF vacuum filter unit (Sartorius AG, Goettingen, Germany). The vials were placed on a freeze-drying tray with two rows of placebo filled vials as outer radiation shield and semi-stoppered with West 13-mm Lyo Nova Pure RS 1356 4023/50 G stoppers (West Pharmaceutical Services, Inc, Exton, PA, USA).

Table IV.I Used formulations

Formulation ID	Sucrose [gl^{-1}]	Trehalose [gl^{-1}]	PS20 [gl^{-1}]	IgG_1 mab [gl^{-1}]	Formulation ID
2gl_NoSurf_Suc	79.45	-	-	2	79.45
2gl_PS20_Suc	79.45	-	0.4	2	79.45
2gl_NoSurf_Tre	-	79.45	-	2	-
2gl_PS20_Tre	-	79.45	0.4	2	-
50gl_NoSurf_Suc	79.45	-	-	50	79.45
50gl_PS20_Suc	79.45	-	0.4	50	79.45

** equals the market formulation.*

IV.3.2 Freeze-drying protocols

The protocols were designed to lead to products with similar amounts of residual moisture. Additionally, the product temperature during primary drying has to stay below T_g' for the conventional cycle, between T_g and collapse temperature (T_c) for the aggressive cycle and exceed T_c for the collapse cycle.

For all freeze-drying protocols the same freezing step was used. The shelf was loaded at 20 °C and afterwards ramped with 1 K/min to 5 °C. The temperature was held for 1 h to allow temperature equilibration in all vials. Next the shelf was cooled with 1 K/min to -45 °C and held for 2.5 h for a homogenous freezing of the formulations. a) Primary drying for the conventional cycle was conducted at -25 °C after ramping the temperature with 1 k/min from -45 °C. The time of primary drying was 48 h. For secondary drying, the shelf was ramped from -25 °C to 30 °C with a ramp rate of 0.15 K/min including isothermal steps at -10 °C for 0.5 h as well as 5 °C for 1 h. The chamber pressure was set to 0.09 mbar starting with primary drying. b) For the aggressive cycle, the shelf was ramped to 10 °C with a rate of 1 K/min and the temperature was held for 10 h. Secondary drying was introduced by ramping the shelf to 30 °C with a ramp of 0.15 K/min. The temperature was held for 4 h until the process was stopped. The chamber pressure was set to 0.05 mbar for primary and 0.03 mbar for secondary drying. c) To achieve the products with structural collapse, the shelf was ramped from -45 °C to 45 °C with a ramp rate of 0.7 K/min and a combined primary and secondary drying was performed

by holding the temperature for 16 h. The chamber pressure was set to 1.2 mbar for the first 4 h and to 0.04 mbar for the last 12 h of drying.

After the processes the vials were stoppered under a nitrogen atmosphere with a pressure of 600 mbar. Figure IV.1 graphically displays the freeze-drying protocols.

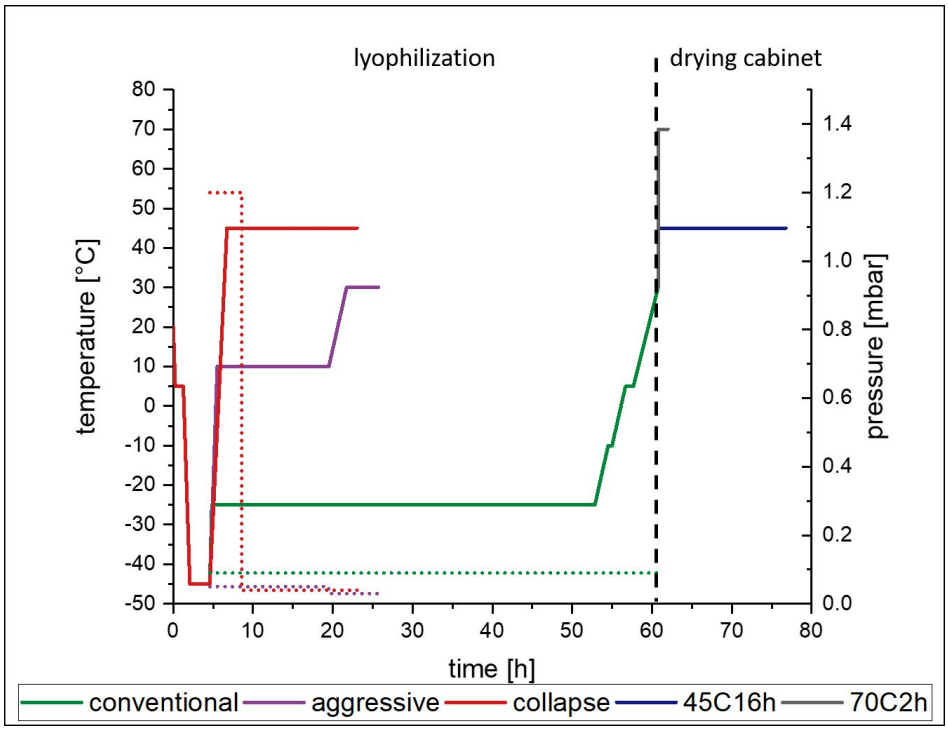

Figure IV.I Applied freeze-drying protocols. The tempered samples are described as acronym of their storage temperature and time with 45C16h = tempered at 45 °C for 16 h and 70C2h = tempered at 70 °C for 2 h.

For the conventional and aggressive drying protocol a Christ ε2-6D laboratory-scale freeze-dryer (Martin Christ Gefriertrocknungsanlagen GmbH, Osterode am Harz, Germany) was used. The collapse cycle was carried out on a FTS LyoStar™ 3 freeze-dryer (SP Scientific, Stone Ridge, NY, USA). The tempering procedure was performed with fully stoppered and crimped vials in a separate drying cabinet at the respective temperatures and times.

IV.3.3 Residual moisture content (r.m.)

The residual moisture content in [% (w/w)] was determined by coulometric Karl-Fischer Titration using an Aqua 40.00 Vario plus head space titrator (ECH Elektrochemie Halle GmbH, Halle (Saale), Germany). The samples were grounded with a spatula under a controlled atmosphere with a humidity < 10 % and about 10 – 30 mg were transferred in a new 2R Vial. For samples without structural collapse, the vials were heated in an oven to 100 °C without further treatment. In the vials including structural collapsed product, 0.5 ml Methanol, Dry, Hydranal™ (Honeywell Chemicals, Charlotte, NC, USA) was injected through the stopper to suspend the sample and dissolve the residual water. The vials were heated in an oven to 70 °C.

In both cases, with and without structural collapse, the water evaporated and was transferred by a dry gas stream into the measurement cell.

IV.3.4 Differential scanning calorimetry (DSC)

A Mettler Toledo DSC 821e (Mettler Toledo, Gießen, Germany) differential scanning calorimeter was used to determine the values of T_g [°C], enthalpy recovery [Jg^{-1}] and the difference in heat capacity before and after the glass transition, Δc_p [$Jg^{-1}K^{-1}$]. About 5 – 15 mg sample mass was transferred to an aluminum crucible in a controlled atmosphere with a humidity < 10 %. The crucible was hermetically sealed and an empty crucible was used as reference pan. A modulated scanning mode was utilized with a heating rate of 2 K/min, a period of 2 min and an amplitude of 1 K. To determine the data, the obtained curve was extracted in a reversing, non-reversing and total curve. For T_g and Δc_p the reversing curve was used whereas the non-reversing curve was utilized for the enthalpy recovery.

IV.3.5 Isothermal microcalorimetry (IMC)

To determine the α-relaxation times, the isothermal microcalorimeter LKB 2277 Thermal Activity Monitor (TAM) (TA Instruments, New Castle, DE, USA) was used at 40 °C operating temperature. 100 – 300 mg sample were transferred in a stainless steel measuring ampoule under a controlled atmosphere with a humidity below 10 %. The empty reference ampoule was purged with the same atmosphere during sample filling. The ampoules were first lowered to the thermal equilibrium position to allow equilibration. After 15 min the sample and reference ampoule were simultaneously lowered to the measurement position. The data collection interval was 2 seconds for the first hour and 10 seconds afterwards. The duration of the measurement was at least 12 h. For the fitting procedure OriginPro 2019b was utilized with the modified stretch exponential function as suggested by Kawakami and Pikal (equation III.1) [22]. $\tau_0 = 2$, $\tau_1 = 1$ and $\beta = 0.1$ were chosen as start parameters with the further conditions $\tau_0 > \tau_1$ and $0 < \beta \leq 1$. The first 0.5 h were left out from the evaluations due to disturbing noises arising from the ampoule insertion.

$$P = 277.8 * \frac{\Delta H_r(\infty)}{\tau_0} * \left(1 + \frac{\beta t}{\tau_1}\right) * \left(1 + \frac{t}{\tau_1}\right)^{\beta-2} * \exp\left[-\left(\frac{t}{\tau_0}\right) * \left(1 + \frac{t}{\tau_1}\right)^{\beta-1}\right] \quad \text{(IV.1)}$$

$$\text{With } \Delta H_r(\infty) = \left(T - T_g\right) * \Delta c_p$$

and P in $\left[\frac{\mu W}{g}\right]$; $\Delta H_r(\infty)$ in $[Jg^{-1}]$; τ_0 and τ_1 = relaxation time constants; t = $[h]$; β = stretch parameter; *Note: the number 277.8 is a numerical factor due to unit conversation.*[8]

The samples intended for IMC measurements were frozen to -80 °C immediately after the freeze-drying process. With this, the α-relaxation process can be considered as stopped and the samples were defrosted 1 h before the measurement.

IV.3.6 Specific surface area (SSA)

The specific surface area was determined with the Brunauer-Emmet-Teller (BET) krypton gas adsorption device (Autosorb 1; 3P-Instruments, Odelzhausen, Germany). About 100 mg sample was transferred in measurement glass tubes in a controlled humidity below 10 %. To do so, 3 sample vials of one product were pooled in the glass tube and measured as n=1. The Autosorb 1 software was used to fit the resulting BET curve.

IV.3.7 X-ray powder diffraction (XRD)

A MiniFlex benchtop XRD instrument (Rigaku Corporation, Tokyo, Japan) was utilized to check for the presence or absence of crystals in the freshly prepared samples. The grounded samples were placed on a silica sample holder and the diffraction was measured ranging from 3° to 60° 2θ in 0.02° measurement intervals with a speed of 10 °/min. A copper anode at 40 kV and 15 mA with the wavelength of 1.540593 Å was used to generate the radiation.

IV.3.8 High performance size exclusion chromatography (HP-SEC)

Separation was conducted with a Waters 2695 Separation Module (Waters GmbH, Eschborn, Germany). A Tosoh TSKgel G3000 SWXL column (Tosoh Bioscience, Griesheim, Germany) was utilized to determine the content of soluble aggregates. The flowrate was 1 ml/min with an elution buffer consisting of 100 mM sodium phosphate pH 7.0 containing 200 mM sodium chloride. For detection, a Waters 2487 Dual λ Absorbance Detector (Waters) at the wavelength of 280 nm was used. For the 2g/l formulations, 20 µl reconstituted sample was injected, whereas the 50 g/l formulations were diluted to a concentration of 5 g/l and 10 µl were injected. To determine the aggregation rate, the area in mAU of the monomeric protein peak as well as the higher molecular weight species (protein aggregates) was integrated. The area of the protein aggregates was then expressed as percentage area in relation to the total peak area. This value was plotted against the square root of the storage time in months. The slope of the linear fit of this plot equals the aggregation rate k. The procedure to use the square root of time resulted in the best fits and was also used by Wang et al [16]. Furthermore, this kind of “diffusive” kinetic

is a promising condition for the scope of the present study as global α-relaxations are inversely linked to diffusion by the VTF-equation and thus this kinetic should lead to a good correlation with τ^{β} [33]. Additionally, the recovery of the monomer peak area was reviewed to ensure absence of substantial protein precipitation. The monomeric peak recovery was satisfactory in each case (between 95 and 105 %).

IV.3.9 Scanning electron microscopy (SEM)

To study the morphology of the freeze-dried cakes a scanning electron microscope (Dual beam FEI Helios G3 UC, Fisher Scientific, Waltham, MA, USA) was used. The cake was carefully cut to extract a sample from its core. The small pieces were placed on a carbon conductive cement to analyze the breakage border and images were recorded at 2kV.

IV.4 Results

IV.4.1 3.1 Characterization of the dried products

7 formulations were studied (see Table IV.1) in 5 different freeze-drying processes (see Figure IV.1). For clarity, the tempering processes are designated with their tempering temperature and time leading, e.g., to the ID 45C16h for the process conducted at 45 °C for 16 h as well as 70C2h for the process at 70 °C for 2h. Table IV.2 shows selected results. Complete data from solid state analysis can be found in the appendix, Tables IV.A1-IV.A6 and representative DSC traces in Figure IV.A1. Table IV.2 exemplifies how the solid state parameters are reported by presenting the data for the 2gl_NoSurf_Suc formulation.

Figure IV.2 shows the macroscopic and scanning electron microscopy (SEM) pictures of the 2gl_PS20_Tre and 50gl_PS20_Tre samples as they are representative for all formulations, independent of being based on sucrose or trehalose. No macroscopic or microscopic difference was observable between conventional and tempered products. Both processes resulted in elegant looking cakes. In contrast, the aggressive cycle led to a triangle shaped shrinkage at the side of the cake and the SEM pictures made microcollapse visible all over the cake structure. The collapse cycle resulted in a bubbled foam with a full loss of a cake structure in the samples with low antibody content, whereas in the formulations with high antibody content, at least a cake shape but with strong ruptures was recognizable. Both variants, low and high antibody content, appeared equally in the SEM showing scales without a porous surface.

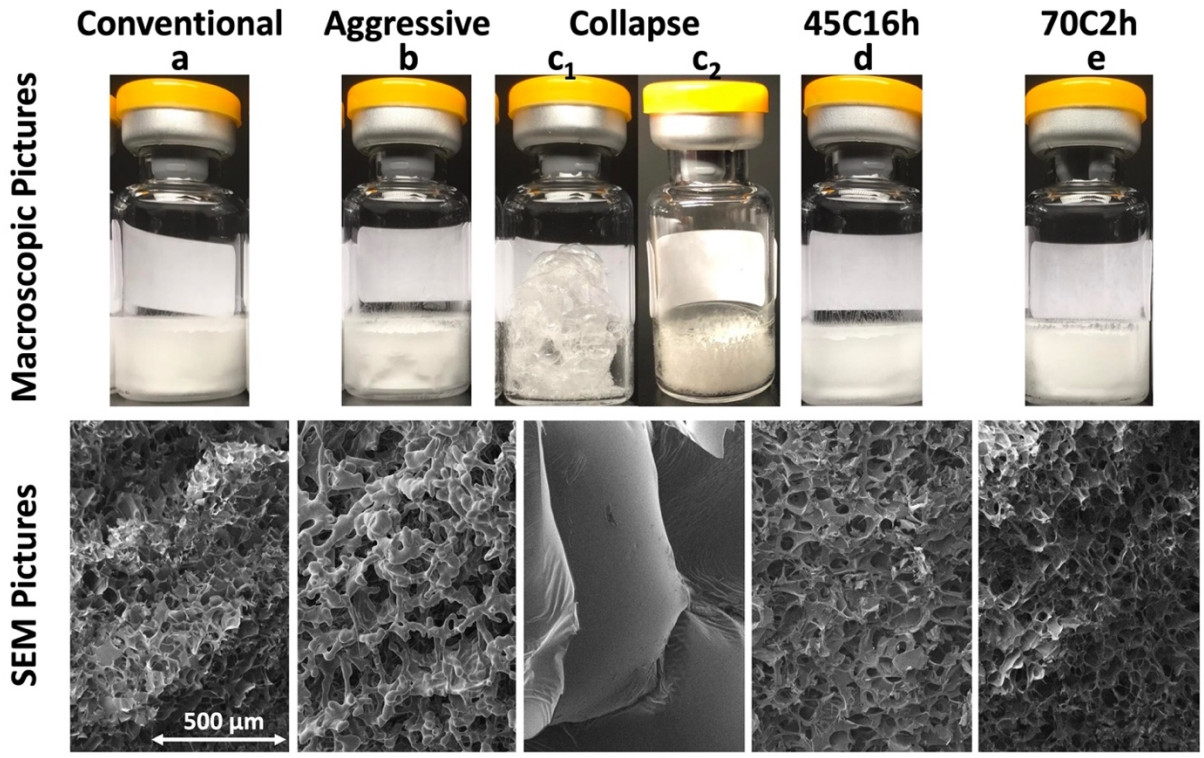

Figure IV.2 Macroscopic and microscopic appearance of the 2gl_PS20_Tre formulation. In the case of the collapsed cycle an additional picture of 50gl_PS20_Tre is included as the high concentrated formulations differ in der macroscopic appearance of the collapse cycle. (c_1 = 2gl_PS20_Tre; c_2 = 50gl_PS20_Tre)

The residual moisture levels were independent of the process, leading to 1.5 % residual moisture (r.m.) for the 2gl_Suc formulations, 1.2 % r.m. for 2gl_Tre, 1.0% r.m. for 50gl_Suc and 0.8 % r.m. for 50 gl_Tre (Tables IV.2 and appendix Table IV.A1 – IV.A6).

The only exception occurred in the 2gl_Tre samples. Here, the collapse cycle ended up significantly wetter with levels about 3.0 % (Appendix Tables IV.A1 + IV.A3).

For each product, the residual moisture level stayed constant during the whole observation time of 9 months.

Table IV.2 Solid state parameter of the 2gl_NoSurf_Suc formulation. n = 3, values represent the mean value and the corresponding standard deviation. The results of the remaining formulations can be found in appendix A.

process	Glass transition [°C]	Δc_p [$Jg^{-1}K^{-1}$]	Enthalpy recovery [Jg^{-1}]	SSA [m^2g^{-1}]	Residual moisture [%]
conventional	48.60 ± 4.18	0.64 ± 0.04	2.21 ± 0.65	0.842	1.55 ± 0.11
aggressive	52.57 ± 0.53	0.64 ± 0.04	3.89 ± 1.05	0.575	1.50 ± 0.00
collapse	60.45 ± 0.36	0.35 ± 0.14	2.17 ± 0.29	0.004	1.59 ± 0.05
45C16h	50.39 ± 3.02	0.58 ± 0.01	6.06 ± 0.65	0.761	1.62 ± 0.03

For all products, except certain collapsed samples, the glass transitions were found at about 50 °C for 2gl_Suc formulations, 70 °C for 50gl_Suc formulations, 90 °C for the 2gl_Tre formulations and 110 °C for the 50gl_Tre formulations, respectively. The Δc_p-values, used for the relaxation time calculation according to equation IV.1, were comparable within a certain formulation group independent of the process. Only the collapsed 2gl_Suc variants resulted in a higher T_g of 60 °C and a lower c_p compared to the other 2gl_Suc formulations.

The parameters of the collapsed 2gl_Tre formulation are described separately as the DSC parameters are strongly influenced by the higher residual moisture content compared to the other 2gl_Tre products. In the collapsed variants, 75 °C for the glass transition temperature were obtained and they reached the strongest enthalpy relaxation at t(0). In contrast to the remaining 2gl_Tre formulations neither an exo- nor an endothermal event was observed.

As expected, the specific surface area (SSA) of the cakes from different processes can be ranked from highest to lowest in the order of conventional > tempered > aggressive > collapse, thereby, resulting in about 10 % reduction of SSA from conventional to tempered, 25 % from tempered to aggressive and 80 % from aggressive to collapse. In the foam bubbled samples, the SSA was barely measurable, with a high measurement error in the BET fitting procedure.

The absence of peaks in the XRD-diffractogram proved a full amorphous phase for all products.

An overview of the relaxation data at 40 °C is presented in Figure IV.3. Most measurements resulted in an expected exothermal relaxation curve with an exponential like decay[22]. However, a few curves showed an ascending part with a subsequent maximum for the exothermal decay. This part might origin from an endothermal event consuming the energy

from the relaxation process at the beginning of the measurement, which is also described in literature and suggested as an enthalpy recovery process [22,26]. In those curves, the start time for the fitting procedure was set with the start of the exponential decay neglecting the endothermal event. The measurement of the conventional dried 2gl_Suc formulations (Figure IV.3a and IV.3d) showed a curve with a particularly strong decay resulting in a bulbous shape of the curve. In general, the conventional dried cakes had the shortest relaxation time, followed by the aggressive dried cakes and then the collapsed ones. The order between collapsed and tempered samples changed depending on the formulation, but the relaxation times of both were always longer than for conventionally or aggressively dried ones.

IV.4.2 Protein aggregation rate determined by high performance size exclusion chromatography (HP-SEC)

Figure IV.4 displays the aggregation rate of the products at the investigated storage temperatures of 4 °C, 25 °C and 40 °C over 9 months. In the formulations with 50 g/l antibody the degradation rate constantly increased with increasing storage temperature (Figure IV.4). The 50gl_PS20_Tre formulations showed the highest aggregation rate, followed by the 50 g/l sucrose formulations without PS20. Notably, the aggregation rate was often lower in the samples without PS20.

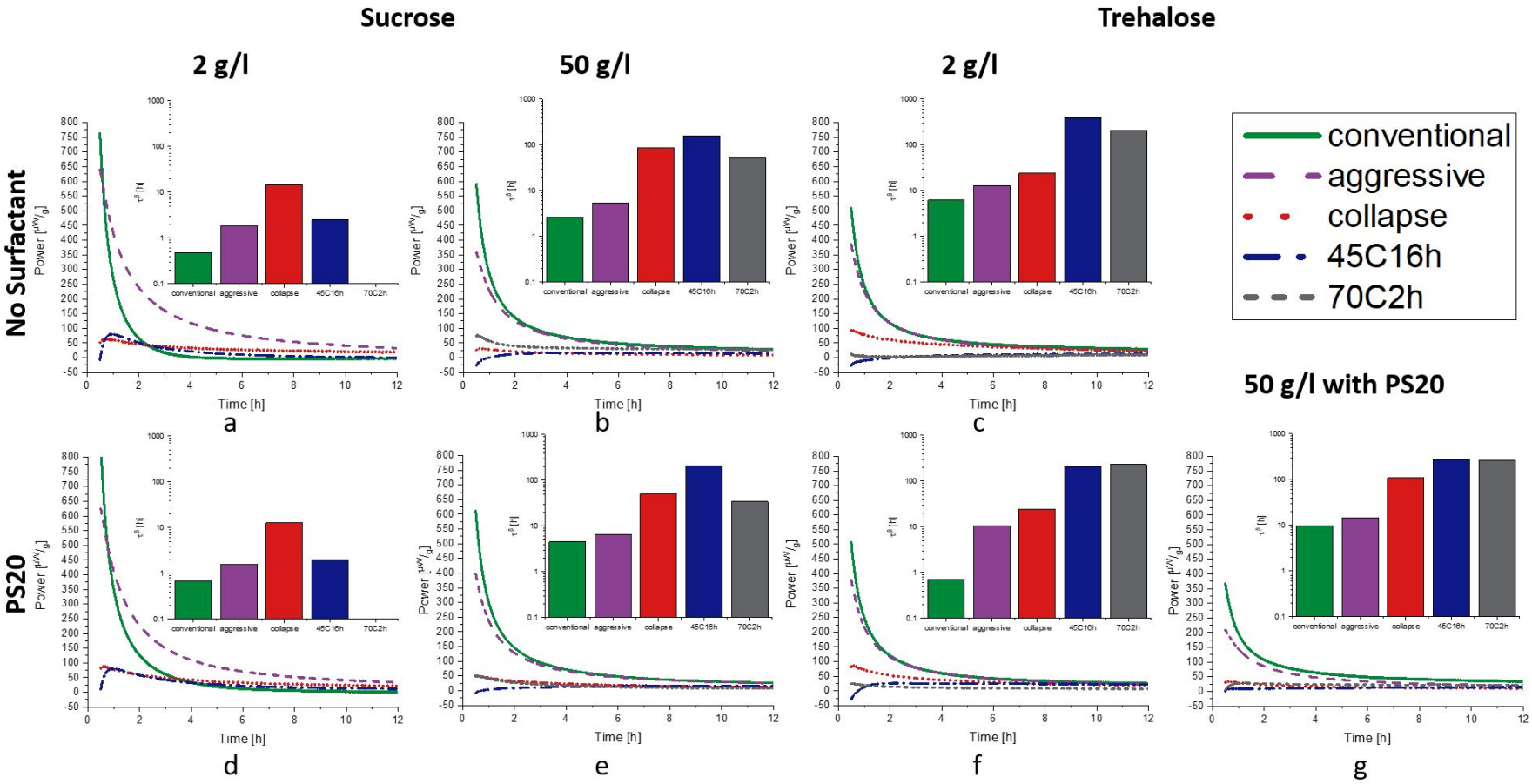

Figure IV.3 Relaxation data obtained from isothermal microcalorimetry at 40 °C. The line diagram presents the relaxation curve and the bar chart the calculated τβ-values.

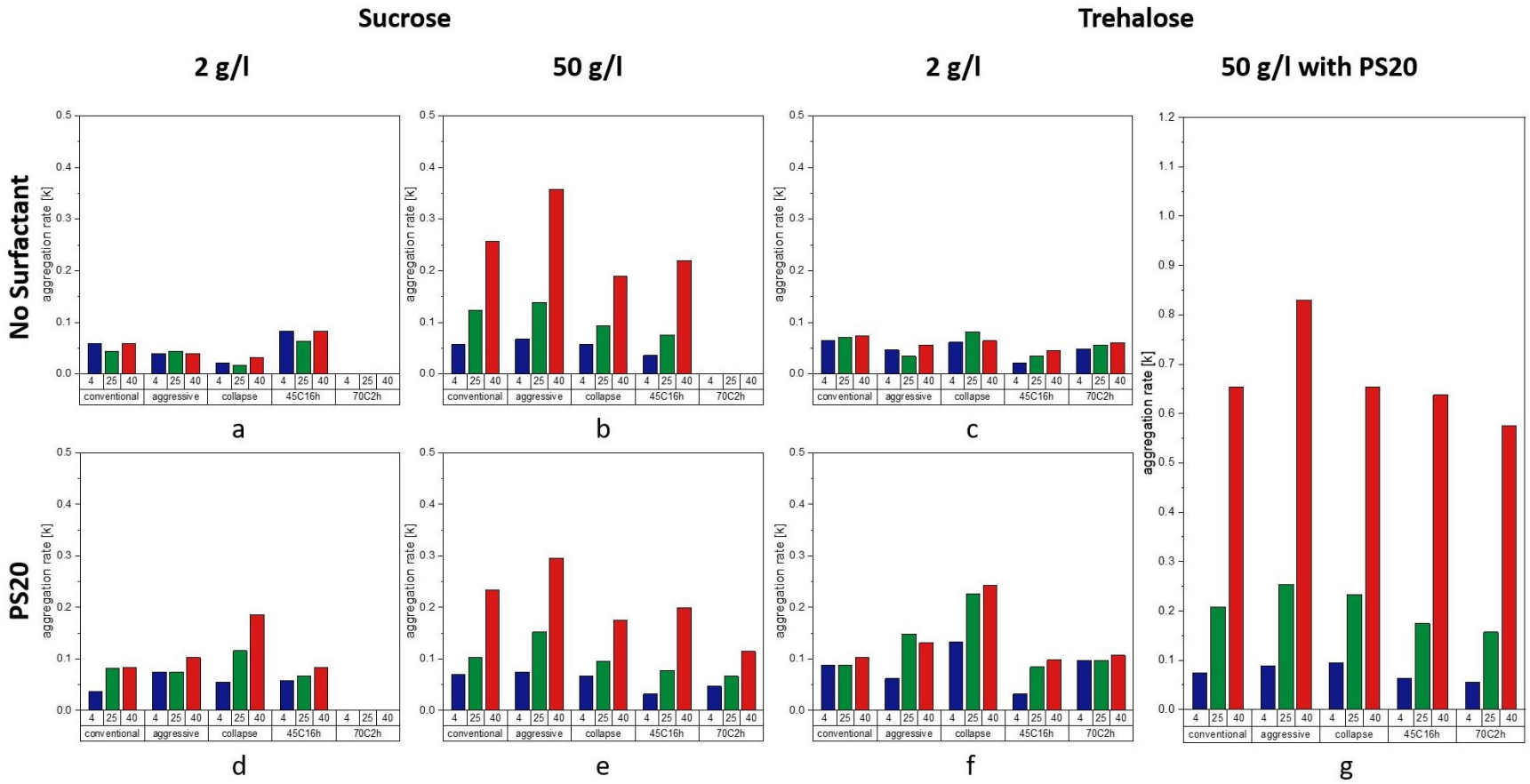

Figure IV.4 Protein aggregation rate at 40 °C (red bars), 25 °C (green bars) and 4 °C (blue bars) of the different products. 2gl_NoSurf_Suc (a), 50gl_NoSurf_Suc (b), 2gl_NoSurf_Tre (c), 2gl_PS20_Suc (d), 50gl_PS20_Suc (e), 2gl_PS20_Tre (f), 50gl_PS20_Tre (g). rate expressed as %/month^{-1}

IV.4.3 Pre-Study with high mobility

Before the main data of the study are discussed, a pre-study is presented in Figure IV.5 (and appendix B) as a proof of concept with the 2gl_PS20_Suc and 50gl_PS20_Suc formulations. Because stable market like formulations were utilized in the main study, the pre-test should clarify whether these products would in general be suitable for the planned approach. So, freeze-drying protocols that led to a high amount of residual water are used. This high amount of residual water (> 2.0%) dramatically increased the overall mobility in the amorphous cake and would not be reasonable for a market formulation.

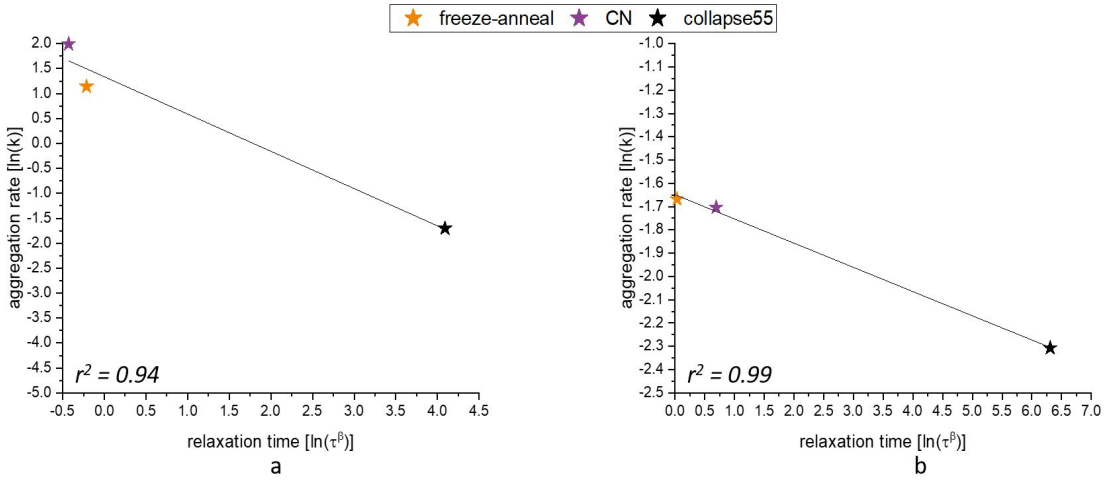

Figure IV.5 Relaxation of samples with increased molecular mobility due to high residual moisture levels > 2 %. Purple = controlled nucleation, orange = annealing in the freezing step and black =collapse at 55 °C. Diagram a presents the 2gl_PS20_Suc formulation and diagram b the 50gl_PS20_Suc formulation. The solid line represents the linear fit between the data points.

With the high residual moisture content, regardless of the protein concentration, the correlation between α-relaxation and protein aggregation is very strong leading to a fit with a correlation coefficient of r^2 = 0.94 for 2gl_PS20_Suc and r^2 = 0.99 for 50gl_PS20_Suc. Therefore, the correlation between α-relaxation and protein aggregation could be demonstrated in case of an overall high mobility in the presence of high residual moisture. Thus, the formulations are suggested to be suitable for the study and were then systematically investigated with industry relevant freeze-drying processes that led to reasonably low residual moisture levels. Furthermore, in the main study more data-points were created to increase the quality of the fit.

IV.5 Discussion

First of all, analysis of the dried formulations confirmed the successful preparation of products with different solid state characteristics as intended. Residual water molecules in the solid matrix act as plasticizer, which leads to faster α-relaxations (short τ^{β}) [34]. It is discussed in literature that a thermal treatment of an amorphous matrix levels off the impact of residual moisture on α-relaxations, given that the differences in r.m. are below 0.5 – 1.0 % [28]. Therefore, in the present study residual moisture levels within a formulation can be considered as equivalent with respect to the impact on α-relaxations, as the ranged between 1.5 – 1.62 % for 2gl_NoSurf_Suc (Table IV.2) 1.31 – 1.54 % for 2gl_PS20_Suc (Table Appendix IV.A2), 1.12 – 1.19 % for 2gl_NoSurf_Tre (Table appendix IV.A1, collapse excluded), 0.98 – 1.20 for 2gl_PS20_Tre (Table appendix IV.A3, collapse excluded), 0.80 – 1.00 for 50gl_NoSurf_Suc (Table appendix IV.A4), 0.84 – 1.06 for 50gl_PS20_Suc (Table appendix IV.A5) and 0.47 – 0.89 for 50gl_PS20_Tre (Table appendix IV.A6). There is however one exemption, the r.m. in the 2gl_Tre formulations with full collapse remained at about 3.0 %. Even with a prolonged drying time the moisture content could not be reduced further. The corresponding, collapsed sucrose formulations resulted in low moisture contents of 1.5 %. Still, the collapsed 2gl_Tre formulations were further investigated in the study.

The results for the specific surface area (SSA) were as expected. Drying below T_g' with either sucrose or trehalose using the conventional process led to well-structured cakes with many pores and a high SSA. The aggressive cycle resulted in microcollapse of the cake (Figure IV.2). As intended, drying above T_c with the collapse cycle led to a complete loss of structure. Interesting is the small reduction for SSA in the tempered cakes. From theory it is consistent that the tempering procedure and a reduction in α-relaxation time is connected with a volume loss [35–37]. However, in literature it was not reported so far[28,38] and the volume shrinkage in the tempered samples was also not visible in the macroscopic and microscopic appearance of the cakes (Figure IV.2).

IV.5.1 Impact of thermal history and morphology on protein stability

Independent of relaxation time, the following can be noted concerning the protein aggregation of conventionally dried, tempered and aggressively dried protein formulations. In the most cases, the conventional dried formulation, without further heat treatment, resulted in products with the lowest amount of aggregates at t(0) (appendix D). It has to be noted here, that the "worst" overall formulation had only 0.52 % protein aggregates at t(0). However, thermal treatment led to a lower aggregation rate and thus, corresponding products resulted in a lower

amount of aggregates after 9 months of storage. This observation is valid for all formulations, except the 2gl_PS20_Suc, which crystallized and is therefore not within the scope of the investigation. These results support the usage of thermal treatment of freeze-dried pharmaceutical formulations like suggested in several publications [14,21,33].

The best way how to apply thermal treatment is not fully clear, but some estimations can be made. Of course, the process must deliver products with reasonable moisture content. Thus, structural collapse with low residual moisture in the "cake", has a high probability to end up in products with very low aggregation rates (Figure IV.4). In products without surfactants the collapse process even led to products with the lowest aggregation rate (Figure IV.4a and IV.4b). This can be explained by the low SSA of these products, which correlates with stability, e.g., in the studies of Bosch et al.[39]. An overall low SSA could have similar effects as the addition of a surfactant, which acts as surface shield to protect the protein from surface stress. So, it could be considered to use structural collapse on purpose to reduce the amount of added surfactant. Studies of Xu et al. showed that proteins on surfaces degrade faster than within the amorphous surface [40]. Furthermore, they showed that the ratio of protein amount on the surface to the bulk is similar for conventional dried, freeze-annealed and tempered products. Thus, it can be assumed for the present study, that the ratio between surface and bulk protein of conventional, 45C16h, and 70C2h was the same. Additionally, these processes result in cakes with quite similar SSA and differences in protein aggregation are therefore due to different α-relaxation times.

Summarized, structural collapse of a formulation introduced by the freeze-drying process did not lead to more or faster protein aggregation. The protein stability is at least comparable to conventional dried counterparts and even better in some cases. This is shown here for practically relevant market like formulations at standard, long-term storage conditions.

IV.5.2 Correlation of α-relaxations with long-term protein stability

The correlation between the aggregation rate and the relaxation time was performed by plotting the logarithm of both values and applying a linear fit as described by Abdul-Fattah and coworkers [14].

For the formulations where a 45C16h as well as a 70C2h tempering process were conducted (6c, 6e-6g), the mean value of the aggregation rate and the relaxation time of both tempering procedures were used for the correlation procedure. This was done because, the relaxation data of these formulations cannot be distinguished very well (Figure IV.3). In the 2gl_Tre formulations, the datapoint for the collapsed products is shown in the plot but not used for the

linear fitting as the residual moisture in these samples was too high with approx. 3.0 % and did not fulfil the inclusion criteria that were set for the full study.

The 2gl_NoSurf_Suc formulation stored at 40 °C was one of the best correlating formulations (Figure IV.6a). If the 45C16h process is excluded from the correlation, a r^2 of 0.99 could be reached. The exclusion of the 45C16h data for both 2gl_Suc formulations can be justified with the small distance between the tempering temperature of 45 °C and the sample's T_g of approx. 52 °C. With a tempering temperature so close to T_g the relaxation process is thermodynamically instead of kinetically controlled [41–43]. Consequently, the relaxation process can be considered as interrupted for those formulations because the state of an equilibrated supercooled liquid is already reached during the tempering process [25]. This most likely has disturbed the data in a similar manner as a crystallization process. A more detailed discussion regarding this phenomenon can be found in the appendix C.

The 2gl_PS20_Suc was the only formulation where crystallization occurred during the storage at 40 °C. As the overall T_g (approximately 52 °C) of these lyophilizates was very close to the storage temperature, the tendency to crystallize was not surprising. It was observed in other studies that PS20 can accelerate the crystallization of sucrose [44,45], explaining this particular behavior. It is reasonable that a prediction concept that is based on matrix relaxations is not suitable for a crystalline matrix, where movements stop and kthermodynamic equilibrium is reached. When crystallizing, the excipient sucrose leaves the amorphous phase and thus cannot be protective for the protein anymore [46–48]. Thus, in Figure IV.6d (marked with #) only the data points of the first 3 month of observation time were used for the correlation procedure. Furthermore, in both of the 2gl_Suc formulations the collapse process led to products with the lowest aggregation rate and the longest relaxation time (Figure IV.6a and IV.6d). This supports the hypothesis, that tempering protocols can be included in the freeze-drying process itself.

When evaluating the data set in Figure IV.6 it must be considered that a market like formulation and 6 small variations of it were utilized for this study. This setup led to an overall highest aggregation rate in the least stable formulation/process combination of k = 0.83 [%/month$^{-0.5}$]. In contrast, in other studies the lowest aggregation rate in the most stable samples were for example k = 1.04 [%/month$^{-0.5}$] [23] and k = 6.69 [%/month$^{-0.5}$][28]. Thus, in the present study, the differences in protein

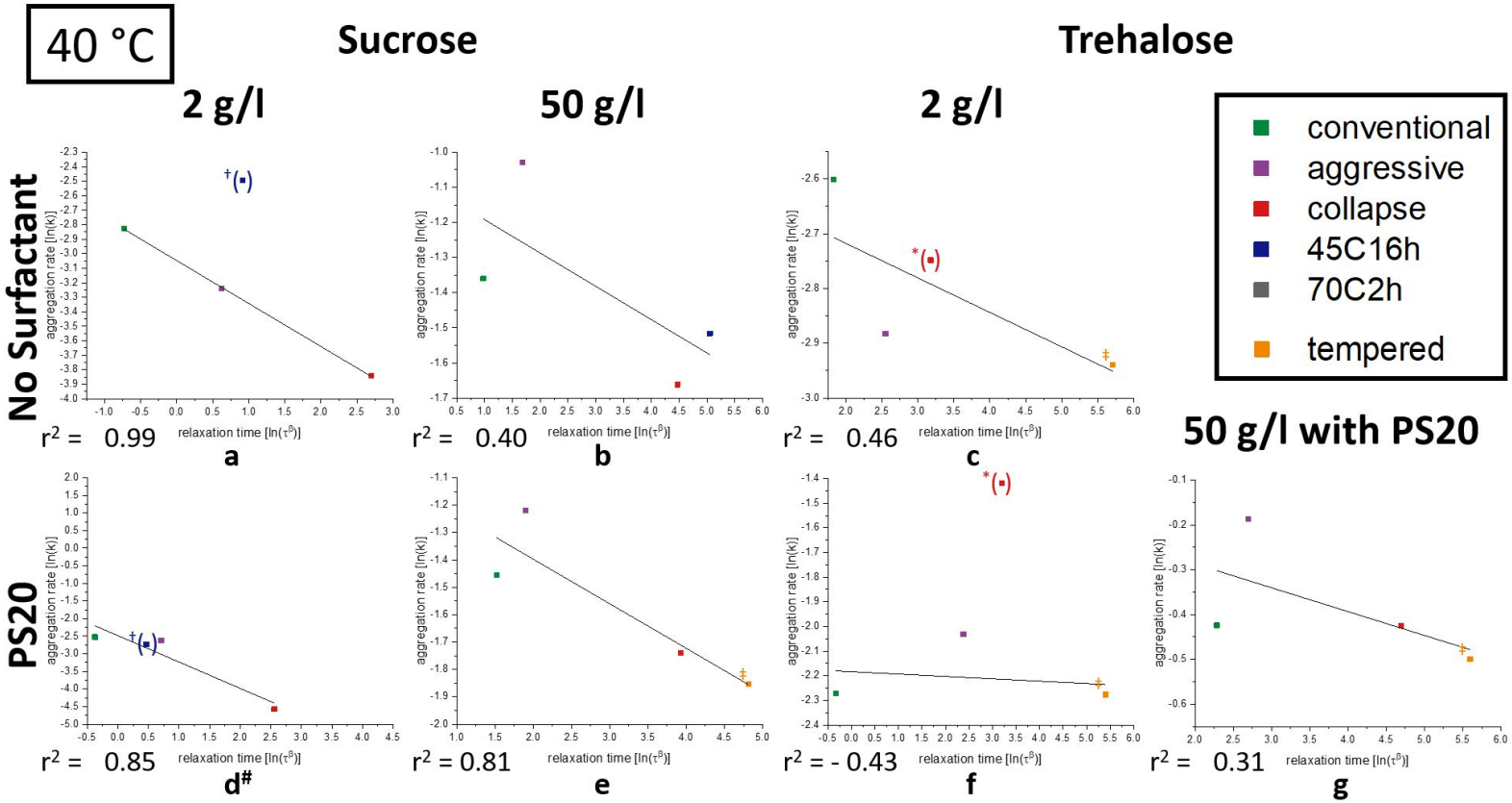

Figure IV.6 Correlation of the protein aggregation rate determined by HP-SEC with α-relaxation obtained with IMC. Small figures a-g represent the correlation of the different formulations at 40 °C. Formulations and processes as described in the legend. The respective correlation coefficients of the linear fit is presented at the left bottom of each chart. The orange dot named tempered and indicated by the double cross (‡) presents the mean value of both tempering processes (45C16h + 70C2H). The asterisc (*) in the 2gl_Tre formulations (c+f) marks the collapsed products as outlier as the residual moisture is significantly increased compared to the other products. The cross (†) in the 2gl_Suc formulations marks the 45C16h proces a outlier due to the tempering temperature close to Tg (see Appendix C). Those datapoint was left out of the fit procedure. In 2d marked with the hash, only the SEC data from the first 3 months of investigation time were used as the onset of crystalliation in this formulations made an correlation at later time points not possible.

aggregation rates among the processes were so small, that small errors were able to disturb the correlation procedure.

The proximity of the storage temperature to the glass transition temperature ($T_{storage} - T_g \approx 15\ °C$) of the 2gl_Suc formulations (Table IV.2 + IV.A2) could have been the reason why the correlation was the best in those formulations (Figure IV.6a and IV.6c), due to the fact that α-relaxations are temperature dependent and dominate the behavior of a matrix near the T_g[33]. With this, it could be that the higher T_g and with that the larger distance to the storage temperature for the other formulations (e.g. $T_{storage} - T_g \approx 50\ °C$ for trehalose formulation) made the correlation less strong as other temperature independent degradation mechanisms can superimpose the aggregations driven by α-relaxations. Figure IV.7 supports this hypothesis. There, the quality of the respective fits from figure IV.6 expressed as r^2 is plotted against the T_g distance of the formulations to the measurement and storage temperature of 40 °C. To estimate the T_g distance, the mean value of the Tg temperature of a formulation was calculated and subtracted by 40. When the 2gl_PS_Tre formulations was left out, a coupling factor $r^2_{T_g-distance}$ of 0.72 was achieved. The relation between T_g and storage temperature must be kept in mind when the stability predictions are carried out with α-relaxations.

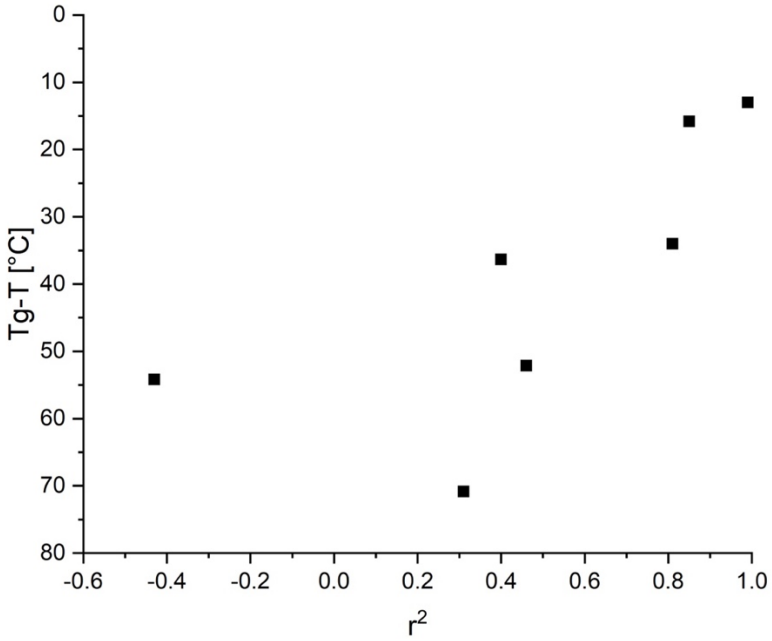

Figure IV.7 Dependency of the fit quality (aggregation rate with α-relaxations) with the distance of the average Tg of the formulations to the measurement and storage temperature of 40 °C. The average Tg for a formulation was calculated as mean value of all Tg from the respective tables 2, A1-A6 leaving out the collapsed samples for the 2gl_Tre formulations. r^2= 0.40, without the 2gl_PS20_Tre as negative values r^2 = 0.72

In summary, the present study supports the principle to correlate α-relaxation with protein aggregation but also shows the difficulties in the application on rather stable market formulations. Besides the idea to apply "external" tempering steps after drying it is possible to include the heat energy for tempering directly in the freeze-drying procedure (e.g., by a collapse cycle) to save time and costs. In the case of 2gl_Suc formulations the lowest aggregation rate of all processes was achieved by the collapse process. With an individual adaption and optimization of the process for formulations containing trehalose or a high amount of protein, intended collapse might led to the most stable products.

IV.6 Conclusion

The obtained data show that the direct correlation of α-relaxation and long-term aggregation is meaningful and even led to a prediction power for several formulations, but only when the storage temperature and the T_g are not too far apart. Furthermore, the IMC method works very well to determine and confirm the state of relaxation. However, the theoretical direct coupling of α-relaxations with protein aggregation could not be confirmed in a statistically valid manner over a broader range of different ratios of T_g to measurement temperature. It should be noted that in the main study very stable, market-like, relevant drug product formulations were used, instead of moist samples which would have created an artificial scenario triggering fast relaxation and strong correlations, like in the pre-study.

Furthermore, a number of very relevant observations was made and allows the following conclusions and practical advice.

1) Thermal treatment, either during the freeze-drying process or afterwards, improves the stability of protein formulations with respect to aggregation, not only relative but also in absolute numbers of protein aggregates after 9 months of storage (Appendix D).
2) Structural collapse introduced during the freeze-drying process could be used not only to safe time but also to achieve good stability and also to reduce the concentration of surfactant.
3) When external tempering after the freeze-drying process is utilized, short time and hot temperatures appear better than longer time at moderate warm temperatures (Figure IV.4). Eventually, collapse drying is the most "elegant" way of tempering as it is fast and can be carried out in one process.
4) The setup of the study allows the conclusion that the theoretical assumptions and experimental observations also apply to protein rich matrices (protein content of the

solid phase 38.5 %), not only to more or less to pure sugar matrices with a tiny amount of protein (protein content of the solid phase 2.4 %).

IV.7 Appendix A

Table IV.A1 Results from analysis of the matrix in solid state of the 2gl_NoSurf_Tre formulation. n = 3, values represent the mean value and the corresponding standard deviation.

process	Glass transition [°C]	Δc_p [$Jg^{-1}K^{-1}$]	Enthalpy recovery [Jg^{-1}]	SSA [m^2g^{-1}]	Residual moisture [%]
conventional	91.05 ± 2.08	0.52 ± 0.01	0.25 ± 0.17	0.942	1.13 ± 0.00
aggressive	92.73 ± 0.10	0.53 ± 0.09	0.47 ± 0.64	0.598	1.00 ± 0.12
collapse	76.43 ± 0.17	0.30 ± 0.05	1.83 ± 0.20	0.047	2.89 ± 0.26
45C16h	91.21 ± 1.77	0.43 ± 0.08	0.56 ± 0.33	0.845	1.19 ± 0.09
70C2h	93.59 ± 2.04	0.56 ± 0.05	*	0.887	1.12 ± 0.04

Table IV.A2 Results from analysis of the matrix in solid state of the 2gl_PS20_Suc formulation. n = 3, values represent the mean value and the corresponding standard deviation.

process	Glass transition [°C]	Δc_p [$Jg^{-1}K^{-1}$]	Enthalpy recovery [Jg^{-1}]	SSA [m^2g^{-1}]	Residual moisture [%]
conventional	48.81 ± 0.10	0.61 ± 0.07	3.83 ± 0.38	0.699	1.51 ± 0.00
aggressive	56.53 ± 5.19	0.60 ± 0.02	3.00 ± 0.51	0.154	1.31 ± 0.10
collapse	65.30 ± 2.26	0.33 ± 0.03	3.79 ± 0.25	0.099	1.38 + 0.10
45C16h	52.56 ± 0.23	0.54 ± 0.07	5.62 ± 0.07	0.668	1.54 ± 0.02

Table IV.A3 Results from analysis of the matrix in solid state of the 2gl_PS20_Tre formulation. n = 3, values represent the mean value and the corresponding standard deviation.

process	Glass transition [°C]	Δc_p [$Jg^{-1}K^{-1}$]	Enthalpy recovery [Jg^{-1}]	SSA [m^2g^{-1}]	Residual moisture [%]
conventional	91.16± 2.48	0.52 ± 0.02	0.43 ± 0.18	0.923	1.17 ± 0.19
aggressive	100.19 ± 0.01	0.40 ± 0.02	0.40 ± 0.16	0.660	0.98 ± 0.14
collapse	78.89 ± 2.34	0.35 ± 0.05	2.43 ± 0.20	0.074	2.72 ± 0.11
45C16h	92.63 ± 0.05	0.43 ± 0.00	0.33 ± 0.03	0.746	1.20 ± 0.03
70C2h	92.72 ± 0.08	0.62 ± 0.02	0.25 ± 0.19	0.873	1.15 ± 0.07

** Value not determinable.*

Table IV.A4 Results from analysis of the matrix in solid state of the of the 50gl_NoSurf_Suc formulation. n = 3, values represent the mean value and the corresponding standard deviation.

process	Glass transition [°C]	Δc_p [$Jg^{-1}K^{-1}$]	Enthalpy recovery [Jg^{-1}]	SSA [m^2g^{-1}]	Residual moisture [%]
conventional	74.43 ± 2.51	0.39 ± 0.08	*	0.824	1.00 ± 0.03
aggressive	78.24 ± 3.00	0.35 ± 0.03	*	0.641	0.80 ± 0.05
collapse	80.30 ± 0.15	0.46 ± 0.14	*	0.170	0.88 ± 0.12
45C16h	72.47 ± 0.01	0.42 ± 0.06	*	0.794	0.94 ± 0.03
70C2h	76.17 ± 0.03	0.50 ± 0.05	*	-	0.94 ± 0.14

** Value not determinable. – Not measured.*

Table IV.A5 Results from analysis of the matrix in solid state of the 50gl_PS20_Suc formulation. n = 3, values represent the mean value and the corresponding standard deviation.

process	Glass transition [°C]	Δc_p [$Jg^{-1}K^{-1}$]	Enthalpy recovery [Jg^{-1}]	SSA [m^2g^{-1}]	Residual moisture [%]
conventional	72.58 ± 1.51	0.62 ± 0.03	*	0.839	1.05 ± 0.04
aggressive	77.82 ± 1.82	0.44 ± 0.05	*	0.638	0.84 ± 0.06
collapse	78.33 ± 2.63	0.46 ± 0.03	*	0.148	1.01 + 0.13
45C16h	68.68 ± 0.06	0.46 ± 0.08	*	0.636	0.98 ± 0.09
70C2h	72.66 ± 0.10	0.41 ± 0.03	*	0.637	1.06 ± 0.0

** Value not determinable.*

Table IV.A6 Results from analysis of the matrix in solid state of the 50gl_PS20_Tre formulation. n = 3, values represent the mean value and the corresponding standard deviation.

process	Glass transition [°C]	Δc_p [$Jg^{-1}K^{-1}$]	Enthalpy recovery [Jg^{-1}]	SSA [m^2g^{-1}]	Residual moisture [%]
conventional	108.77 ± 0.44	0.34 ± 0.06	*	1.010	0.81 ± 0.02
aggressive	116.35 ± 0.20	0.27 ± 0.07	*	0.695	0.47 ± 0.07
collapse	116.24 ± 5.35	0.30 ± 0.10	*	0.143	0.70 ± 0.11
45C16h	104.43 ± 0.32	0.29 ± 0.02	*	0.918	0.86 ± 0.05
70C2h	108.42 ± 0.01	0.33 ± 0.07	*	0.937	0.89 ± 0.03

** Value not determinable.*

Table IV.A7 Relaxation times τ^{β} in h as obtained by isothermal microcalorimetry.

	Relaxation time τ^{β} [h]									
	Conventional		**Aggressive**		**Collapse**		**45C16h**		**70C2h**	
	25 °C	**40 °C**	**25 °C**	**40 °C**	**25 °C**	**40 °C**	**25 °C**	**40 °C**	**25 °C**	**40 °C**
2gl_NoSurf_Suc	4	1	11	2	23	15	206	3	-	-
2gl_NoSurf_Tre	18	6	20	13	30	24	471	391	535	212
2gl_PS20_Suc	5	1	26	2	40	13	203	2	-	-
2gl_PS20_Tre	25	1	44	11	72	24	717	211	328	232
50gl_NoSurf_Suc	12	3	38	5	48	87	718	156	*	52
50gl_PS20_Suc	15	5	67	7	97	51	105	212	71	35
50gl_PS20_Tre	22	10	39	15	140	110	599	273	102	266

*- combination of process with formulation did not exist due to T_g < tempering temperature of 70 °C. * combination of process with formulation not measured due to material limitations.*

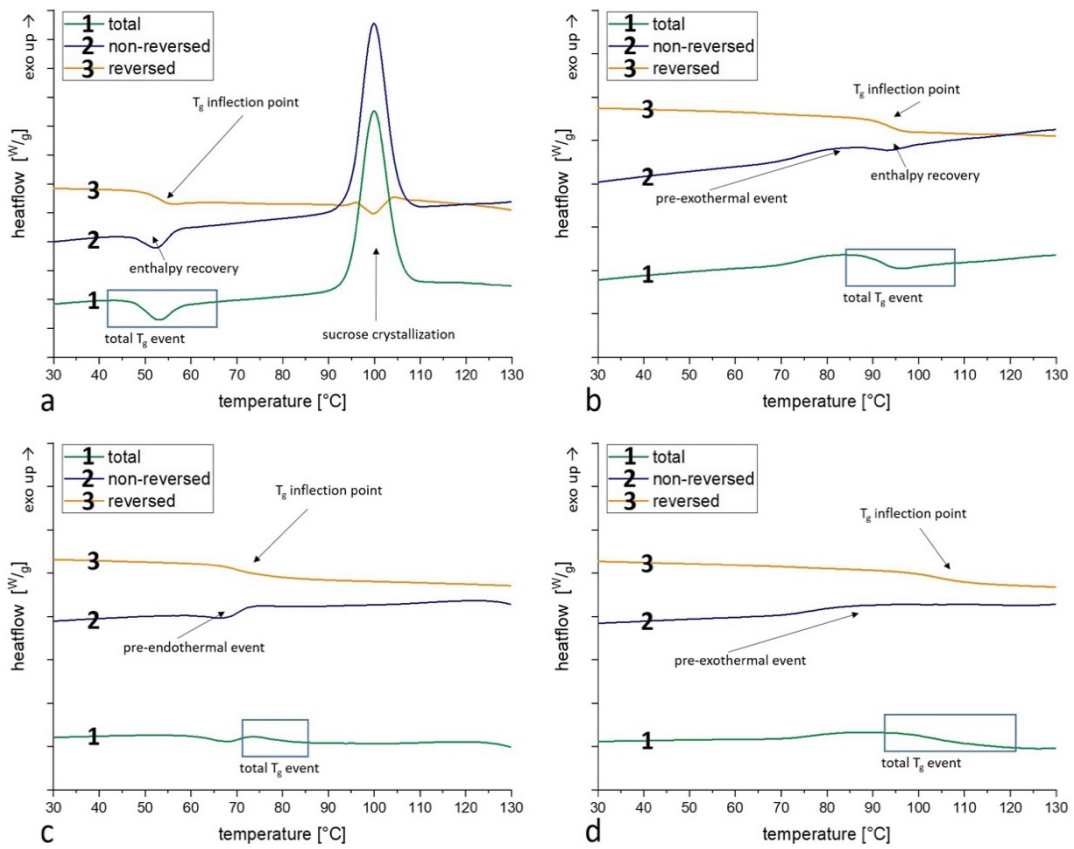

Figure IV.A1: Selected DSC curves from 45C16h process as example. Curve 1 (green) represents the total heat curve, curve 2 (blue) the non-reversed heat curve and curve 3 (orange) the reversed heat curve. The curves are presented with an y-axis offset for b etter clarity and a value of 0.05 µW/g between each auxiliary line. With diagram (a) 2gl_PS20_Suc, (b) 2gl_PS20_Tre, (c) 50gl_PS20_Suc and (d) 50gl_PS20_Tre.

IV.8 Appendix B

The utilized freeze-drying protocols for the pre-study are summarized as follows:

- Freeze-anneal (annealing step during the freezing procedure): Corresponds to the conventional process but an additional annealing step during the freezing procedure is added by ramping the samples with 1 K/min to - 4 °C after the 2.5 h hold time at – 45 °C. The temperature of - 4 °C was held for 6 h. Afterwards the samples were cooled back to - 45 °C again with 1 K/min and held for 2.5 h. From then, primary and secondary drying are conducted as for the conventional cycle.
- CN (controlled nucleation): The freezing procedure corresponds to the controlled nucleation procedure from a previous study[45]. Primary and secondary drying are conducted as for the conventional cycle.
- Collapse55 (more aggressive drying cycle that led to a full collapse of the product): The freezing step equals the freezing step from the collapse cycle. The pressure was then set to 1.2 mbar and the shelfs were ramped from -45 °C to 55 °C with 0.7 K/min. The 55 °C were held for 16 h with a pressure of 1.2 mbar for the first 3.5 h and 0.04 mbar for the rest of the process.

Table IV.B1 Solid state parameter of the 2gl_PS20_Suc formulation. n = 1, values represent the mean value and the corresponding standard deviation.

process	Glass transition [°C]	Δc_p [$Jg^{-1}K^{-1}$]	Enthalpy recovery [Jg^{-1}]	SSA [m^2g^{-1}]	Residual moisture [%]
freeze-anneal	72.58 ± 1.51	0.62 ± 0.03	*	0.839	1.05 ± 0.04
CN	77.82 ± 1.82	0.44 ± 0.05	*	0.638	0.84 ± 0.06
collapse55	78.33 ± 2.63	0.46 ± 0.03	*	0.148	1.01 + 0.13

– *Not measured.*

Table IV.B2 Solid state parameter of the 2gl_PS20_Suc formulation. n = 1, values represent the mean value and the corresponding standard deviation.

process	Glass transition [°C]	Δc_p [$Jg^{-1}K^{-1}$]	Enthalpy recovery [Jg^{-1}]	SSA [m^2g^{-1}]	Residual moisture [%]
freeze-anneal	60.20	0.45	0.64	-	2.03
CN	64.20	0.54	1.64	-	2.06
collapse55	70.52	0.45	2.06	-	0.54

– Not measured.

IV.9 Appendix C

As mentioned in the main text, a detailed explanation for the optimum tempering temperature and protocols can be found elsewhere[25,33]. The relevant information for the 2gl_Suc formulations is the following. The greater the temperature distance below T_g, the bigger is the energy excess of the glass compared to the thermodynamic equilibrated state at T_g or higher (purple line Figure IV.C1b). This means at lower temperatures the sample must release more energy to reach the state of equilibrium. However, at lower temperatures, overall reactions are slowed down kinetically. Usually, tempering protocols are performed with enough distance to T_g that the relaxation process is kinetically controlled (Figure IV.C1b, green and blue dots). Being too close to T_g for the tempering procedure, the process is not kinetically but rather thermodynamically controlled (Figure IV.C1b red dot) [41,49]. Thus, already during the tempering procedure the thermodynamic equilibrium is reached, and the sample is unnecessarily stressed by the higher temperature without the possibility to relax further. By bringing the sample back to a lower storage temperature of 40 °C (open red circle Figure IV.C1b), the thermodynamic limit increases, and the sample can proceed to relax. However, at this point in time the sample possesses still a higher energy excess (shorter τ^{β}) compared to the tempered samples at lower temperature. This means the tempering procedure was not affective but the mAb is already pre-damaged by the thermal stress at higher temperature. When a conventionally dried 2gl_NoSurf_Suc sample was stored for 7 days at 25 °C, 35 °C and 45 °C, the shortest τ^{β} values were observed for the highest tempering temperature at 45 °C (Figure IV.C1a). This supports the observation that a tempering temperature too close to T_g, in this case a T_g value of approx. 50 °C, will result in short relaxation times although the energy excess is low, which is counterintuitive. With these

theoretical considerations, the 45C16h process of the 2gl_Suc data may corrupt the correlation and is left out for the correlation procedure.

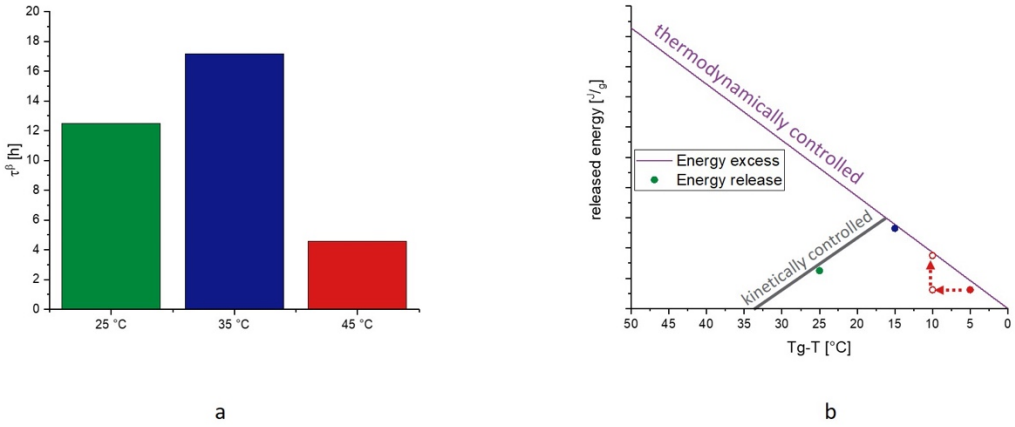

Figure IV.C1 Graphical explanation for the thermodynamic restriction for the tempering process of 2gl_Suc formulations at 45 °C. a) presents α-relaxation times measured at 40 °C of the 2gl_NoSurf_Suc formulation after storing it on the respective temperatures of 25°C, 35 °C or 45 °C for 7 days. b) is a graphical sketch explaining why the product stored at 45 °C has a smaller relaxation time than at 25 °C or 35 °C which is counterintuitive. Dots are the released energies as measured (green = tempered at 25 °C, blue = at 35 °C and red = at 45 °C). The grey line represents the kinetically controlled restriction and the thermodynamically controlled area (purple line). The x-axis shows the distance below Tg in [°C] and on the y-axis the released energy in J/g. More details about the energy transfer in amorphous matrices can be found in further literature.

IV.10 Appendix D

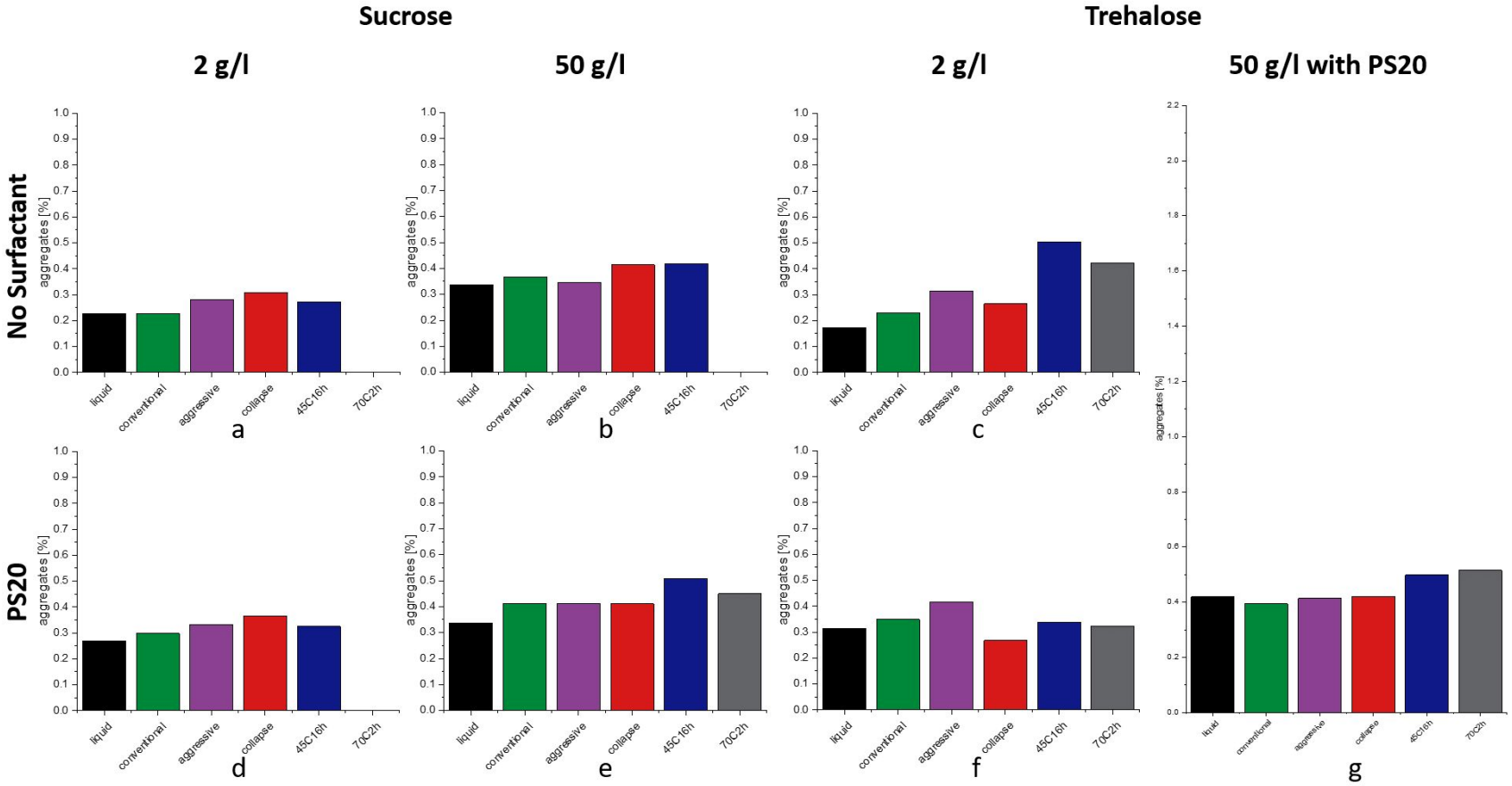

Figure IV.D1 The level of aggregates at t(0) of the products.

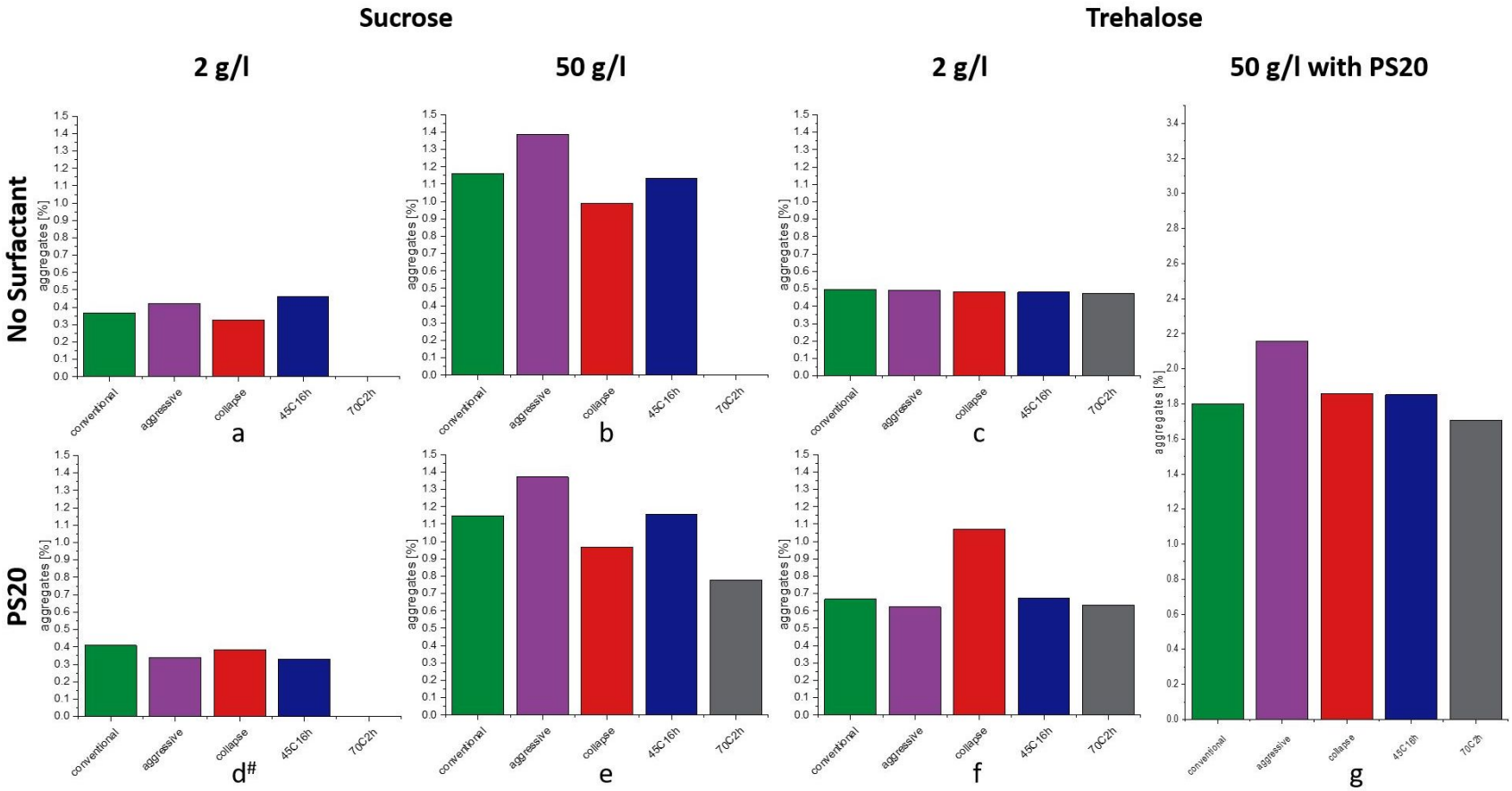

Figure IV.D2 The level of the relative amount aggregates at 9 month of storage at 40 °C of the products. For formulation 2d marked with the hash, only the data after 3 month of storage are displayed as discussed above.

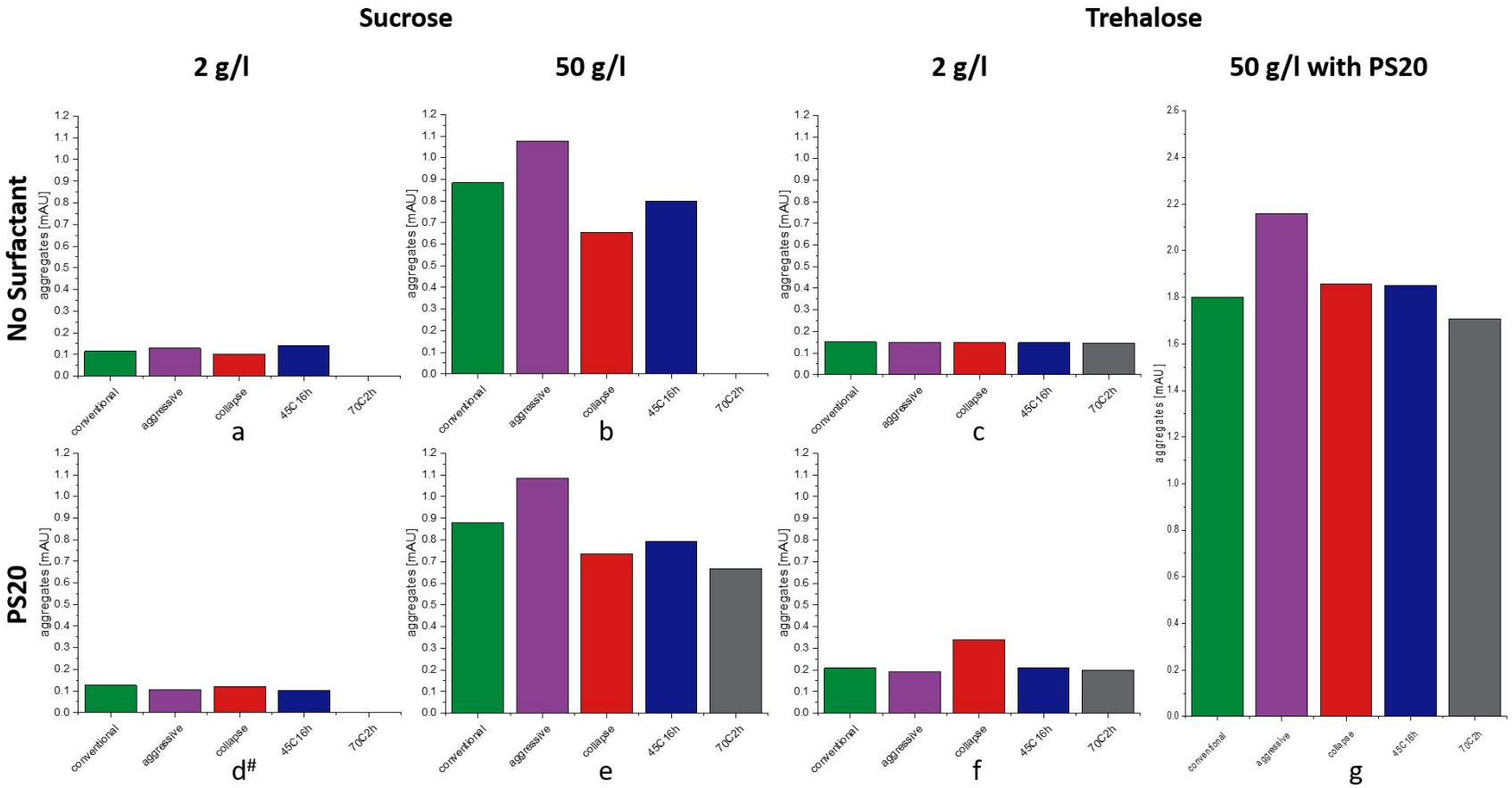

Figure IV.D3 The absolute level of aggregates after 9 month of storage at 40 °C. For formulation 2d marked with the hash, only the data after 3 month of storage are displayed as discussed above

IV.11 References

1. Mullard, A. 2020 FDA Drug Approvals. *Nat. Rev. Drug Discov.* **2021**, *20*, 85–90, doi:10.1038/d41573-021-00002-0.
2. Randolph, T.W.; Schiltz, E.; Sederstrom, D.; Steinmann, D.; Mozziconacci, O.; Schöneich, C.; Freund, E.; Ricci, M.S.; Carpenter, J.F.; Lengsfeld, C.S. Do Not Drop: Mechanical Shock in Vials Causes Cavitation, Protein Aggregation, and Particle Formation. *J. Pharm. Sci.* **2015**, *104*, 602–611, doi:10.1002/jps.24259.
3. Wang, W. Instability, Stabilization, and Formulation of Liquid Protein Pharmaceuticals. *Int. J. Pharm.* **1999**, *185*, 129–188, doi:10.1016/S0378-5173(99)00152-0.
4. Xu, Y.; Jiang, B.; Samai, P.; Tank, S.-M.; Shameem, M.; Liu, D. Genome DNA Leakage of Adeno–Associated Virus under Freeze–Thaw Stress. *Int. J. Pharm.* **2022**, *615*, 121464, doi:10.1016/j.ijpharm.2022.121464.
5. Crommelin, D.J.A.; Anchordoquy, T.J.; Volkin, D.B.; Jiskoot, W.; Mastrobattista, E. Addressing the Cold Reality of MRNA Vaccine Stability. *J. Pharm. Sci.* **2021**, *110*, 997–1001, doi:10.1016/j.xphs.2020.12.006.
6. Carpenter, J.F.; Pikal, M.J.; Chang, B.S.; Randolph, T.W. Rational Design of Stable Lyophilized Protein Formulations: Some Practical Advice. *Pharm. Res.* **1997**, *14*, 969–975, doi:10.1023/A:1012180707283.
7. Carpenter, J.F.; Chang, B.S.; Garzon-Rodriguez, W.; Randolph, T.W. Rational Design of Stable Lyophilized Protein Formulations: Theory and Practice. In *Rational Design of Stable Protein Formulations*; Carpenter, J.F., Manning, M.C., Eds.; Pharmaceutical Biotechnology; Springer US: Boston, MA, 2002; Vol. 13, pp. 109–133 ISBN 978-1-4613-5131-3.
8. Liu, J.; Rigsbee, D.R.; Stotz, C.; Pikal, M.J. Dynamics of Pharmaceutical Amorphous Solids: The Study of Enthalpy Relaxation by Isothermal Microcalorimetry. *J. Pharm. Sci.* **2002**, *91*, 1853–1862, doi:10.1002/jps.10181.
9. Grzybowska, K.; Capaccioli, S.; Paluch, M. Recent Developments in the Experimental Investigations of Relaxations in Pharmaceuticals by Dielectric Techniques at Ambient and Elevated Pressure. *Adv. Drug Deliv. Rev.* **2016**, *100*, 158–182, doi:10.1016/j.addr.2015.12.008.
10. Butreddy, A.; Janga, K.Y.; Ajjarapu, S.; Sarabu, S.; Dudhipala, N. Instability of Therapeutic Proteins — An Overview of Stresses, Stabilization Mechanisms and Analytical Techniques Involved in Lyophilized Proteins. *Int. J. Biol. Macromol.* **2021**, *167*, 309–325, doi:10.1016/j.ijbiomac.2020.11.188.

11. Telikepalli, S.; Kumru, O.S.; Kim, J.H.; Joshi, S.B.; O'berry, K.B.; Blake-Haskins, A.W.; Perkins, M.D.; Russell Middaugh, C.; Volkin, D.B. Characterization of the Physical Stability of a Lyophilized IgG1 MAb after Accelerated Shipping-Like Stress. *J. Pharm. Sci.* **2015**, *104*, 495–507, doi:10.1002/jps.24242.
12. Pikal, M.J. Chemistry in Solid Amorphous Matrices: Implication for Biostabilization. In *Amorphous Food and Pharmaceutical Systems*; Levine, H., Ed.; The Royal Society of Chemistry, 2002; pp. 257–272 ISBN 978-0-85404-866-3.
13. Pikal, M.J. Mechanisms of Protein Stabilization During Freeze-Drying Storage: The Relative Importance of Thermodynamic Stabilization and Glassy State Relaxation Dynamics. In *Freeze drying/lyophilization of pharmaceutical and biological products*; Rey, L., May, J.C., Eds.; Informa Healthcare: New York, 2010 ISBN 978-0-429-15185-9.
14. Abdul-Fattah, A.M.; Dellerman, K.M.; Bogner, R.H.; Pikal, M.J. The Effect of Annealing on the Stability of Amorphous Solids: Chemical Stability of Freeze-Dried Moxalactam. *J. Pharm. Sci.* **2007**, *96*, 1237–1250, doi:10.1002/jps.20947.
15. Yoshioka, S.; Aso, Y.; Kojima, S. Usefulness of the Kohlrausch-Williams-Watts Stretched Exponential Function to Describe Protein Aggregation in Lyophilized Formulations and the Temperature Dependence Near the Glass Transition Temperature. *Pharm. Res.* **2001**, *18*, 256–260, doi:10.1023/A:1011082309058.
16. Wang, B.; Tchessalov, S.; Cicerone, M.T.; Warne, N.W.; Pikal, M.J. Impact of Sucrose Level on Storage Stability of Proteins in Freeze-Dried Solids: II. Correlation of Aggregation Rate with Protein Structure and Molecular Mobility**This Work Is a Product of the U.S. Government and Is Not Subject to Copyright in the United States. *J. Pharm. Sci.* **2009**, *98*, 3145–3166, doi:10.1002/jps.21622.
17. Ellis, E.F.; Henney, C.S. Adverse Reactions Following Administration of Human Gamma Globulin. *J. Allergy* **1969**, *43*, 45–54, doi:10.1016/0021-8707(69)90019-7.
18. Kotarek, J.; Stuart, C.; De Paoli, S.H.; Simak, J.; Lin, T.-L.; Gao, Y.; Ovanesov, M.; Liang, Y.; Scott, D.; Brown, J.; et al. Subvisible Particle Content, Formulation, and Dose of an Erythropoietin Peptide Mimetic Product Are Associated With Severe Adverse Postmarketing Events. *J. Pharm. Sci.* **2016**, *105*, 1023–1027, doi:10.1016/S0022-3549(15)00180-X.
19. Joubert, M.K.; Hokom, M.; Eakin, C.; Zhou, L.; Deshpande, M.; Baker, M.P.; Goletz, T.J.; Kerwin, B.A.; Chirmule, N.; Narhi, L.O.; et al. Highly Aggregated Antibody

Therapeutics Can Enhance the in Vitro Innate and Late-Stage T-Cell Immune Responses. *J. Biol. Chem.* **2012**, *287*, 25266–25279, doi:10.1074/jbc.M111.330902.

20. Shamblin, S.L.; Hancock, B.C.; Dupuis, Y.; Pikal, M.J. Interpretation of Relaxation Time Constants for Amorphous Pharmaceutical Systems. *J. Pharm. Sci.* **2000**, *89*, 417–427, doi:10.1002/(SICI)1520-6017(200003)89:3<417::AID-JPS12>3.0.CO;2-V.
21. Luthra, S.A.; Hodge, I.M.; Utz, M.; Pikal, M.J. Correlation of Annealing with Chemical Stability in Lyophilized Pharmaceutical Glasses. *J. Pharm. Sci.* **2008**, *97*, 5240–5251, doi:10.1002/jps.21391.
22. Kawakami, K.; Pikal, M.J. Calorimetric Investigation of the Structural Relaxation of Amorphous Materials: Evaluating Validity of the Methodologies. *J. Pharm. Sci.* **2005**, *94*, 948–965, doi:10.1002/jps.20298.
23. Abdul-Fattah, A.M.; Truong-Le, V.; Yee, L.; Nguyen, L.; Kalonia, D.S.; Cicerone, M.T.; Pikal, M.J. Drying-Induced Variations in Physico-Chemical Properties of Amorphous Pharmaceuticals and Their Impact on Stability (I): Stability of a Monoclonal Antibody. *J. Pharm. Sci.* **2007**, *96*, 1983–2008, doi:10.1002/jps.20859.
24. Descamps, M.; Aumelas, A.; Desprez, S.; Willart, J.F. The Amorphous State of Pharmaceuticals Obtained or Transformed by Milling: Sub-Tg Features and Rejuvenation. *J. Non-Cryst. Solids* **2015**, *407*, 72–80, doi:10.1016/j.jnoncrysol.2014.08.055.
25. Groël, S.; Menzen, T.; Winter, G. Calorimetric Investigation of the Relaxation Phenomena in Amorphous Lyophilized Solids. *Pharmaceutics* **2021**, *13*, 1735, doi:10.3390/pharmaceutics13101735.
26. Luthra, S.A.; Hodge, I.M.; Pikal, M.J. Investigation of the Impact of Annealing on Global Molecular Mobility in Glasses: Optimization for Stabilization of Amorphous Pharmaceuticals. *J. Pharm. Sci.* **2008**, *97*, 3865–3882, doi:10.1002/jps.21255.
27. Wang, B.; Pikal, M.J. The Impact of Thermal Treatment on the Stability of Freeze Dried Amorphous Pharmaceuticals: I. Dimer Formation in Sodium Ethacrynate. *J. Pharm. Sci.* **2010**, *99*, 663–682, doi:10.1002/jps.21959.
28. Wang, B.; Cicerone, M.T.; Aso, Y.; Pikal, M.J. The Impact of Thermal Treatment on the Stability of Freeze-Dried Amorphous Pharmaceuticals: II. Aggregation in an IgG1 Fusion Protein. *J. Pharm. Sci.* **2010**, *99*, 683–700, doi:10.1002/jps.21960.
29. Pikal, M.J.; Dellerman, K.M. Stability Testing of Pharmaceuticals by High-Sensitivity Isothermal Calorimetry at 25°C: Cephalosporins in the Solid and Aqueous Solution States. *Int. J. Pharm.* **1989**, *50*, 233–252, doi:10.1016/0378-5173(89)90127-0.

30. Waghmare, R.B.; Choudhary, P.; Moses, J.A.; Anandharamakrishnan, C.; Stapley, A.G.F. Trends in Approaches to Assist Freeze-Drying of Food: A Cohort Study on Innovations. *Food Rev. Int.* **2022**, *38*, 552–573, doi:10.1080/87559129.2021.1875232.
31. Schersch, K.; Betz, O.; Garidel, P.; Muehlau, S.; Bassarab, S.; Winter, G. Systematic Investigation of the Effect of Lyophilizate Collapse on Pharmaceutically Relevant Proteins I: Stability after Freeze-drying. *J. Pharm. Sci.* **2010**, *99*, 2256–2278, doi:10.1002/jps.22000.
32. Schersch, K.; Betz, O.; Garidel, P.; Muehlau, S.; Bassarab, S.; Winter, G. Systematic Investigation of the Effect of Lyophilizate Collapse on Pharmaceutically Relevant Proteins, Part 2: Stability During Storage at Elevated Temperatures. *J. Pharm. Sci.* **2012**, *101*, 2288–2306, doi:10.1002/jps.23121.
33. Luthra, S.A. Impact of Optimum Annealing on Chemical Stabilization of Model Amorphous Pharmaceuticals. PhD Thesis, University of Connecticut: Connecticut, 2007.
34. Chang, L. (Lucy); Shepherd, D.; Sun, J.; Tang, X. (Charlie); Pikal, M.J. Effect of Sorbitol and Residual Moisture on the Stability of Lyophilized Antibodies: Implications for the Mechanism of Protein Stabilization in the Solid State. *J. Pharm. Sci.* **2005**, *94*, 1445–1455, doi:10.1002/jps.20363.
35. Luthra, S.A.; Hodge, I.M.; Pikal, M.J. Effects of Annealing on Enthalpy Relaxation in Lyophilized Disaccharide Formulations: Mathematical Modeling of DSC Curves. *J. Pharm. Sci.* **2008**, *97*, 3084–3099, doi:10.1002/jps.21186.
36. Hodge, I.M.; Berens, A.R. Effects of Annealing and Prior History on Enthalpy Relaxation in Glassy Polymers. 2. Mathematical Modeling. *Macromolecules* **1982**, *15*, 762–770, doi:10.1021/ma00231a016.
37. Struik, L.C.E. *Physical Aging in Amorphous Polymers and Other Materials*; Elsevier Scientific Pub. Co. ; distributors for the U.S. and Canada, Elsevier North-Holland: Amsterdam ; New York : New York, 1978; ISBN 978-0-444-41655-1.
38. Surana, R.; Pyne, A.; Suryanarayanan, R. Effect of Aging on the Physical Properties of Amorphous Trehalose. *Pharm. Res.* **2004**, *21*, 867–874, doi:10.1023/B:PHAM.0000026441.77567.75.
39. Bosch, Thomas Aggressive Freeze-Drying: A Fast and Suitable Method to Stabilize Biopharmaceuticals, Ludwig-Maximilians-Universität München, 2014.
40. Xu, Y.; Grobelny, P.; Von Allmen, A.; Knudson, K.; Pikal, M.; Carpenter, J.F.; Randolph, T.W. Protein Quantity on the Air–Solid Interface Determines Degradation

Rates of Human Growth Hormone in Lyophilized Samples. *J. Pharm. Sci.* **2014**, *103*, 1356–1366, doi:10.1002/jps.23926.

41. Chung, H.-J.; Lim, S.-T. Physical Aging of Glassy Normal and Waxy Rice Starches: Effect of Aging Temperature on Glass Transition and Enthalpy Relaxation. *Carbohydr. Polym.* **2003**, *53*, 205–211, doi:10.1016/S0144-8617(03)00077-8.
42. Montserrat, S. Vitrification and Further Structural Relaxation in the Isothermal Curing of an Epoxy Resin. *J. Appl. Polym. Sci.* **1992**, *44*, 545–554, doi:10.1002/app.1992.070440319.
43. Cook, WayneD.; Mehrabi, M.; Edward, GrahamH. Ageing and Yielding in Model Epoxy Thermosets. *Polymer* **1999**, *40*, 1209–1218, doi:10.1016/S0032-3861(98)00343-7.
44. Vollrath, I.; Friess, W.; Freitag, A.; Hawe, A.; Winter, G. Does Controlled Nucleation Impact the Properties and Stability of Lyophilized Monoclonal Antibody Formulations? *Eur. J. Pharm. Biopharm.* **2018**, *129*, 134–144, doi:10.1016/j.ejpb.2018.05.025.
45. Groël, S.; Menzen, T.; Winter, G. Prediction of Unwanted Crystallization of Freeze-Dried Protein Formulations Using α-Relaxation Measurements. *Pharmaceutics* **2023**, *15*, 703, doi:10.3390/pharmaceutics15020703.
46. Cicerone, M.T.; Douglas, J.F. β-Relaxation Governs Protein Stability in Sugar-Glass Matrices. *Soft Matter* **2012**, *8*, 2983, doi:10.1039/c2sm06979b.
47. Allison, S.D.; Chang, B.; Randolph, T.W.; Carpenter, J.F. Hydrogen Bonding between Sugar and Protein Is Responsible for Inhibition of Dehydration-Induced Protein Unfolding. *Arch. Biochem. Biophys.* **1999**, *365*, 289–298, doi:10.1006/abbi.1999.1175.
48. Schammé, B.; Couvrat, N.; Tognetti, V.; Delbreilh, L.; Dupray, V.; Dargent, É.; Coquerel, G. Investigation of Drug–Excipient Interactions in Biclotymol Amorphous Solid Dispersions. *Mol. Pharm.* **2018**, *15*, 1112–1125, doi:10.1021/acs.molpharmaceut.7b00993.
49. Haque, Md.K.; Kawai, K.; Suzuki, T. Glass Transition and Enthalpy Relaxation of Amorphous Lactose Glass. *Carbohydr. Res.* **2006**, *341*, 1884–1889, doi:10.1016/j.carres.2006.04.040.
50. Petit, S.; Coquerel, G. The Amorphous State. In *Polymorphism*; Hilfiker, R., Ed.; Wiley-VCH Verlag GmbH & Co. KGaA: Weinheim, FRG, 2006; pp. 259–285 ISBN 978-3-527-60788-4.

Chapter V Further investigations and analyses

V.1 Introduction

In addition to the results presented in chapter III and IV, this chapter provides further elaborations of findings from our research on relaxation of amorphous cakes. While the published papers focused on specific aspects of the research questions, this chapter presents a partly more comprehensive analysis of the data, including results that were not presented in the previous chapters. The aim of this chapter is to provide a deeper understanding of amorphous freeze-dried protein formulations in connection with α-relaxations and to expand upon the insights gained from the initial analysis.

By these results, a more nuanced perspective on the calorimetric investigation should be provided.

The chapter is organized into sections that reflect the main themes of the research project, and each section includes a detailed discussion of the relevant findings. If not stated otherwise, the used materials and methods correspond to those in chapter IV.

V.2 Investigation of semicrystalline matrices

In the area of freeze-dried protein formulations crystalline bulking agents can be used to support the freeze-drying process [1,2]. By annealing, agents like mannitol or glycine can be forced to crystallize on purpose [3–5]. Crystallized, the excipients are no longer able to preserve the protein well which is why they are mixed with other components that must stay amorphous, but the crystals are able to form a stable network that preserves the structure of the amorphous cake [6,7]. Thus, optical defects of the cake are prevented and harsher freeze-drying cycles can be used without visible damage of the product [1].

For this reason, semi-crystalline matrices were also considered in our α-relaxation stability study. To check the influence crystalline agents would have on relaxation, mixtures out of trehalose and KCl (Merck KGaA, Darmstadt, Germany) were generated in different ratios and freeze-dried in a pre-study, with the annealing cycle from chapter IV. KCl was chosen as agent that fully crystallizes in any case to minimize the risk of remaining amorphous parts like it could have happened with mannitol or glycine [2,3]. Figure V.1a shows the obtained α-relaxation curves.

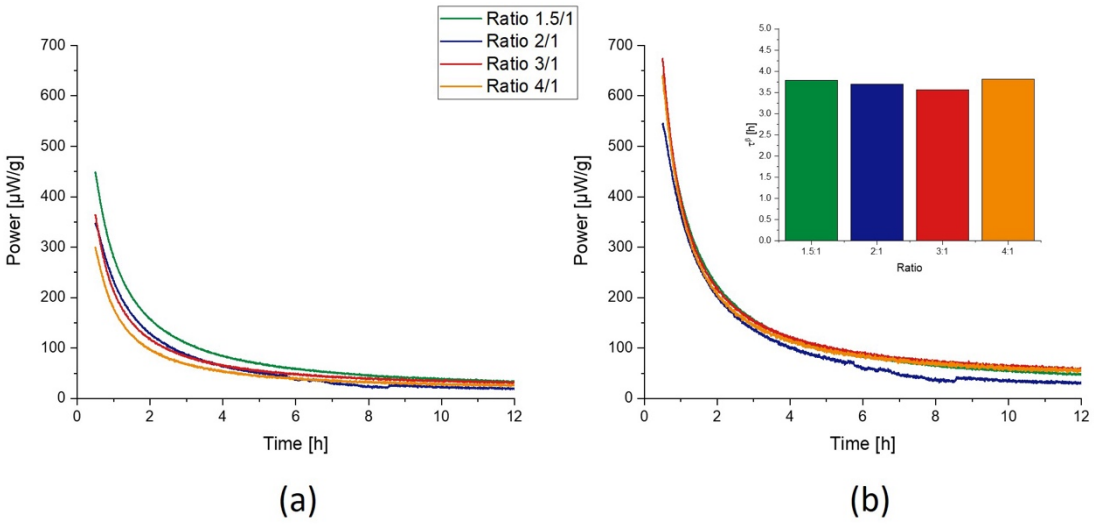

Figure V.1 Relaxation data of the KCl:Trehalose mixtures. (a) presents the untreated data whereas the power curve is normalized to the weight ratio of trehalose in (b). The small bar chart presents the relaxation time of the normalized relaxation curves from (b).

It can be seen in in figure V.1a, that the data normalized on the weight of the complete formulation clearly led to different relaxation curves with higher absolute maxima and energy release for formulations with a higher trehalose content. However, when the curves were normalized on the weight of trehalose only (Figure V.1b), as the disaccharide is the only expected amorphous part of the cake, the curves can be overlayed very well and the calculated values for τβ for each curve are very similar.

The obtained results fit to the expectations. As the crystallized KCl leaves the amorphous part of the formulation by phase separation, it has no impact on the relaxation of the latter. The crystalline phase itself does not show any energy signal, as a crystal is the most stable state and possesses no energy excess or energy lack. The possibility that the crystalline part of the formulation might change the relaxation behavior of the amorphous phase for example by steric hindrance can now be ruled out. For this reason, only full amorphous matrices were considered in the investigations of chapter IV. With this, a maximally clean and high signal level could be obtained in the IMC instrument and also very small changes in α-relaxations between the processes can be carved out. If the amorphous phase would be „diluted“ with a crystalline part, that does not contribute to the power signal, more sample mass (than the typically used 100 - 300 mg) would have been needed for the measurement. Furthermore, the relaxation signal will not be interrupted by a subsequently crystallizing agent.

V.3 The use of microwave radiation as alternative tempering procedure

As further method to change the relaxation state of freeze-dried products, microwave radiation was tested. This technique can be applied during primary drying, secondary drying and after the freeze-drying process [8,9].

Recent studies of Härdter et al. provide further insights in the function of microwave assisted freeze drying (MFD) [8]. In their studies the authors achieved a clear reduction of the process time by the application of microwave radiation during primary drying, without loss of product quality compared to conventional dried formulations. With the similar idea as used in chapter IV, to apply energy not in a subsequent tempering process but already in the freeze-drying process itself (to gently increase the relaxation time of the product and simultaneously shorten the process time), a verum and placebo sample dried with microwave radiation added to the primary drying was investigated. The pertaining samples were provided by N. Härdter and consist out of 20 mg/ml sucrose in 10 mM Histidine buffer pH 5.5 as well as additional 70 mg/ml IgG_1-antibody for the verum formulations. To examine, whether the microwave radiation during primary drying is absorbed by the amorphous matrix and an increased relaxation time can be achieved, from each formulation a conventional dried version (CFD) was compared to a counterpart that was dried with microwave radiation (MFD). Figure 2 presents the α-relaxation curves and τ^{β} values of the products.

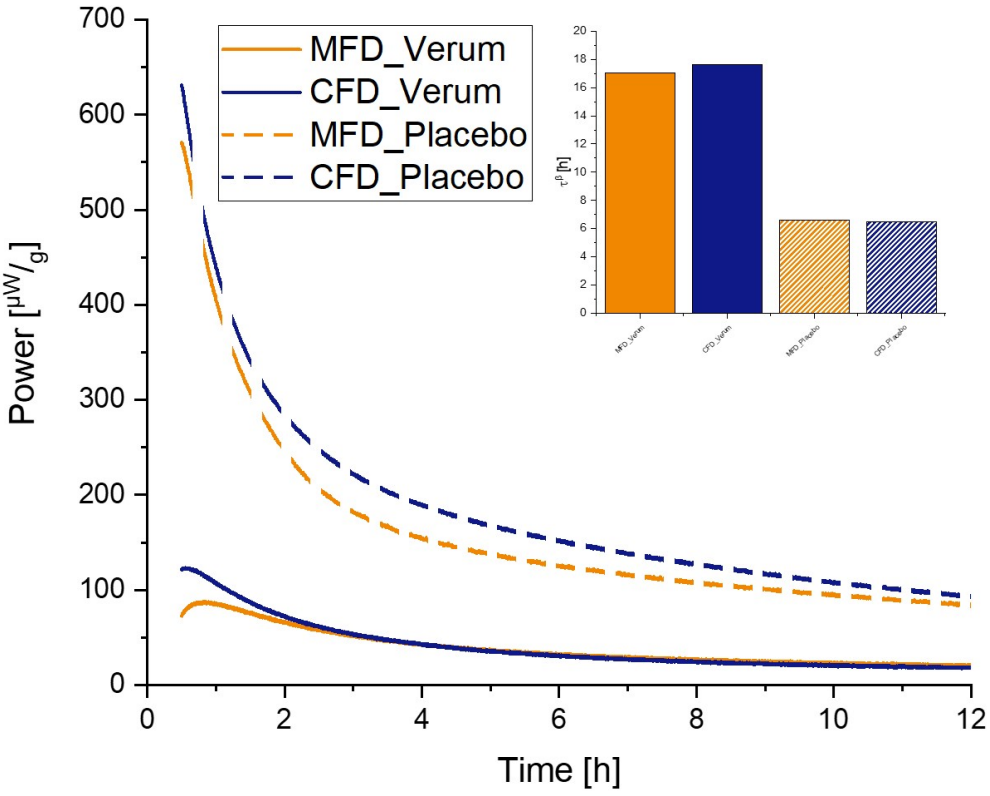

Figure V.2 α- relaxation times of conventional and microwave assisted freeze-dried products. Solid lines display verum formulations and dashed lines placebo formulations, respectively. The orange line shows the microwave assisted freeze dried product and the blue line the conventional dried counterparts. The bar chart presents the corresponding τ^{β}-values.

The data in figure V.2 indicates that there is only a very small difference in the relaxation behavior between the tested CFD and MFD products. The curves possess a quite similar course. Only during the first 2.5 h of the measurement in the verum samples, a more distinct difference between the MFD and CFD version of the product is evident and in both products a peak maximum is observable during the measurement, like in the 45C16h products of chapter IV. Thus, it seems like the amorphous matrix is not absorbing the energy of the microwave radiation during primary drying or is able to transfer the absorbed energy into the sublimation of ice. Further studies are necessary to provide more insights in the mechanisms, however this experiment supports the use of microwave assisted freeze drying in that way, that the amorphous matrix seems to be unaffected by the microwave radiation and only the sublimation of ice is accelerated without a strong energy input into the growing solid matrix.

In a further experiment microwave radiation was applied on an already dried product. Similar to tempering, the treatment should lead to a longer α-relaxation time τ^{β}. Maybe a direct correlation to the remaining inner energy of the amorphous phase can be drawn depending on the energy input of the microwave, which would make a rational design of the tempering process more easy. A Bosch HMT84M421 microwave (Robert Bosch Hausgeräte GmbH, Munich, Germany) was utilized for this experiment with the 50gl_PS20_Tre formulation from chapter IV. The sample vials were decrimped to remove aluminum and plastic materials and placed in the middle of the microwave plate. The microwave was set to 90 W for different time points of 1, 10 and 20 min. The power level settings of 180 W and higher led to a detachment of the stopper and thus, could not be utilized in this study. Figure V.3 presents the results of this experiment.

It is noticeable, that the presented curve parameters are in good correlation with the energy entry by microwave radiation. The energy entry was calculated by multiplying the set power with the radiation time.

The maximum of the relaxation curve and the enthalpy recovery from DSC in the other hand can be determined more precisely and with this can achieve correlation values of $r^2 = 0.99$ and $r^2 = 0.93$, respectively.

Overall, the main goal of this short study was achieved. Applying microwave radiation on finalized freeze-dried formulations allows a very fast and precise control of the relaxation state of the amorphous phase. In freeze-dryers equipped with microwave modules, a tempering of the formulations could be applied within time spans of 20 min or even less instead of adding an additional tempering step. Stability studies must be performed to ensure, that with microwave radiation as tempering procedure, no side reactions are triggered. For the study in chapter IV, microwave tempered vials could not be included, as it was technically impossible to temper all needed vials in a microwave.

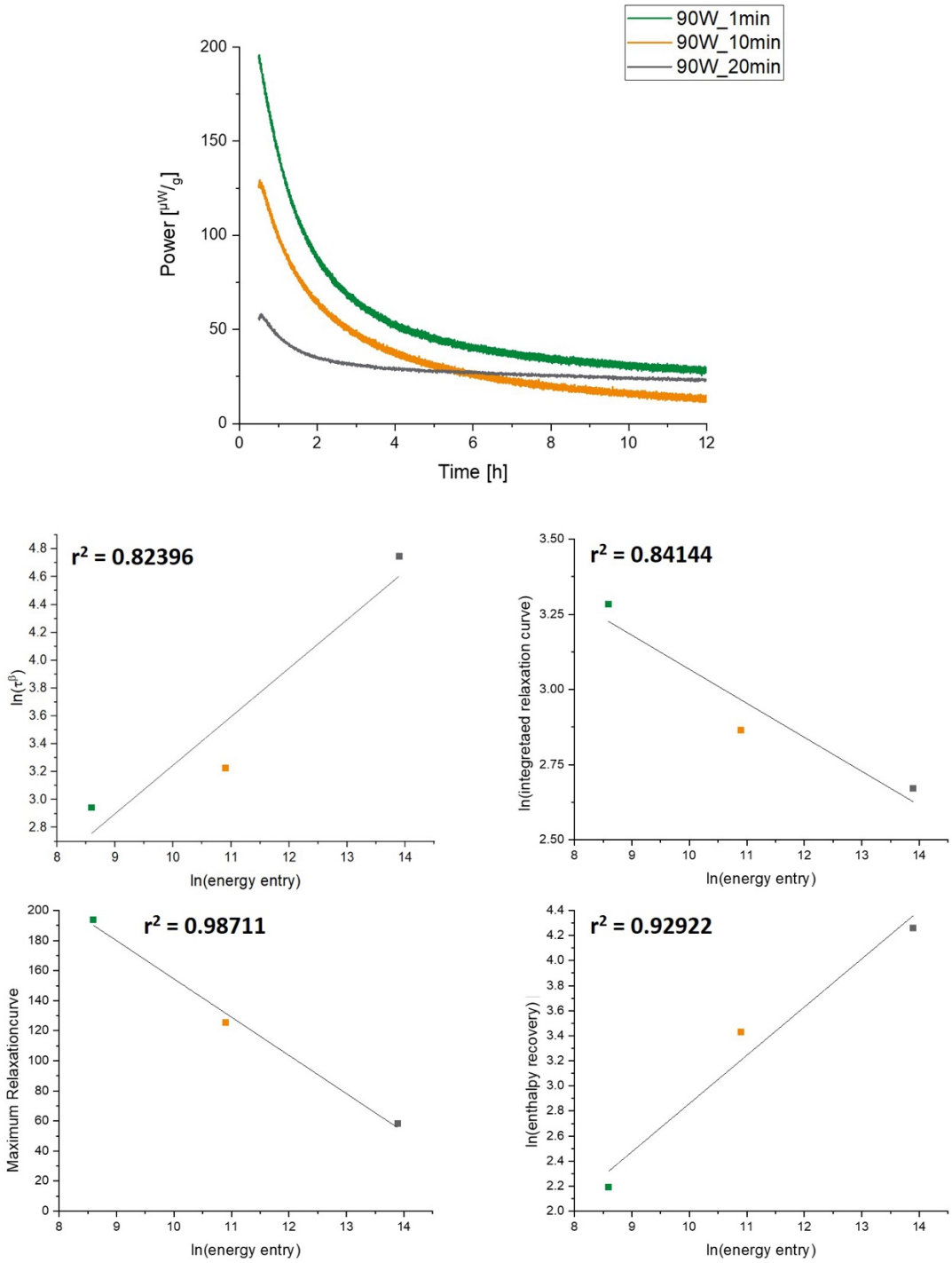

Figure V.3 Summarized correlations of α-relaxation curve parameters with the energy entry of microwave radiation. The top graph presents the normalized α-relaxation curves and the lower 4 graphs the correlation of the logarithmized energy entries with either logarithmized values of τ^{β}, integrated relaxation curve (energy), maximum of relaxation curve or enthalpy recovery from DSC experiments respectively.

V.4 Correlation of protein stability and α-relaxation at 25 °C

As an addition to the correlation of IgG_1 aggregation with α-relaxation times during storage and IMC measurement at 40 °C, the data obtained for storage and measurement at 25 °C are presented in this part. The methodology corresponds to the one presented in chapter IV with the only exception that for determining the relaxation times at 25 °C the sample preparation time was also noted and added to the measurement time recorded by the calorimeter. As the sample preparation was conducted near 25 °C it can be assumed that a relevant amount of relaxation happened already during the sample transfer to the measurement system. For this reason, the relaxation curves start at slightly different times and always later than 0.5 h. Figure V.4 displays the obtained relaxation curves with corresponding α-relaxation time τ^{β}.

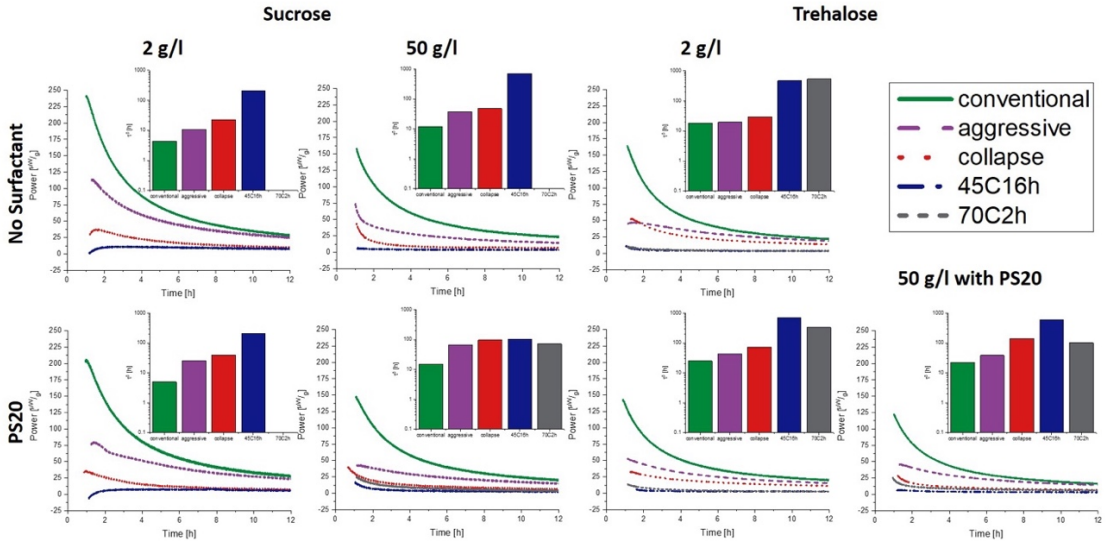

Figure V.4 Relaxation data obtained from isothermal microcalorimetry at 25 °C. The line diagram presents the relaxation curve and the bar chart the calculated τ^{β}-values.

Compared to the measured relaxation times at 40 °C, the overall relaxation times were longer at 25 °C (Figure IV.3). This was expected, due to the fact that overall reactions should be slowed down at lower absolute temperature and with this of course also the relaxation reactions. It could be observed that the resolution and differences between the process parameters are more distinct at 25 °C. For example, in the 2gl_Suc samples the curve of the collapse process is well distinguishable from the 45C16h curve, which was not the case at 40 °C. The reason might be the decelerated reactions at 25 °C compared to 40 °C. This made it possible to record some relaxation modes and energies that vanish at a measurement temperature of 40 °C under the friction noises within the first 0.5 h of measurement time. At 25 °C the slower reactions made it possible to record those relaxation modes and made them visible in the relaxation curves.

The correlations of protein aggregation at 25 °C with relaxation times can be found in figure V.5. For the 50gl_NoSurf_Suc (Figure V.5i), 2gl_PS20_Tre (Figure V.5m), and the 50gl_PS20_Tre (Figure V.5n), the quality of the correlation fit was improved compared to the measurement at 40 °C (Table V.1). For the other formulations the fit went worse at 25 °C.

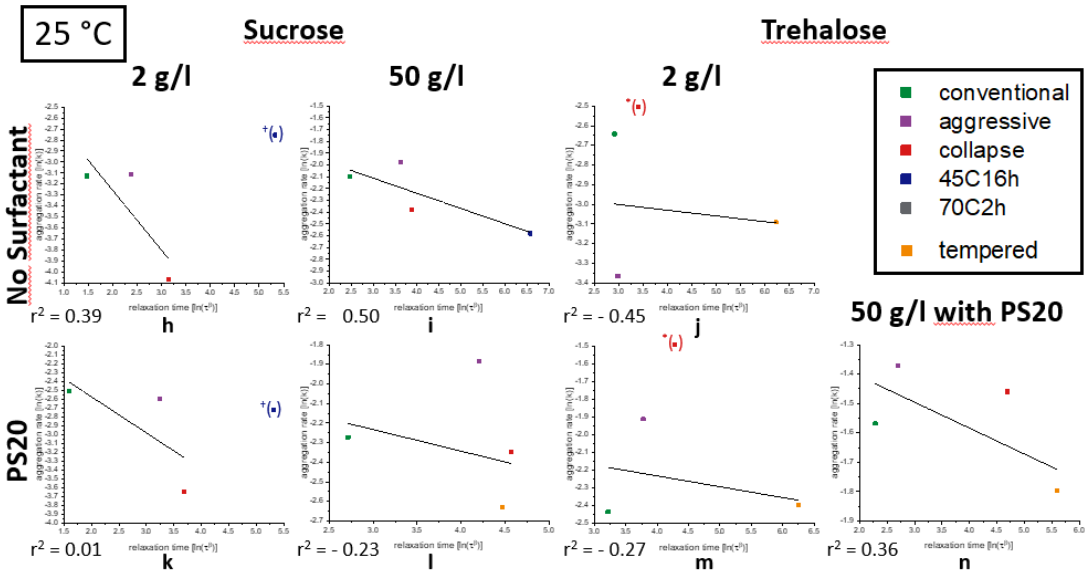

Figure V.5 Correlation of the protein aggregation rate determined by HP-SEC with α-relaxation obtained with IMC. Small figures h-n represent the correlation of the different formulations at 25 °C. Formulations and processes as described in the legend. The respective correlation coefficients of the linear fit is presented at the left bottom of each chart. The orange dot named tempered and indicated by the double cross (‡) presents the mean value of both tempering processes (45C16h + 70C2H). The asterisc (*) in the 2gl_Tre formulations (j+m) marks the collapsed products as outlier as the residual moisture is significantly increased compared to the other products. The cross (†) in the 2gl_Suc formulations marks the 45C16h proces a outlier due to the tempering temperature close to Tg (see Appendix C).

The reason might be the balance between a better resolution of the α-relaxation measurement at 25 °C and a more difficult estimation of the aggregation rate at the lower temperature. As mentioned in chapter IV, the model antibody used for this study was in its stable market formulation and 6 small variations of it. Accordingly, the aggregation rates were very low at 25 °C with the highest aggregation rate for the 50gl_PS20_Tre formulation with only 0.25 [%/month$^{-0.5}$]. Other studies were performed mostly at storage temperatures of 40 °C or higher and thus found much higher aggregation rates than in the present study. As a result, at 25 °C the differences in aggregation rates in our study were lower than at 40 °C and also the correlation got less good compared to the one at 40°C. For the formulations with a high aggregation rate, 50gl_NoSurf_Suc and 50gl_PS20_Tre, the quality of the fit stayed at the same quality level as at 40 °C and proves, that the correlation of relaxation with protein aggregation

is possible at lower temperatures but needs enough “instability” to result in numbers above the limit of quantification for aggregates.

Table V.1 Comparison of the quality of the correlation of aggregation with α-relaxation at 25 °C and 40 °C

formulation	r^2 at 25°C	r^2 at 40°C
2gl_NoSurf_Suc	0.39	0.99
2gl_PS20_Suc	0.01	0.85
50gl_NoSurf_Suc	0.50	0.40
50gl_PS20_Suc	–0.23	0.81
2gl_NoSurf_Tre	–0.45	0.46
2gl_PS20_Tre	–0.27	–0.43
50gl_PS20_Tre	0.36	0.31

V.5 Matrices with further excipients and polymers added

In addition to the used disaccharide formulations in chapter IV, blends with further excipients and polymers were investigated. As the research about the behavior of glasses and relaxations is mainly driven by polymer science, the idea is to improve the correlation of α-relaxations with the stability of an IgG1-antibody when adding polymers to the matrix [10–12]. It could be, that the behavior and response of polymers towards relaxation is stronger and also better transferable to protein stability. Following this concept, additional sucrose formulations were created, presented in table V.3. 40 % of the solid content of the sucrose (79.45 mg/ml, 88% w/w in dried form) was replaced by the respective polymer, to reach a ratio of sucrose to polymer of 1.5:1 as suggested by Haeuser et al. [13]. The used polymers were either Dextran (Dex) or Hydroxethylstarch (HES) and the excipient 2-Hydroxypropyl-β-cyclodextrin (HPβCD) was also tested.

Table V.3 Composition of the additional sucrose formulation blends. Concentrations given in mg/mL

Excipient	Dex	HES	HPβCD
LMU1	10	10	10
sucrose	31.78	31.78	31.78
PS20	0.4	0.4	0.4
Dextran	47.67	-	-
Hydroxyethylstarch	-	47.67	-
2-Hydroxypropyl-β-cyclodextrin	-	-	47.67

The LMU1 formulations were created according to the protocol in chapter IV, where stock solutions of the substances dextran from Leuconostoc spp. with a mean molecular ratio of 40.000 (Sigma-Aldrich, Steinheim, Germany), hydroxyethylstarch (HES) (Fresenius Kabi, Bad Homburg vor der Höhe, Germany), and 2-Hydroxypropyl-β-cyclodextrin (HPβCD) (Sigma-Aldrich, Steinheim, Germany) were spiked into the protein buffer stock to achieve the respective formulations of table V.3.

The different formulations were freeze-dried according to the conventional, collapse and freeze-anneal protocols of chapter IV. Also, the analytics were performed like before. Results are summarized in tables V.4-V.7.

The residual moisture of the dried products is considered as equal depending on literature values as discussed in chapter IV as the differences were lower than 0.5 – 1.0 % [14] (table V.4-V.6). However, the differences were bigger than for the disaccharide formulations from chapter IV, where the differences were only between 0.1 – 0.2 % in most cases. The only formulation where a difference in residual moisture higher than 0.5 – 1.0 % was found, was the HPβCD-mixture with a difference of 2.4% between the conventional and collapsed dried sample.

Interestingly, the T_g-values of the collapsed polymer formulations reached the same temperature levels as the conventional dried formulation although the residual moisture was increased (Table V.4 and V.5). A similar phenomenon was already observed in chapter IV with the 2gl_Suc formulations, where the same amount of residual moisture was reached but the T_g of the collapsed formulations was about 10 °C higher compared to the other formulations. Thus,

the structural collapse of the samples might be connected with other parameters of the amorphous matrix that increase the T_g-values as well as reduce the Δc_p- values of the products. Both parameters are considered to indicate a stable product.

Figure V.7 displays the correlation of the aggregation rate [%/month$^{-0.5}$] with the relaxation time τ^{β} [h]. The corresponding relaxation times can be found in table V.7. Both were determined as described in chapter IV. The correlation in the polymer containing samples (Dex and Hes) were good, in both cases a correlation coefficient of $r^2 = 0.94$ was achieved. It must be noted that the linear fit was performed with only three data points. However, the data gave a positive indication of the usage of relaxation time τ^{β} to estimate long-term protein stability in freeze-dried polymer containing formulations. The samples including HPβCD resulted in a correlation quality of $r^2 = 0.72$.

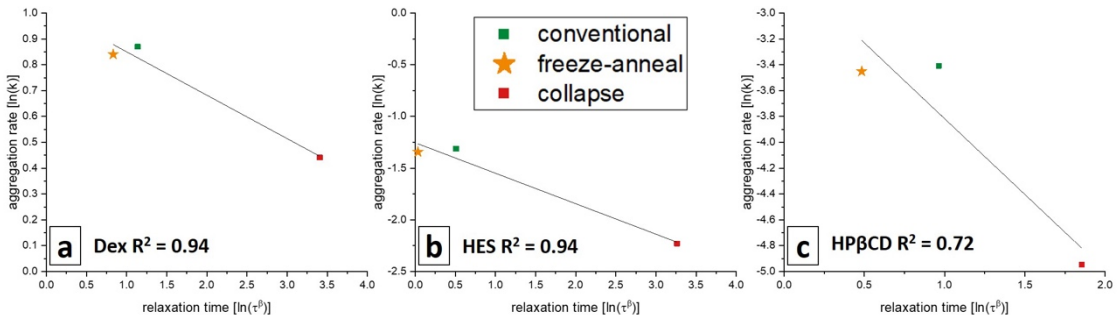

Figure V.7 Correlation of Correlation of the protein aggregation rate determined by HP-SEC with α-relaxation obtained with IMC. Small figures a-c represent the correlation of the different formulations at 40 °C. Formulations and processes as described in the legend. The respective correlation coefficients of the linear fit is presented at the left bottom of each chart.

Tabelle V.4 Solid state parameter of the dextran containing formulations.

process	Glass transition [°C]	Δc_p [Jg^{-1}K^{-1}]	Enthalpy recovery [Jg^{-1}]	SSA [m^{2}g^{-1}]	Residual moisture [%]
conventional	84.21	0.52	*	-	1.36
freeze-anneal	72.53	0.481	*	-	1.86
collapse	84.2	0.312	*	-	1.89

** value not determinable*
- value not recorded

Table V.5 Solid state parameter of the HES containing formulations.

process	Glass transition [°C]	Δc_p [$Jg^{-1}K^{-1}$]	Enthalpy recovery [Jg^{-1}]	SSA [m^2g^{-1}]	Residual moisture [%]
conventional	68.59	0.468	0.69	-	1.23
freeze-anneal	56.58	0.626	0.66	-	1.52
collapse	68.4	0.395	2.02	-	1.74

** value not determinable*
- value not recorded

Tabelle V.6 Solid state parameter of the HPβCD containing formulations.

process	Glass transition [°C]	Δc_p [$Jg^{-1}K^{-1}$]	Enthalpy recovery [Jg^{-1}]	SSA [m^2g^{-1}]	Residual moisture [%]
conventional	72.59	0.521	1.01	-	0.43
freeze-anneal	64.53	0.468	0.85	-	1.00
collapse	44.91	0.378	3.7	-	2.84

** value not determinable*
- value not recorded

Tabelle V.7 Relaxation times oft he achieved products determined at 40 °C.

	Relaxation time τ^{β} [h]		
	Conventional	**Freeze-Anneal**	**Collapse**
Dex	3	2	30
HES	2	1	26
HPβCD	3	2	6

V.6 Conclusions

Excipients that crystallize during the freeze-drying process, are not interfering in α-relaxation measurements using IMC. However, the usage of those excipients should be well considered to prevent a crystallization after the freeze-drying process because in that case the crystallizing agent will interfere with the protein aggregation rate (chapter IV 2gl_PS20_Suc samples 40 °C) and the IMC measurements.

In addition to the presented methods in chapter I, to reduce relaxation in freeze-dried formulations (tempering, aggressive freeze-drying) also microwave radiation applied on the dried product seems to be a suitable method. However, for a deeper analysis and to perform full stability studies, more professional microwave devices must be used. The advantage in using microwave radiation is the very precise control of the relaxation state.

Polymers as additive to a disaccharide formulation led to a better fit in the correlation of α-relaxations with protein aggregation. The character of polymers to build tangled networks and to naturally form glasses seemed to increase the connection of α-relaxations with aggregation promoting processes.

All in all, this chapter provides a short overview of concepts that could be investigated in future experiments to strengthen the relevance of using calorimetric α-relaxations. DSC instruments to determine α-relaxations are generally provided in laboratories working with freeze-drying. Especially, in the early development where higher aggregation rates are common α-relaxation studies are a very suitable method to estimate the long-term stability of a protein formulation.

V.7 References

1. Horn, J.; Tolardo, E.; Fissore, D.; Friess, W. Crystallizing Amino Acids as Bulking Agents in Freeze-Drying. *Eur. J. Pharm. Biopharm.* **2018**, *132*, 70–82, doi:10.1016/j.ejpb.2018.09.004.

2. Johnson, R.E.; Kirchhoff, C.F.; Gaud, H.T. Mannitol–Sucrose Mixtures—Versatile Formulations for Protein Lyophilization. *J. Pharm. Sci.* **2002**, *91*, 914–922, doi:10.1002/jps.10094.

3. Hawe, A.; Fries, W. Impact of Freezing Procedure and Annealing on the Physico-Chemical Properties and the Formation of Mannitol Hydrate in Mannitol–Sucrose–NaCl Formulations. *Eur. J. Pharm. Biopharm.* **2006**, *64*, 316–325, doi:10.1016/j.ejpb.2006.06.002.

4. Kasraian, K.; Spitznagel, T.M.; Juneau, J.A.; Yim, K. Characterization of the Sucrose/Glycine/ Water System by Differential Scanning Calorimetry and Freeze-Drying Microscopy. *Pharm. Dev. Technol.* **1998**, *3*, 233–239, doi:10.3109/10837459809028500.

5. Varshney, D.B.; Kumar, S.; Shalaev, E.Y.; Sundaramurthi, P.; Kang, S.-W.; Gatlin, L.A.; Suryanarayanan, R. Glycine Crystallization in Frozen and Freeze-Dried Systems: Effect of PH and Buffer Concentration. *Pharm. Res.* **2007**, *24*, 593–604, doi:10.1007/s11095-006-9178-z.

6. Costantino, H.R.; Carrasquillo, K.G.; Cordero, R.A.; Mumenthaler, M.; Hsu, C.C.; Griebenow, K. Effect of Excipients on the Stability and Structure of Lyophilized Recombinant Human Growth Hormone. *J. Pharm. Sci.* **1998**, *87*, 1412–1420, doi:10.1021/js980069t.

7. Mutukuri, T.T.; Wilson, N.E.; Taylor, L.S.; Topp, E.M.; Zhou, Q.T. Effects of Drying Method and Excipient on the Structure and Physical Stability of Protein Solids: Freeze Drying vs. Spray Freeze Drying. *Int. J. Pharm.* **2021**, *594*, 120169, doi:10.1016/j.ijpharm.2020.120169.

8. Härdter, N.; Geidobler, R.; Presser, I.; Winter, G. Accelerated Production of Biopharmaceuticals via Microwave-Assisted Freeze-Drying (MFD). *Pharmaceutics* **2023**, *15*, 1342, doi:10.3390/pharmaceutics15051342.

9. Gitter, J.H.; Geidobler, R.; Presser, I.; Winter, G. Significant Drying Time Reduction Using Microwave-Assisted Freeze-Drying for a Monoclonal Antibody. *J. Pharm. Sci.* **2018**, *107*, 2538–2543, doi:10.1016/j.xphs.2018.05.023.

10. Angell, C.A. Formation of Glasses from Liquids and Biopolymers. *Science* **1995**, *267*, 1924–1935, doi:10.1126/science.267.5206.1924.

11. Shamblin, S.L.; Hancock, B.C.; Dupuis, Y.; Pikal, M.J. Interpretation of Relaxation Time Constants for Amorphous Pharmaceutical Systems. *J. Pharm. Sci.* **2000**, *89*, 417–427, doi:10.1002/(SICI)1520-6017(200003)89:3<417::AID-JPS12>3.0.CO;2-V.

12. Austen Angell, C.; Sivarajan, S. Glass Transition. In *Reference Module in Materials Science and Materials Engineering*; Elsevier, 2017; p. B9780128035818031000 ISBN 978-0-12-803581-8.

13. Haeuser, C.; Goldbach, P.; Huwyler, J.; Friess, W.; Allmendinger, A. Excipients for Room Temperature Stable Freeze-Dried Monoclonal Antibody Formulations. *J. Pharm. Sci.* **2020**, *109*, 807–817, doi:10.1016/j.xphs.2019.10.016.

14. Wang, B.; Cicerone, M.T.; Aso, Y.; Pikal, M.J. The Impact of Thermal Treatment on the Stability of Freeze-Dried Amorphous Pharmaceuticals: II. Aggregation in an IgG1 Fusion Protein. *J. Pharm. Sci.* **2010**, *99*, 683–700, doi:10.1002/jps.21960.

Chapter VI Summary of the thesis

The number of biological drug products to treat severe diseases continuously increased over the last decades. Advantages like improved targeting or rapid generation of vaccines still accelerates the interest in their development. However, even today, the often very restricted biological and chemical stability make formulation, shipment and storage of such products difficult. Often, dry, solid formulations of biological entities are superior regarding stability compared to their liquid counterparts but are challenging and more time consuming in their development. There is no universal rule for selecting formulation compounds as well as freeze-drying process parameters. Even if a reasonable product is achieved after the lyophilization process, stability studies must be performed to determine and ensure the therapeutic function after a long shelf life as well as to select the most promising formulation candidate. Thus, methods that predict shelf life immediately after lyophilization are still urgently needed to accelerate the formulation and lyophilization process development of biologic pharmaceuticals.

In **chapter I**, a literature review combined with pre-experiments, methods to study and to evaluate α-relaxations were presented as one possible predictive method to determine long-term protein stability in freeze-dried pharmaceuticals. An amorphous state of the lyophilized matrix is required to maintain the function of the protein. In such amorphous, glassy systems, the activation energy for reactions itself is temperature dependent and an Arrhenius-like behavior if often not applicable. This leads to special kinetics in those systems, that differ strongly depending on the investigation temperature of interest compared to the glass transition temperature. Changing relaxation kinetics at corresponding temperatures leading to different mobility might explain that phenomenon. Models like the Vogel-Tammann-Fulcher equation (VTF-equation) were developed in order to describe glassy kinetics. This equation is a deviation of the Arrhenius equation with additive constants that try to take temperature dependent activation energies into account. However, the constants have to be determined for each specific glass, i.e., for each individual lyophilized formulation or process candidate, which is very time consuming. Thus, it is easier and practically more feasible to determine the relaxation behavior only at the temperature of interest. This can be done with isothermal microcalorimetry, for example. In the context of pharmaceutical freeze-dried products, the temperature of interest is of course the intended storage temperature of 2-8 °C or even 25 °C and not the accelerated conditions at 40 °C or even higher.

α-relaxations were discussed in **chapter** I and several methods to measure those were described (e.g. Differential Scanning Calorimetry (DSC), Isothermal Microcalorimetry (IMC), Dielectric

Relaxation Spectroscopy (DRS)). IMC turns out as superior for α-relaxation measurements and was hence used for the extensive studies carried out in this thesis. Relaxation times are captured with the respective instrument in the value of τ^{β} [h]. Short α-relaxations times, are a marker for a less rigid matrix. With this, more and stronger movements occur in matrices with a low τ^{β}-value that allow more pronounced protein degradation in form of protein aggregation. Consequently, in the area of protein formulation an increase of α-relaxation time is considered to lead to an increase in long-term stability of the matrix embedded proteins.

Methods to increase α-relaxations times were presented in **chapter I** and short experiments were performed that suggest further options. The classical way includes the exposure of the amorphous matrix to elevated temperatures for a short amount of time which is called tempering. Nevertheless, in a freeze-drying process, more possibilities to increase the α-relaxation time are possible. For example, α-relaxation time could be increased, by influencing the structure of the matrix in the freezing process or by a primary drying process above T_g'. Furthermore, residual moisture was carved out as a parameter that strongly influences α-relaxation times.

The performed pre-experiments in **chapter I** together with the cited literature work out the concept, that different formulation parameters cannot be compared regarding their stability with α-relaxation. Material properties like the tendency to crystallize or the glass transition temperature are too strong and possess effects that cannot be captured with α-relaxations. An impressive example was given with the pre-experiment using small amounts of PS20 that accelerates the crystallization in sucrose containing formulations without significant changes in α-relaxation times. In contrast, with a constant formulation, the effects of different drying processes can be measured in different relaxation behavior and correlated with product stability parameters.

The crystalline state is the thermodynamic most stable form and due to this fact, every amorphous phase will sooner or later transform into it. As this transformation depends on the mobility in the freeze-dried cake, **Chapter III** focuses on the use of α-relaxations times to predict the onset of crystallization in amorphous protein containing pharmaceuticals at an early stage of development. This would save a lot of time as instead of performing long lasting investigations with several sample aliquots for XRD measurements, only a few vials have to be investigated.

Moreover, the influence of the freezing-step on α-relaxations was more deeply investigated. If it were possible to significantly prolong relaxation time by varying the structure of the amorphous phase through the freezing-step, a very gentle method would be given compared to a tempering process after the lyophilization.

In a pre-experiment in **chapter III,** it was proven that the freezing-step influences the α-relaxation behavior. Processes that differ only in their freezing step (random nucleation, annealing with 1.5 h duration and with 3.0 h duration, controlled nucleation and quench cooling) were compared.

The long-term inspection of the crystallization behavior of the products with the classical methods like DSC and XRD revealed, that the matrix behavior at 40 °C storage cannot be extrapolated to 25 °C as the order of crystallization changes. For example, a sucrose based product generated by a certain freezing step that crystallized at last at 40 °C already crystallized as second sample at 25 °C. This observation was in agreement with the non-Arrhenius behavior of glasses as already described above and showed the importance of product investigation at the intended storage temperatures – not at accelerated conditions through higher temperature.

Above all, this observation was also in agreement with the predicted order in α-relaxation times and the main question of the study was successfully answered. All formulations containing 1.6 mg/ml PS20 crystallized during the investigation period and the onset of crystallization could be correlated with the α-relaxation times τ^{β}. At 40 °C as well as at 25 °C a successful fit between the α-relaxation and crystallization time was achieved. Thus, the method to correlate α-relaxation times with crystallization onset was superior when compared with classical methods like DSC and XRD. To conclude, it should be considered to use IMC measurements for process optimization regarding long-term crystallization after freeze drying.

Furthermore, only a few formulations containing 0.4 mg/ml PS20 crystallized and all vials without PS20 stayed amorphous. The observations of Vollrath et al. were reproduced in **chapter III** in a larger set of samples. PS20 clearly accelerates the crystallization of protein containing sucrose matrices and thus, the use of it has to be well considered to balance its function to protect the protein from aggregation and the attribute to accelerate crystallization.

In **chapter IV**, aggressive drying cycles were used to apply the heat of tempering within the freeze-drying cycle and to correlate α-relaxations with protein stability in stable market like formulations. The main question to be answered with this study was the suitability of α-relaxation measurements as tool for process optimization.

The increased relaxation time τ^{β} in the aggressive and collapse dried formulations compared to the conventional dried products proved that it is possible to relax the amorphous matrix by heat application during the freeze-drying process. In some cases, the collapse cycle led to even longer relaxation times than subsequent tempering. However, a universal rule for the best "tempering procedure" could not be derived from this study and requires further investigations.

The correlation of protein aggregation with relaxation time was also shown in **chapter IV** but the quality of the fit varies in dependency of the formulation T_g compared to the measurement temperature. Although this was expected from the beginning of the study, this effect turned out to be stronger than considered and thus, a statistical valid manner was only achieved in 2gl_Suc formulations. Covering a broad range of T_g temperatures with stable market like formulations made the correlation of the already very stable formulations even more difficult but was intended for this study. Nevertheless, the study achieved the main goal and can give some implications for the further process development.

When the storage temperature is very close to T_g relaxation measurements can be performed, which help to rank the stability of IgG_1 antibody against aggregation with certainty depending on the drying process. Although perfect correlations could not be drawn in the cases where the T_g of the formulation was at least 25 °C higher than the storage temperature, tempered or aggressively dried products showed a better long-term stability than conventional dried counterparts. Structural collapse introduced by harsh drying cycles did not necessarily increase the protein damage but rather on the opposite lead to products with the same stability and when compared to tempered samples a lower initial amount of aggregates.

Furthermore, when external tempering after the freeze-drying is used to relax the products, shorter times at higher absolute temperatures seem to be better than long at lower temperatures.

In **chapter V** further background information about α-relaxations is given. It was shown that in a semi crystalline matrix the α-relaxations of the amorphous phase were not changed by the crystalline phase. Before using α-relaxations as predictive methods for protein stability it should carefully be reviewed whether parts of the crystallizing agent stay amorphous after freeze-drying. If the latter is not the case, interference in the measurement from subsequent crystallizing can be expected by the heat of crystallization.

Microwave radiation as further method to increase the relaxation time τ^{β} was presented in **chapter V**. By the use of a domestic microwave, experiments were performed that confirmed

microwave radiation applied on an already dried product as fast and suitable method for tempering.

More correlations of α-relaxations with protein stability in form of soluble aggregates determined by size exclusion chromatography were presented in **chapter V**. Correlations at 25 °C are better for the resolution of the relaxation curves in the IMC measurement, but the lower aggregation rate of the antibody at 25 °C in comparison to 40 °C made the determination of the aggregation rate more difficult.

Also, the suitability of further excipients for the correlation of α-relaxations with protein stability are investigated in **chapter V**. Blends including polymer excipients showed a good correlation at 40 °C. Thus, it can be considered, that polymers response more to α-relaxations through their stronger ability to build entangled networks and glasses in comparison to disaccharides.

In summary, the correlation of α-relaxations with reactions in the amorphous phase like crystallization or protein aggregation is possible. However, a direct coupling seems not to be present and in some cases led to errors and deviations in the correlation procedure. Especially in relatively stable formulations, low degradation rates can strongly reduce the correlation quality. For products with aggregation as main source for degradation, relaxation times could be a suitable method to predict the long-term stability and help to select the best freeze-drying process.

Appendix 1: Publications associated with this thesis

Groël, S.; Menzen, T.; Winter, G. (2021). Calorimetric Investigation of the Relaxation Phenomena in Amorphous Lyophilized Solids. *Pharmaceutics* 2021, 13, 1735: https://doi.org/10.3390/pharmaceutics13101735

Groël, S.; Menzen, T.; Winter, G. (2023). Prediction of Unwanted Crystallization of Freeze-Dried Protein Formulations Using α-Relaxation Measurements. *Pharmaceutics* 2023, 15, 703: https://doi.org/10.3390/pharmaceutics15020703

Groël, S.; Menzen, T.; Winter, G. (2023). Possibilities and limitations of α-relaxation data of amorphous freeze-dried cakes to predict long term IgG_1 antibody stability. *International Journal of Pharmaceutics* 2023, 123445: https://doi.org/10.1016/j.ijpharm.2023.123445

Appendix 2: Presentations associated with this thesis

Oral presentations:

Groel S., Seidel J., Menzen T., Winter G. α-relaxations studied by isothermal microcalorimetry to develop freeze dried products with improved shelf life from a thermodynamical point of view.
Die 24. Kalorimetrietage Braunschweig, May 26 – 28, 2021, Virtual Conference

Groel S., Menzen T., Winter G. α-relaxation studies to improve long term stability of lyophilized products from a thermodynamical point of view.
12th World Meeting on Pharmaceutics, Biopharmaceutics and Pharmaceutical Technology, May 11 – 14, 2021, Virtual Conference

Groel S., Seidel J., Menzen T., Winter G. Using Isothermal Calorimetry to Study the Influence of Excipients and Processes on the Glassy Dynamics of Lyophilized Products.
PDA Europe Pharmaceutical Freeze Drying Technology, September 24 – 25, 2020, Virtual Conference

Poster presentations:

Groël, S., Menzen, T., Winter G. Optimization of aggressive freeze-drying protocols using α-relaxation in the amorphous cake as predictive factor for long term protein stability
2022 Colorado Protein Stability Conference, August 8 – 11, 2022, Breckenridge

Awarded with the student poster competition price as 2nd runner up.

Groël, S., Menzen, T., Winter G. Application of isothermal microcalorimetry to predict unwanted crystallization in amorphous lyophilisates.
13th World Meeting on Pharmaceutics, Biopharmaceutics and Pharmaceutical Technology, March 28 – 31, 2022, Rotterdam